MICROFLUIDIC FOCAL INJURY MODELS OF THROMBOSIS AND HEMOSTASIS

Sean Francis Maloney

A DISSERTATION

in

Chemical and Biomolecular Engineering

Presented to the Faculties of the University of Pennsylvania in Partial Fulfillment of the Requirements for the Degree of Doctor of Philosophy

2010

Scott L. Diamond, Ph.D., Arthur E. Humphrey Professor
Department of Chemical and Biomolecular Engineering
Supervisor of Dissertation

Matthew J. Lazzara, Ph.D., Assistant Professor
Department of Chemical and Biomolecular Engineering
Graduate Group Chairperson

Dissertation Committee

Lawrence F. Brass, M.D., Ph.D., Professor of Medicine
Department of Medicine, Division of Hematology and Oncology

John C. Crocker, Ph.D., Associate Professor
Department of Chemical and Biomolecular Engineering

Daniel A. Hammer, Ph.D., Alfred G. and Meta A. Ennis Professor
Department of Chemical and Biomolecular Engineering

Acknowledgements

As is the case with any successful project, the work of this thesis was aided by the help of many. The first recognition and thanks go to my advisor, Dr. Scott Diamond. For over four years, he has been invaluable in developing my ability to assess, analyze, take action on scientific matters of all shapes and sizes. His vast experiences inform his ability to look beyond the immediate problem and quickly extract the pertinent nuggets of information and relating them to the issue at hand.

A great deal of thanks also is in order to the members of my thesis committee: Dr. Skip Brass, Dr. John Crocker, and Dr. Dan Hammer. I have been fortunate in being able to discuss some of the issues presented in this thesis with three expert scientists that have vastly disparate backgrounds, which provide for inspiration and insight into complicated biological and engineering problems. Their willingness to take time and discuss aspects of research, perhaps outside of their immediate interests, with enthusiasm and interest was an inspiration throughout the course of this work. Special thanks are in order for Skip, whose patience in bringing an engineer into the wonderfully complicated and diverse world of medicine, specifically platelet biology.

A special mention must be made to Dr. Keith Neeves, now at the Colorado School of Mines. As a post-doctoral researcher, Keith brought the experience of microfabrication and nanocharacterization techniques to the lab. However, on a personal note, Keith taught me more about the design, conduct, and analysis of experiments than anyone throughout my career. Perhaps equally as important, he was able to guide my development as a scientific critic of both my and others work,

as well as sage advice on marriage, music, and baseball. I will be forever grateful for his influence on my life and career.

I have been fortunate to have had the pleasure of working with a number of brilliant and kind individuals throughout the execution of this work. All past and current members of the Diamond Lab have been helpful in every aspect of this work; special recognition to Dr. Uzoma Okorie, Dr. Bill Denney, Dr. Jeremy Purvis, Manash Chatterjee, Matt Flamm, Dan Jaeger, and Tom Colace as members of the Blood Systems Biology research team. Additionally, Dr. Greg Barker, Dr. Dave Fein, Joel Outten, Matt Furlow, and Alexis Wallen were great sources of help. Other members of the Department of Chemical and Biomolecular Engineering at Penn: students, faculty, and staff, especially Marge Addario, made this work possible. Also, the Institute for Medicine and Engineering members and staff, especially Marvin Jackson, provided help throughout my time at Penn. I also owe a debt of thanks to Dr. Abraham Lenhoff and Dr. J.J. Langford, for it was their guidance and inspiration that led me to pursue a doctoral degree by instilling a love of research in me as an undergraduate at the University of Delaware.

Finally, I am eternally grateful to family and friends that supported me throughout the work described in this thesis. Preston, Steve, Kathy, Casey, Nick, and Marisa provided daily reprieves from the constant reality of the research world with their podcast, which I will always remember as an integral part of my time in the lab. Numerous friends and family members have provided kind words of encouragement during the tough times and reassurances that the goal was, in fact, worth the effort, and I am indebted to them. The last, and most important thanks, is to my wife, Kristen. She has been an inspiration and motivator for longer than anyone would believe, and her work ethic and dedication are among the countless characteristics of hers that I admire and strive to emulate. In her, I have found my best friend, my college sports co-fanatic, a voice of confidence and reason, and a beautiful inspiration for all that I do; for that I am and will be eternally thankful.

ABSTRACT

MICROFLUIDIC FOCAL INJURY MODELS OF THROMBOSIS AND HEMOSTASIS

Sean Francis Maloney

Scott L. Diamond

Current *ex vivo* models of thrombosis either fail to accurately recreate the hemodynamics and focal nature of injuries commonly found throughout the vasculature or require excess amounts of material. Development of a novel microfluidic thrombosis model has allowed for the measurement of thrombus stability of platelet aggregates formed on collagen from a single non-lethal murine blood draw. It was observed that platelet accumulation exhibits a biphasic behavior, with maximum accumulation at an average wall shear rate of 400 sec^{-1}, with engagement of $\alpha_2\beta_1$ integrin a mandatory factor due to complete loss of adhesion in blood from a knockout animal. It was found that PAR4 stimulation of pre-formed thrombi increased aggregate stability by 50%. Subsequent device designs were made to simultaneously measure platelet accumulation on collagen of eight samples under independent bulk pharmacological intervention. This provided a platform for rapidly and repeatable assessing the potency of receptor antagonists under relevant flow conditions with half-maximal inhibitor concentrations ($P2Y_1$ inhibitor MRS 2179 $IC_{50} = 0.23$ μM, $P2Y_{12}$ inhibitor 2-MeSAMP $IC_{50} = 2.56$ μM) comparable to published data, while an enzyme commonly used failed to have any effect due to transport limitations. Finally, investigation into the effects of tissue factor initiated coagulation in addition to collagen-induced platelet accumulation and activation revealed a number of technical hurdles required for further experimentation. The use of custom functional liposomes as linkers for surface immobilization provides a platform for careful titration of active tissue factor onto a surface at high densities (up to 35 active tissue factor molecules per μm^2) for illumination into the role and extent of thrombin and fibrin formation during hemostatic injury. Additionally, geometries akin to late stage atherosclerotic vessels open

the possibility of shear history affecting the growth and stability of platelet thrombi formed on collagen. Investigation of bulk phase shear-mediated von Willebrand Factor conformational changes could illuminate both mechanistic processes involved in pathological thrombosis and provide a basis for new biomarkers for patients at risk for a catastrophic thrombotic event.

Contents

List of Tables

List of Figures

Chapter 1

Introduction

1.1 Background

1.1.1 Blood, the vasculature, and hemostasis

The development of a high-pressure closed circulatory system necessarily required the adaptation of mechanisms to rapidly stop blood loss upon injury while maintaining bulk fluidity during homoeostatic periods. The delicate balance is dependent on both the removal of procoagulant species from the circulation and the active passivization. Whole blood consists of numerous cellular components suspended in a milieu of dissolved gases, ionic species, molecules, and proteins. The cellular fraction of blood is significant, red blood cells (RBCs) comprise between 35 and 50 % of blood volume, which has implications on both blood rheology [65] hemostatic processes [1, 108]. While RBCs make up a majority of the cellular component of blood, nucleated cells including, but not limited to, neutrophis, eiosinophils, monocytes, and macrophages are critical components of immunity and host defense. The final major cellular class found in blood is platelets. These small anuclear cells are the second most plentiful, with normal circulation levels between 150 and 400 $\times 10^9$ cells per L. Platelets are small irregularly shaped discoid cells between 2 and 4 μm in diameter. They are the

major cellular player in hemostasis and thrombosis, and are conserved throughout the Class Mammalia, though nucleated thrombocytes are found throughout other classes of animals [66].

The second half of the hemostasis and thrombosis process is a series of enzymatically catalyzed proteolysis reactions that is referred to as the coagulation cascade, as shown in Figure 1.1. These proteins are found a wide range of levels in the circulation, most as inactive zymogens, which are, upon proteolytic cleavage, converted into either active enzymes or cofactors. As is indicated by Figure 1.1, there are numerous feed-back and feed-forward processes that serve to both amplify and dampen the response of the coagulation cascade's most functional product, the enzyme thrombin (IIa). Thrombin acts as the nexus of the coagulation cascade by both rapidly feeding back to accelerate its formation and by initiating events that will lead to its inactivation and subsequent clearance from the circulation.

A closed vascular system is, at the most basic level, a pump, series of pipes, and mass contactors. The heart acts as the pump, which moves the process fluid, blood, through the arteries and the vasculature system through series of smaller vessels to tissues throughout the body where dissolved gases, ions, molecules, and proteins are exchanged. The system operates under a positive pressure, i.e. blood is forced from a high pressure (immediately exiting the left ventricle into the aorta) down pressure gradients throughout the vasculature , recollected into the right atrium via the venous system, all the while at pressures greater than atmospheric. Upon return to the heart, the right ventricle pumps the blood through the lungs where gaseous species are exchange with inhaled air, after which blood returns through the left atrium, where it is cycled back into the left ventricle for circulation back to the body. The blood vessels that run throughout the body are lined with a monolayer of endothelial cells which serve numerous functions both in hemostasis and other biological processes. Beneath the endothelial cells are subendothelial matrix proteins, including collagen, vitronectin, and laminin. The endothelial cells and subendothelial matrix comprise

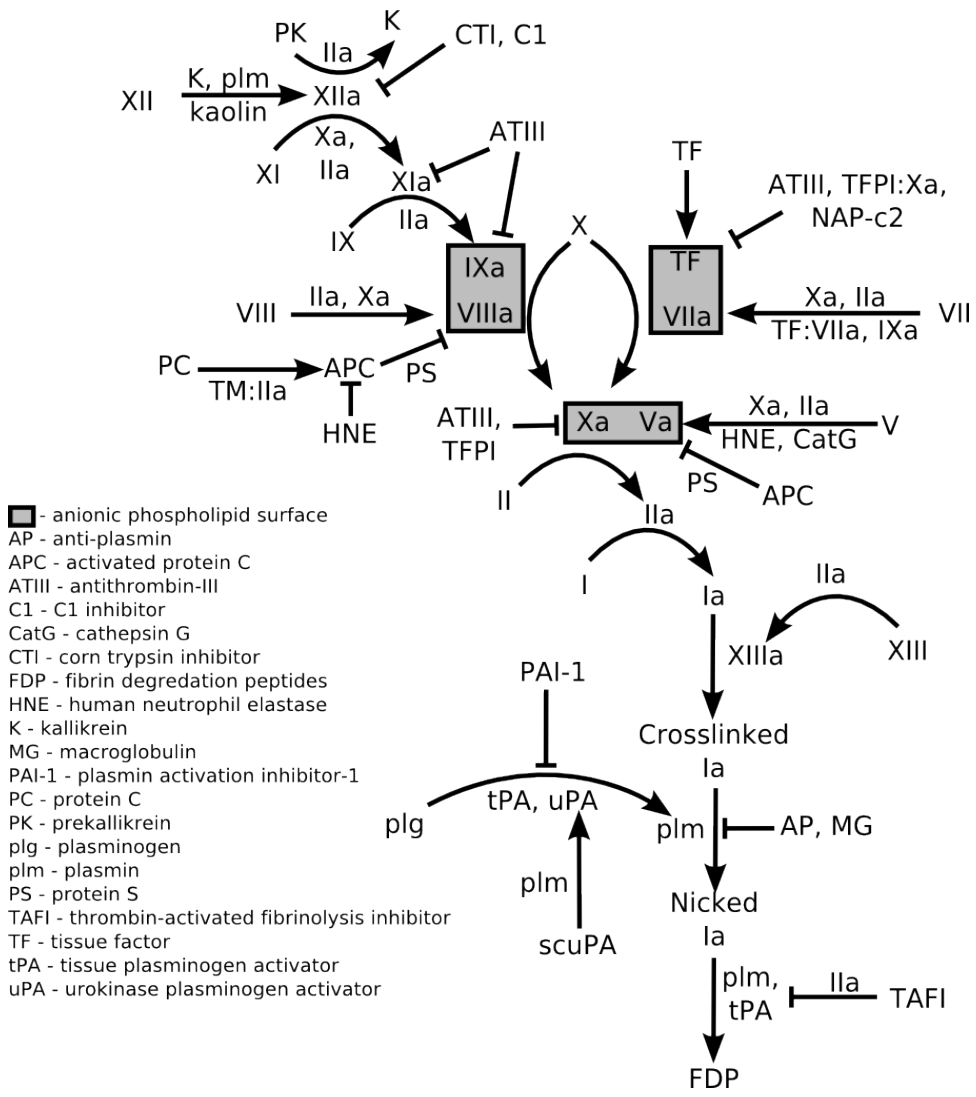

Figure 1.1: The enzymatic reactions of the coagulation cascade (courtesy of Bill Denney).

the intima of the blood vessel. Beneath this layer is the media, comprising of smooth muscle cells which control vaso-constriction and -dilation to regulate blood pressure and flow rate to different regions of the body. The final layer of vessel composition is the adventitia, which is dominated by connective tissue and fat to insulate and provide structural integrity to the overall system.

In order to maintain the fluidity of blood under physiological conditions, the endothelial cell layer performs a number of important functions. Protein expressed constitutively on the luminal side are active nucleotide phosphatases (CD39) which act by hydrolyzing adenosine diphosphate (ADP), a platelet agonist, to its monophosphorolated form which is not recognized by platelet receptors. Also, endothelial cells synthesize nitric oxide and prostacyclin (PGI_2) which serve to keep platelets in a quiescent state by increasing intracellular levels of cyclic adenosine monophosphate (cAMP) inside the platelets. Cyclic AMP acts on calcium pumps within the platelet which actively move calcium ions from the cytoplasm into either dense tubular storage or into the extracellular milieu. In addition to serving biochemical functions, endothelial cells serve as a physical barrier to keep blood cells, specifically platelets, from interacting with the subendothelial matrix. Platelet are specially adept at quickly recognizing sites of injury, adhering and activating to quell blood loss and maintain vascular integrity.

1.1.2 Platelets

Platelets have evolved to fit a very unique niche within the context of a closed, high-pressure vascular system. The loss of sufficient blood flow to organs due to either excessive blood loss through a failure of vessel integrity (hemorrhage) or blockage of flow through the vessel (ischemia) results in tissue death if not rectified. Platelets are the primary cell type involved with keeping the balance between these two states when blood vessels are breached due to injury and are ideal for this purpose for several reasons. Firstly, platelets are generated by thrombopoiesis, by which they are

shed from mature megakaryocytes, which are found in the bone marrow throughout the body. As a result, platelets contain mRNA and other translational machinery found throughout the cytoplasm of megakaryocytes, enabling them to synthesize new proteins upon stimulation, but lack DNA and the transcriptional proteins that would be required for generating new messages.

Platelets express a range of surface proteins that are critical for proper function as hemostatic agents. The most well studied platelet surface proteins fall into three categories: integrins, glycoproteins, and G-protein coupled receptors. Integrins are heterodimeric proteins consisting of an α and β subunit. These receptors are expressed in a variety of levels on both the apical and luminal side of the plasma membrane. Upon platelet activation, membrane sections are flipped and granules released, causing the copy number and types of membrane proteins on the platelet surface to greatly change. Subsequently, throughout the platelet activation process, some surface proteins are shed from the surface while others are internalized upon ligand binding or other signaling events. The exposure of certain proteins is accompanied by exposure of different types of lipids on the platelet surface, specifically the negatively charged phospholipid phosphatidylserine (PS). This negative lipid surface is crucial for the proper assembly and proteolytic cleavage of several enzymes in the coagulation cascade (as shown in the gray boxes in Figure 1.1). While circulating in a quiescent state, platelet integrins, mainly $\alpha_{IIb}\beta_3$, $\alpha_2\beta_1$, and $\alpha_V\beta_3$, are in an inactive or low-affinity state. Upon platelet activation via an independent route, the integrins undergo a conformational change, setting the ligand binding region into a high-affinity state. This 'inside-out' signaling allows platelets to interact modularly with species that are found ubiquitously throughout the blood, like the soluble protein fibrinogen. Complementary, upon ligand binding, additional changes are induced on the stalk and cytoplasmic tail of the integrin proteins, allowing for both intracellular signaling and scaffold protein binding as an 'outside-in' signal. Glycoproteins are an important class of platelet surface molecules that, like integrins,

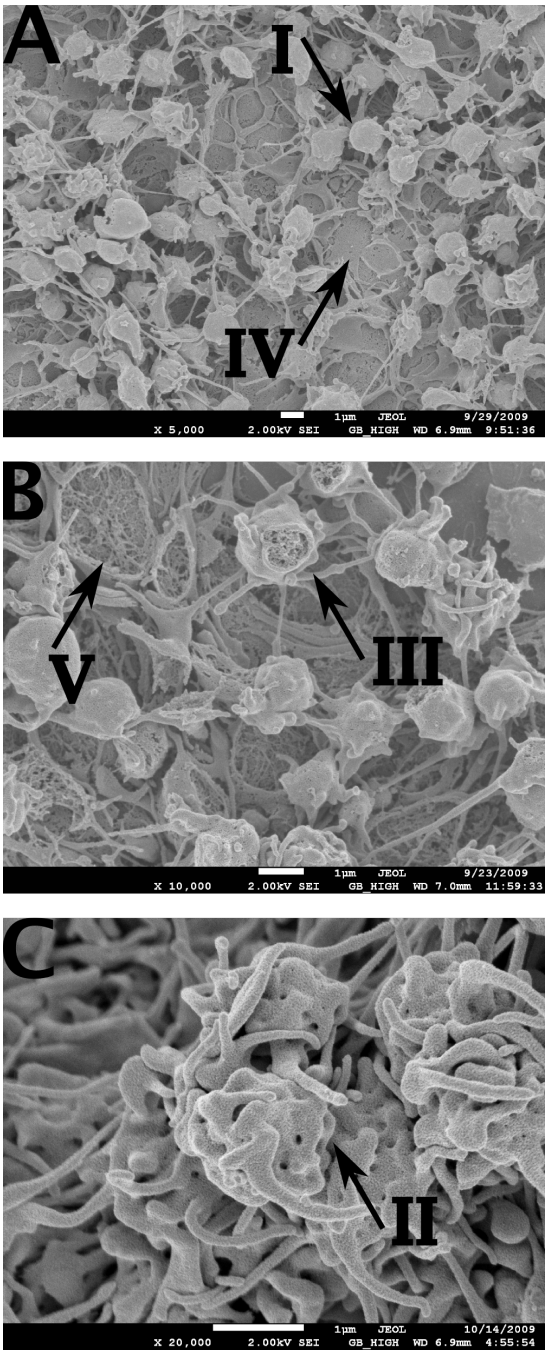

Figure 1.2: Different phases of platelet activation: I. Initial adhesion (A), II. Pseduopod extension and membrane ruffling (C), III. Granule fusion and membrane peeling (B), IV. Compression and collapse (A) V. Membrane disintegration leaving only microtubules and cytoskeletal proteins (B).

function both as adhesion molecules and signaling molecules. Glycoproteins are in a constitutively active confirmation, and are post-translationally modified with numerous sugar groups, hence the nomenclature. The two glycoproteins that are active in hemostatic processes on the platelet surface are glycoprotein VI (GPVI) and the glycoprotein Ib-IX-V complex (GPIb-IX-V).

G-protein coupled receptors, or GPCRs, are transmembrane proteins that present extracellular ligand binding sites and are coupled to one or more a subtype of G-protein that activates a signaling cascade upon ligand binding. Among the most studied GPCRs expressed on the platelet surface are the purinergic receptors, $P2Y_1$ $P2Y_{12}$, and $P2X_1$, the thromboxane receptor (TP) and the protease activated receptors, PAR1 and PAR4. While the specifics of G-protein signaling are complicated and still under intense research, their importance in platelet signaling are undoubted. The intrinsic regulation of G-protein signaling via signaling molecules such as kinases and phosphatases within the platelet allows for very complex response behavior. Coupling to feed-forward and feed-back mechanisms allow for a full range from rapid-on/rapid-off signals for fast responses to long, sustained signals depending on the molecules involved. The output of these signaling pathways result in a wide range of signals, including inside-out integrin activation, calcium release, granule fusion. The physical manifestations of platelet activation can be seen in Figure 1.2.

1.1.3 Coagulation

The coagulation cascade describes the collection of proteolytic processes as shown in Figure 1.1. The large interaction web between numerous zymogens, cofactors, enzymes, and reactive surfaces are frequently broken down into three pathways: intrinsic, extrinsic, and common, as shown in Figure 1.3. The role of the contact pathway in thrombin formation *in vivo* is currently under investigation [109], but the classical view of *in vivo* thrombin generation is tissue factor initiated via the

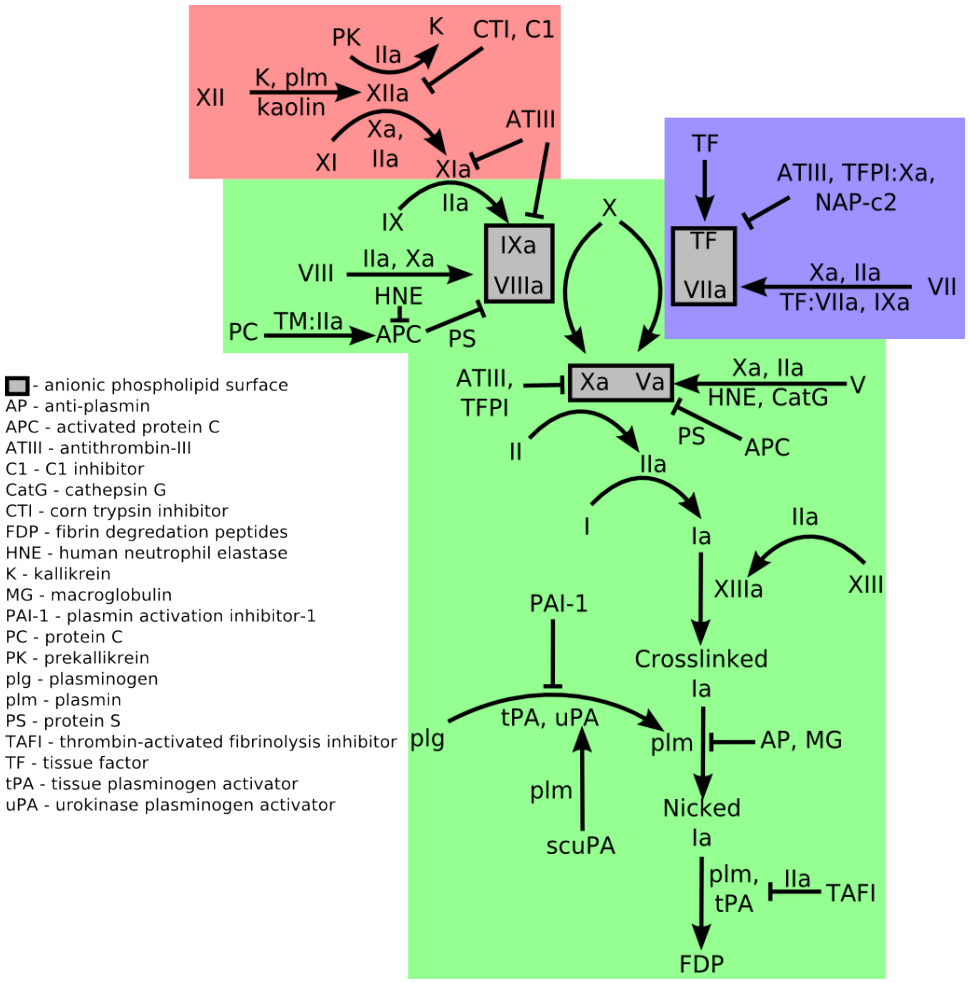

Figure 1.3: Breakdown of the coagulation cascade into the intrinsic (red), extrinsic (blue), and common (green) pathways.

extrinsic pathway. Upon endothelial cell disruption during an injury, tissue factor that is exposed to flowing blood. Small circulating levels of activated Factor VII (FVIIa) bind to the exposed tissue factor and initiate the cascade. There are also a number of other sources of tissue factor, such as monocytes, microparticles, and platelets. Upon binding of FVIIa to tissue factor, small amounts of activated Factor X (FXa) are formed, which can activate Factor V to FVa. The assembly of Factor Xa and Va on a negatively charged phospholipid surface is what is referred to as the prothrombinase complex, the coenzyme that converts prothrombin into thrombin.

Thrombin is the central enzyme in the coagulation cascade and an important link between coagulation, platelets, and the rest of the vascular system, with its involvement in many of the coagulation reactions highlighted in Figure 1.4. A potent serine protease, thrombin is able to cleave and activate other proteases as well as a number of protease activated receptors, or PARs, on the surface of platelets, endothelial cells, neutrophils and other cells associated with vascular integrity. Thrombin serves to rapidly increase its product by feeding back in the common pathway (the green section of Figure 1.4), while also rapidly being deactivated by the serine protease inhibitor, or SERPIN, antithrombin III (ATIII), which is present at high (2.3 μM) concentrations in the circulating plasma. This kinetic competition of feedback and inhibition leads to a very complex and finely regulated system, which is advantageous for such a potent end-product such as thrombin.

Ultimately, thrombin serves as the major component that interacts with both the coagulation cascade and platelets. PARs on the platelet surface respond to thrombin activity, while platelets serves as the major source of negatively charged phospholipid support for coagulation complex assembly and proteolysis. It is this tight integration of the two systems that lends much of the complexity to many of the model systems used to investigate the biology and function of hemostasis and thrombosis and general.

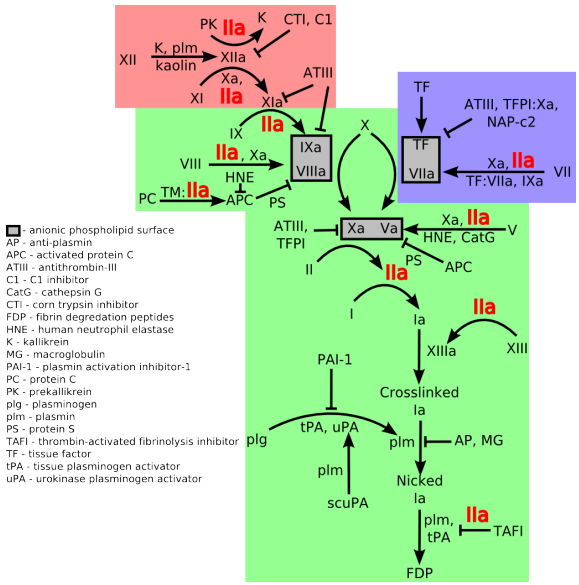

Figure 1.4: The role of thrombin, the central enzyme in the coagulation cascade, is highlighted in its many feed-back and feed-forward roles.

1.2 Motivation

The motivation behind this work is to develop and use new tools to study phenomena in thrombosis and hemostasis. By using well established soft-lithographic techniques to generate a set of microfluidic devices to pattern and then perfuse solutions over a glass substrate. The ability to use small volumes of materials to create focalized models of thrombosis for real-time and *post-hoc* analysis is targeted to a technology gap currently facing researchers in both basic science and clinical applications of platelet biology and coagulation biochemistry. Since blood is necessarily under flow in closed, high-pressure circulatory systems, models for injuries that can capture the hemodynamics and flow characteristics are more realistic and offer better opportunities to accurately describe the phenomena which occur *in vivo*. There are a number of technologies that are currently used to investigate hemostatic processes while under flow *ex vivo*, such as parallel plate flow chambers, capillary flow chambers, and cone-and-plate viscometers; however, each has their shortfall in terms

of material requirement, patterning capability, or realistic hemodynamics. By coupling micropatterning techniques with flexible channel designs, microfluidics allows for realistic, spatially confined injury mimetics to be formed under controlled flow conditions with precise control over initial surface and inlet blood conditions. Each of the subsequent chapters builds upon the complexity and strengths of the previous section, while employing new and novel aspects to the work. By incrementally increasing the complexity and realism of the model system, it is possible to both master the physical fabrication and experimental use of the devices and develop better understanding of successful design aspects and crucial biological implications of using *ex vivo* model systems.

1.3 Problem Statement

The problems addressed in this work include the design, fabrication, characterization, and use of a microfluidic based focal injury model for asking and answering novel questions in thrombosis and hemostasis. One goal includes the development of a system that is amenable to use with small volumes of blood that is mandated by the non-sacrificial techniques of blood obtained from immensely important genetically modified mice lines. Additionally, the ability to measure multiple outputs from a single source blood sample simultaneously provides controls which are paramount in highly variable hemostasis measurements, while serving as preliminary units which could be used as future diagnostic devices. Finally, increasing the complexity of the surface composition and the flow geometry will begin to recreate some of the important complexities of *in vivo* thrombosis and hemostasis.

Chapter 2

Microfluidic Model System

2.1 Abstract

Flow chambers allow the *ex vivo* study of platelet response to defined surfaces at controlled wall shear stresses. However, most assays require 1 to 10 mL of blood and are poorly suited for murine whole blood experiments. The objective of this Chapter is to describe a system used to measure murine platelet deposition and stability in response to focal zones of prothrombotic stimuli using 100 μL of whole blood and controlled flow exposure. Microfluidic methods were used for patterning acid-soluble collagen in 100 μm x 100 μm patches and creating flow channels with a dead volume of 150 nL. Within 1 min of blood draw into PPACK and fluorescent anti-mouse CD41 mAb, whole blood from normal mice or from mice deficient in the integrin α_2 subunit was perfused for 5 min over the patterned collagen. Platelet accumulation was imaged at venous and arterial wall shear rates. After 5 min, thrombus stability was measured with a "shear step-up" to 8,000 sec^{-1}. Wild-type murine platelets adhered and aggregated on collagen in a biphasic shear dependent manner with increased deposition from 100 to 400 sec^{-1}, but decreased deposition at 1,000 sec^{-1}. Adhesion to patterned collagen was severely diminished for platelets lacking functional $\alpha_2\beta_1$ integrin. Those integrin α_2-deficient platelets that did adhere

were removed from the surface when challenged to shear step-up. PAR4 agonist (AYPGKF) treatment of thrombus at 5 min enhanced aggregate stability during shear step-up. This PAR4 signaling enhances aggregate stability by mechanisms independent of other thrombin-dependent pathways such as fibrin formation.

2.2 Background

As anuclear cells, platelets are incompatible with *in vitro* genetic manipulation by transfection or transduction. Consequently, genetically modified mice are a critical tool for researchers studying the roles of platelet receptors and signaling in clot initiation, propagation and stability [92]. Chemical [59], photoactivated [64], and laser-induced [87] injury to vessels within genetically modified mice in combination with intravital microscopy [26] are powerful tools for capturing the complex interplay among platelets, endothelial cells and the subendothelial extracellular matrix. Yet, it is difficult to control or quantify the biochemistry of the wall injury within these models. In addition, local hemodynamic parameters such as wall shear stress are uncontrolled and can vary in vessel injury models.

Useful complements to *in vivo* models are *ex vivo* flow champers that allow for manipulation of shear stresses [8, 93, 104], controlled presentation of platelet stimuli [95, 94], and evaluation of pharmacological agents [54]. Flow chambers for studying platelet rolling, adhesion and aggregation over immobilized ligands have been critical in understanding shear-dependent receptor-ligand dynamics [88, 6, 35]. However, most parallel-plate and annular flow chambers require milliliters of fluid to perform experiments over a relevant time scale. This volume of blood is easily obtained from human subjects, but requires pooling or dilution of murine whole blood owing to the relatively low total blood volume of a single animal ($\sim$1 mL) [56, 96]. The cost of pooling and the sacrifice of difficult to breed animals can be prohibitive when using genetically modified mice to obtain data for a single experimental condition in a

parallel plate flow chamber. Thus, current flow chamber designs are poorly suited for research with murine blood.

We developed a method for characterizing murine platelet function under flow using microfluidic and protein patterning techniques. This method addresses an important need for researchers who want to perform *ex vivo* flow assays using small volumes of blood from genetically modified mice. Owing to the small size of the channels, the small volume ($\sim$100 μL) of blood obtained from a retro-orbital plexus was sufficient to perform an experiment, thus avoiding the need to sacrifice animals. We validated the method by measuring platelet adhesion to patterned collagen at venous and arterial wall shear rates and comparing platelet adhesion of wild-type mice and mice deficient in collagen receptors. The stability of platelet-collagen and platelet-platelet bonds were characterized by a high shear challenge. In addition, the role of PAR4 activation on aggregate stability was measuring in a setting that was independent of fibrin formation.

2.3 Materials and Methods Used

2.3.1 Fabrication of microfluidic devices

Microfluidic channels were fabricated in poly(dimethylsiloxane) (PDMS) using standard soft lithography techniques [22]. Photomasks were designed in LayoutEditor (Jürgen Thies) and exported as '.dxf' files. The dxf files were printed on high-resolution transparencies at 10,000 dpi (OutputCity, Bandon, OR). Prior to photoresist spin coating, four inch <1 0 0> silicon wafers (Virginia Seminconductor, Fredericksburg, VA) were cleaned with acetone and isopropanol then dehydrated on a 200°C hotplate for 10 min. KMPR 1050 (MicroChem, Newton, MA) negative photoresist was spun (CEE 100, Brewer Science Inc., Rolla, MO) to 500 rpm (100 rpm/sec) for 5 sec and then ramped up (300 rpm/sec) to 2,000-3,000 rpm for 30-45 sec to yield a film thickness of 50-80 μm. Following spin casting, the wafers were

placed on a hotplate for 15 min at 100°C to drive the remaining solvent out of the photoresist. The transparency photomask was taped to a glass substrate (5 in x 5 in) and brought into contact with the wafer using a Karl Suss MA4 contact aligner (Karl Suss, Garching, Germany). The photoresist was exposed with a broadband UV source that was filtered to eliminate wavelengths below 365 nm. The intensity of the UV light was between 4.7 and 5.0 mW/cm^2 and the exposure time of 3.25 to 4.25 min was used to achieve the manufacturer's exposure energies (975-1,200 mJ/cm^2). Following exposure, the wafer was placed on a hot plate for 3 min at 100°C to cross-link the photoresist. After cooling to room temperature, the unexposed resist was developed away in AZ300MIF (2.38% tetramethyl ammonium hydroxide and 0.261 N metal-ion-free developer, Clariant Corp., Somerville, NJ) for 7 min. Developed wafers were triple-rinsed in DI water, nitrogen dried, and dehydrated at 80°C for at least 10 hours prior to initial use in order to drive off any remaining water. Feature heights were measured using a Tencor Alpha Step (KLA-Tencor Corp., San Jose, CA).

2.3.2 Casting and preparation

Prior to casting, silicon masters were taped to 6 in polystyrene tissue culture dishes (Fisher Scientific, Pittsburg, PA) and incubated with 1,1,2,2-tetrahydrooctyl -1-trichlorosilane (United Chemical Technologies, Bristol, PA) under vacuum for 3 hr to achieve a hydrophobic surface. Meanwhile, PDMS pre-polymer and curing agent (Sylgard 184, Dow Corning, Midland, MI) were mixed at a ratio of 10:1 and degassed under vacuum. The mixture was poured over the silane-treated master wafers and allowed to set at 65°C for at least 3 hr in a gravity convection oven. After cooling, the molded devices were pealed from the master and cut to size using a #11 Xacto®blade. Fluidic and vacuum ports were punched with 0.75 and 1.2 mm Harris Uni-Core punches (Ted Pella, Redding, CA) respectively. Prior to use, PDMS devices were cleaned in 1 N hydrochloric acid for 10 min, followed by immersion in

an ultrasonic cleaning bath in acetone then ethanol for 10 min each. All surfaces that were contacted with blood were blocked by incubation with 0.5% bovine serum albumin (BSA, Sigma-Aldrich, St. Louis, MO) in HEPES buffered saline (HBS, 20 mM 4-(2-hydroxyethyl) -1-piperazineethanesulfonic acid, 150 mM NaCl, pH 7.4) for 1 hr. Fluidic connections were made using blunt 21 gauge needles inserted into Tygon tubing (0.020 in ID, 0.060 in OD, Small Parts Inc., Miramar, FL). Vacuum was applied (∼10 psig) for reversible bonding using a direct connection between the device and tubing which was connected to a variable pressure vacuum pump (Gast Manufacturing Inc., Benton Harbor, MI).

2.3.3 Collagen patterning

Glass slides (75 x 28 x 1 mm, Fisherbrand, Fisher Scientific, Pittsburg, PA) were cleaned in 1:1 (v:v) methanol : 17.1 N HCl for 30 min, followed by a 5 min rinse in DI water, then dried in an 80°C oven for 30 min. Immediately before patterning, slides were covered with Sigmacote (Sigma-Aldrich, St. Louis, MO), rinsed with DI water, and dried with pressurized air in order to form a hydrophobic surface to aid in protein adsorption. Patterning devices were aligned on the slide and held in place by vacuum. A solution of 100 μL bovine or human solubilized type I collagen (PurCol or VitroCol respectively, Advanced BioMatrix, San Diego, CA), 890 μL HBS, and 10 μL 0.1 N sodium hydroxide (with an optional 2 μL of 1 mM FITC to aid in interaction localization) was mixed and immediately filled through the patterning device. The collagen was allowed to polymerize at room temperature for 90 to 150 min. After the desired incubation, the excess collagen solution was removed and the patterning device removed. The second device to be used for blood perfusion was immediately aligned on the slide in a perpendicular manner to the patterned collagen strip. The flow channels were then immediately filled with a 0.5% BSA solution. This solution prevented non-specific interactions of blood components with both the unreacted glass surface and the PDMS device. As is shown in Figure 2.1, the total system

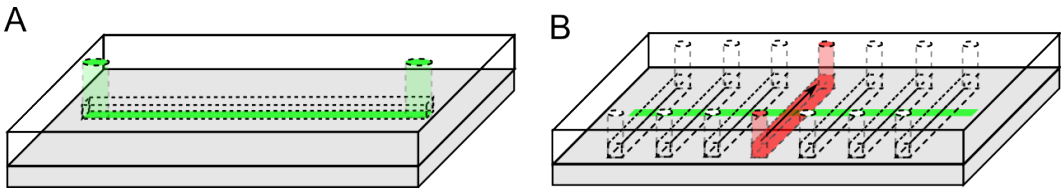

Figure 2.1: Cartoon of patterning procedure with the patterning device (A) and the flow device (B).

consists of two PDMS devices and one slide. By developing the system as a modular pair of independent devices, it is possible to establish a general procedure to be used regardless of the geometry of the flow channels or composition of the solutions used to pattern. Utilizing reversible vacuum bonding techniques has provided this capability: maintaining firm contact between the patterning device and the substrate during the micropatterning procedure, while subsequently being able to remove that device to place the flow device on the same substrate.

2.3.4 Mice

Flow assays were performed with whole blood from wild-type mice and mice deficient in one or both of the primary collagen receptors. Knockout mice deficient in the integrin α_2 subunit were generated as previously described [15]. A double knockout was created by crossing Fc receptor gamma chain (FcRγ)-deficient mice (Taconic Farms, Hudson, NY) with α_2-deficient mice [96]. Mixed background litter-mate animals were used as controls. All mouse studies were approved by the Institutional Animal Care and Use Committee (IACUC) of the University of Pennsylvania.

2.3.5 Blood collection and platelet labeling

Prior to blood draw, rat anti-mouse CD41 (GPIIb, α_{IIb}) monoclonal antibody (clone MWReg30, BD Biosciences, San Jose, CA) was conjugated to AlexaFluor®488 using the AlexaFluor®488 Monoclonal Antibody Labeling Kit (Invitrogen, Carlsbad, CA)

according to manufacturer's instructions. Whole mouse blood, obtained by intra-orbital eye bleed, was anti-coagulated with 93 μM (final concentration) Phe-Pro-Arg-chloromethylketone (PPACK, Haematologic Technologies Inc., Essex Junction, VT) and labeled with 1:100 (v:v) AlexaFluor®488-conjugated monoclonal antibody.

2.3.6 Whole blood flow assay

Channels were initially filled with 0.5% BSA in HBS to ensure that no bubbles were trapped in the channel. Then, a volume of 100 μL of whole blood was placed on the inlet of the device and withdrawn by a syringe pump (Harvard Apparatus PHD2000, Holliston, MA) for 5 min at flow rates of 0.64, 2.5, and 6.4 μL/min to achieve a full channel width-averaged wall shear rate of $\overline{\gamma}_{chan}$ = 100, 400, and 1,000 sec^{-1} respectively. After 5 min of platelet accumulation on the collagen patch, the shear rate was stepped-up to an average wall shear rate of $\overline{\gamma}_{chan}$ = 8,000 sec^{-1} (50 μL/min) for 1 min to probe the stability of the aggregates.

Wall shear rate as a function of flow rate and position was calculated using an analytical solution to the velocity profile in a rectangular duct [111]:

$$u(y,z) = \frac{48Q}{\pi^3 hw} \times \frac{\sum_{n=1,3,5...}^{\infty} \frac{1}{n^3}\left[1 - \frac{cosh\left(n\pi\frac{y}{h}\right)}{cosh\left(n\pi\frac{w}{2h}\right)}\right] sin\left(n\pi\frac{z}{h}\right)}{\left[1 - \sum_{n=1,3,5...}^{\infty} \frac{192h}{n^5\pi^5 w} tanh\left(n\pi\frac{w}{2h}\right)\right]} \tag{2.1}$$

where $u(y,z)$ is the axial velocity at lateral location y and vertical position z in a channel of cross-sectional width w and height h $\left(\frac{-w}{2} \leq y \leq \frac{w}{2}, 0 \leq z \leq h\right)$ for a given volumetric flow rate Q. This equation obeys the no-slip boundary condition at both the bottom and side walls while maintaining the null momentum flux boundary condition across the centerline in both the x-y and x-z planes.

2.3.7 Image capture and anaylsis

The adhesion, aggregation, and fragmentation of platelets were monitored continuously by epifluorescence microscopy. Images were captured using a CCD camera (ORCA-ER, Hamamatsu, Bridgewater, NJ) mounted on an inverted microscope (Olympous IX81, Center Valley, PA) with a 100 W mercury lamp (470 nm Ex / 525 nm Em). Images were captured continuously at 2 frames/sec (500 ms integration) using Slidebook software (Intelligent Imaging Innovations, Denver, CO). The use of fluorescently labeled antibody allowed for continuous illumination of the field of view without additional adhesion as has been reported using dye-loaded platelets [40]. The central 60 μm of the collagen patch (750 $\times$ 372 pixels) and a region upstream (50 $\times$ 372 pixels) of the collagen were defined using a custom MATLAB script (Mathworks Inc., Natick, MA). The average background of the upstream region was calculated for each column and those values were subtracted from the reaction zone pixel value to correct for background gradients across the width of the channel. The background subtracted fluorescence intensity values were integrated over the collagen patch for each time point. Surface coverage was calculated by dividing the area of pixels with a value greater than zero by the area of the collagen patch.

2.3.8 Introduction of platelet agonists to formed platelet aggregates

For stability studies involving PAR activation, platelet aggregates were built up from PPACK-treated whole blood on patterned collagen for 5 min at 400 sec^{-1}. After the deposition phase, the blood in the inlet was replace with HBS. After 30 sec of flow at the same average wall shear rate (400 sec^{-1}), the buffer was then removed and replaced with 1 mM PAR4 agonist peptide (AYPGKF, Bachem, Torrance, CA). Following 30 seconds of agonist presentation at 400 sec^{-1}, the HBS flow rate was increased to an average wall shear rate of 8,000 sec^{-1} to allow measurements of

Table 2.1: Summary of shear settings for murine blood characterization

Animal	$\overline{\gamma}_{chan}$ [sec^{-1}]	$\overline{\gamma}_{central}$ [sec^{-1}]	n
WT (C57BL/6)	100	126 (102-137)	7
WT (C57BL/6)	400	492 (399-537)	6
WT (C57BL/6)	1,000	1,260 (1,021-1,374)	6
WT (BalbC/ByJ)	400	492 (399-537)	8
$\alpha_2^{-/-}$	400	492 (399-537)	7
$\alpha_2^{-/-}/FcR\gamma^{-/-}$	400	492 (399-537)	6

thrombus stability.

2.3.9 Statistical analysis

Each data point represented a single blood draw from one animal. All data are presented as mean ± standard deviation. The Mann-Whiteney U-test was used to compare wild type blood perfused at 400 sec^{-1} (control) to each experimental group. Groups with p-values less than 0.01 were considered significantly different from the control. All calculations were performed using the Statistics Toolbox in MATLAB (Mathworks, Natick, MA).

2.4 Results

2.4.1 Platelet accumulation in microfluidic channels

In developing an *in vitro* analog of a focal vascular injury (albeit without thrombin production), we perfused whole blood over a discrete region of immobilized collagen. A collagen thin film (width of 100 μm) with fiber diameters of ∼15 nm was patterned within a microfluidic channel along the length of a glass slide. Thirteen individual channels with a cross-sectional area of 80 μm (height) × 100 μm (width) were oriented perpendicular to the collagen strip and vacuum-sealed to the slide. A

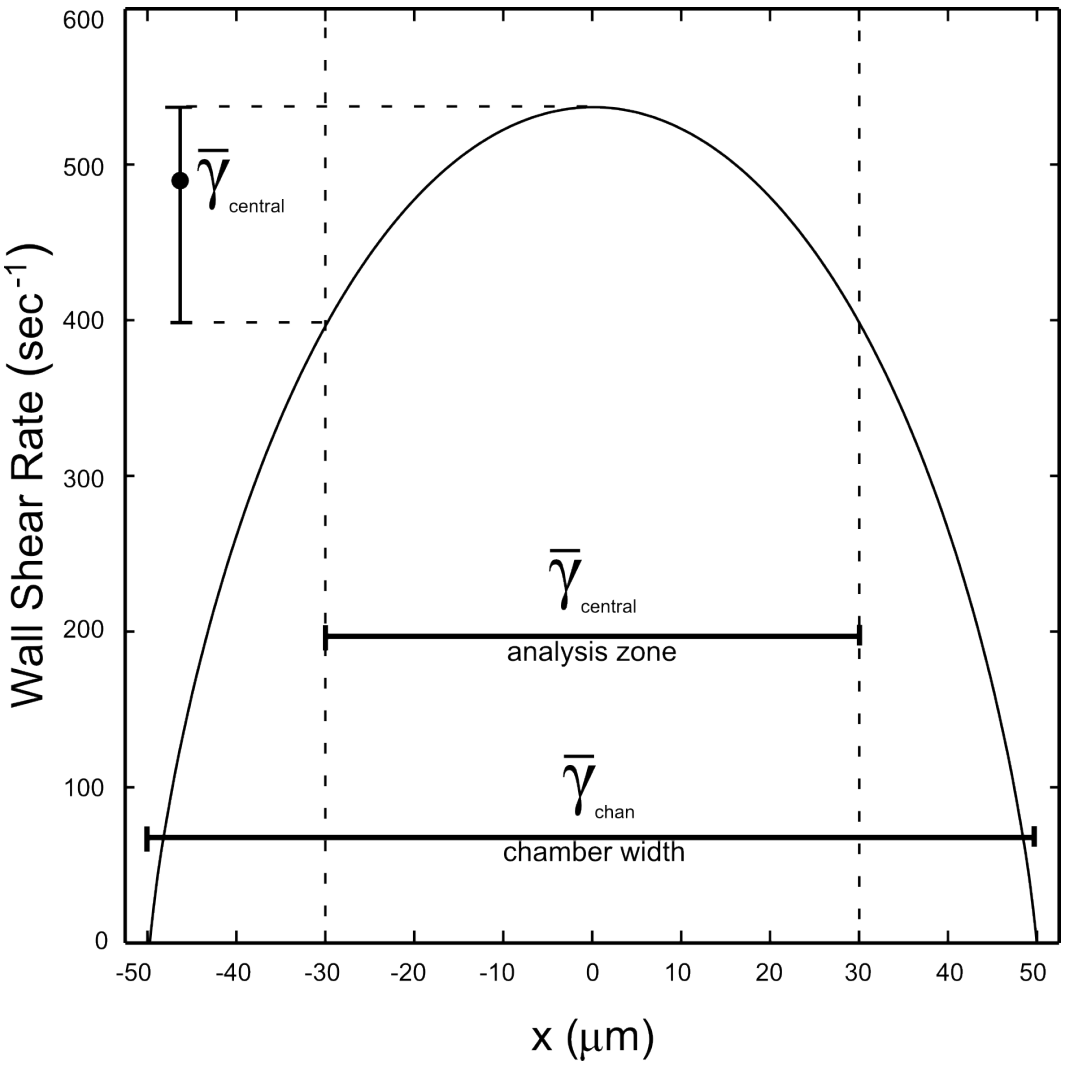

Figure 2.2: Shear profile across the bottom surface of the microfluidic channel.

summary of the experimental specifics (wall shear rates, genetic background, and sample size) are shown in Table 2.1.

Due to the low aspect ratio (the ratio of the cross-sectional width to the cross-sectional height, in this case 100 μm / 80 μm or 1.25) of the channels, the shear rate variation was significant along the bottom channel wall. For example, at a flow rate of 2.5 μL/min (whole channel width-averaged wall shear rate, $\overline{\gamma}_{chan} = 400$ sec^{-1}), the shear rate had a parabolic profile on the bottom channel where it was zero in the corners and reached a maximum of 537 sec^{-1} in the middle as shown in Figure

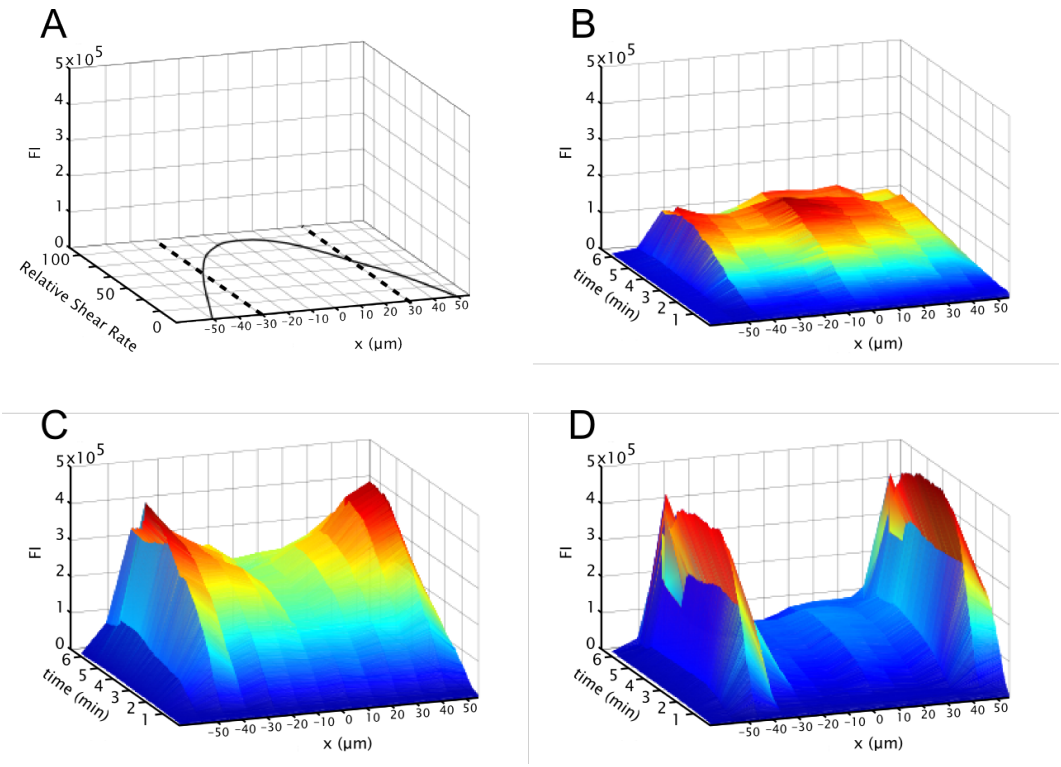

Figure 2.3: The shear profile (A) dictated platelet accumulation as measured by fluorescence intensity (FI) in the channels with average wall shear rates $\overline{\gamma}_{chan} = 100$ (B), 400 (C), and 1,000 (D) sec^{-1}. The width of the channel was broken into 12 bins(10×100 μm) and the fluoresecence intensity represents the average of each bin at each time point.

2.2. The implications of these non-uniform shear profiles are observed throughout the representative micrographs throughout this chapter of work. However, it is important to note that while the flow conditions at the collagen surface do not directly mimic those found in the vasculature due to the rounded nature of blood vessels, the experimental model system remains valid due to the transport of the system, with a Péclet number <1, indicating that lateral diffusion is slow relative to convection downstream and away from the reactive zone.

To account for the non-ideal flow profile due to wall effects of a low aspect ratio channel, only platelet accumulation within the middle 60 μm of the channel ($\overline{\gamma}_{central}$) were used for analysis throughout this Chapter. Within this middle section of the

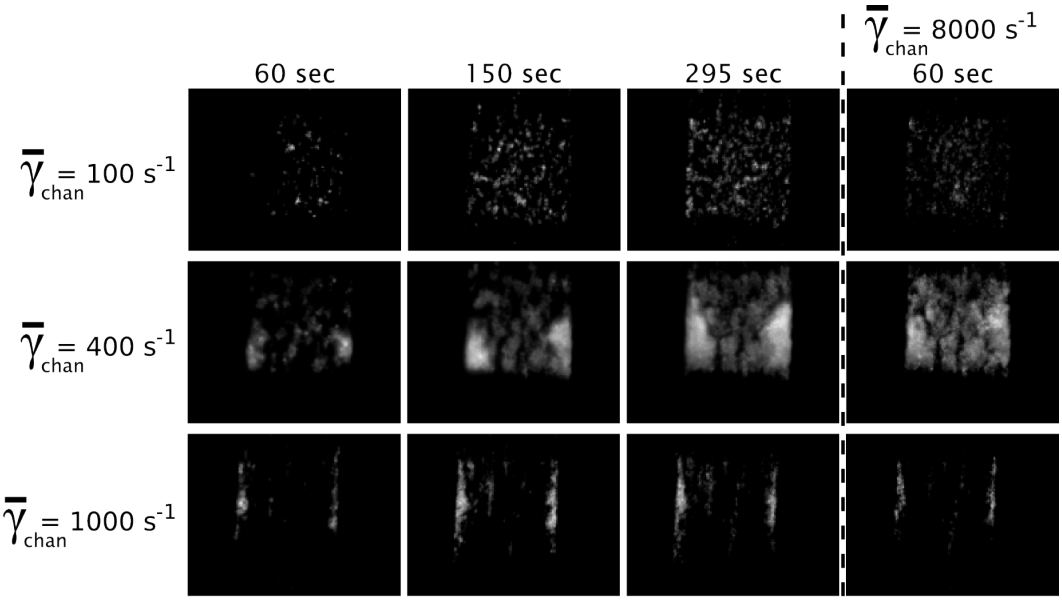

Figure 2.4: Images were taken at the specified time points from characteristic experiments. The direction of flow is from bottom to top.

channel, the range of wall shear rates were small compared with the entire width as shown in Table 2.1, i.e. the wall shear rate was considered to be constant across this section of the surface. The non-constant shear profile at the wall was reflected by the heterogeneous platelet distribution at average wall shear rates of 400 and 1,000 sec^{-1} as shown in Figure 2.3. Platelet accumulation was highest at low shear rates in the corners and less at positions in the middle of the channel at the highest shear rates, while the lowest shear rate did not exhibit the same preference towards the edge. This result, while not intended during experimental design, is one of note. The distribution of platelet adhesion at various wall shear rate regions across the bottom of the channel reflect a competition of phenomena which will be investigated later in this Chapter.

Platelet adhesion was not observed upstream or downstream from the collagen strip at any shear rate as shown in Figure 2.4. The localized platelet accumulation is among the most important aspects of this work that distinguishes it from other experimental systems used to analyze platelet accumulation under whole blood flow.

The most frequently used device, a parallel plate flow chamber mounted on top of a substrate that is uniformly coated with a protein of interest. The focal nature of this system lends itself to investigation of processes confined in space to a relevant yet small injury, i.e. the loss of several endothelial cells from the luminal blood vessel surface. This technique is more sensitive to alterations in both initial adhesion and secondary platelet recruitment to the reactive surface. Significantly shortening the length for potential adhesion, activation, and propagation, bears a more stringent, and possibly more relevant, model system.

For wild-type mouse blood, there was a rapid rise in platelet accumulation for the first 3 min followed by minimal platelet deposition in the fourth and fifth minutes as shown in Figure 2.5A. The dynamics of the platelet deposition curve were similar to those reported in the laser-induced vascular injury model [26]. We observed a delay of ∼20 sec followed by rapid platelet accumulation for 3 to 4 min. The time to saturation in the laser injury model was 50% faster than in this model system, which is likely to be a result of thrombin generation in the *in vivo* system, which was absent in these experiments due to the high concentration of PPACK. By inhibiting thrombin, we limit the thrombus growth to secondary platelet activators such as ADP and TxA_2 once the collagen surface has been covered with platelets. This is in contrast to a system where thrombin is allowed to be formed and signal, recruiting even more platelets and forming fibrin that serves as both a stabilizing network and additional adhesive surface for continued platelet recruitment and activation.

2.4.2 Shear sensitivity of platelet deposition to patterned collagen

In the absence of pre-adsorbed von Willebrand Factor (vWF), we observed a biphasic response of platelet accumulation on patterned collagen. After a 5 min perfusion over collagen, there was a significantly ($P<0.01$) less platelet accumulation and surface coverage in the central zone ($\overline{\gamma}_{central}$) at 126 sec^{-1} and 1,260 sec^{-1} compared with

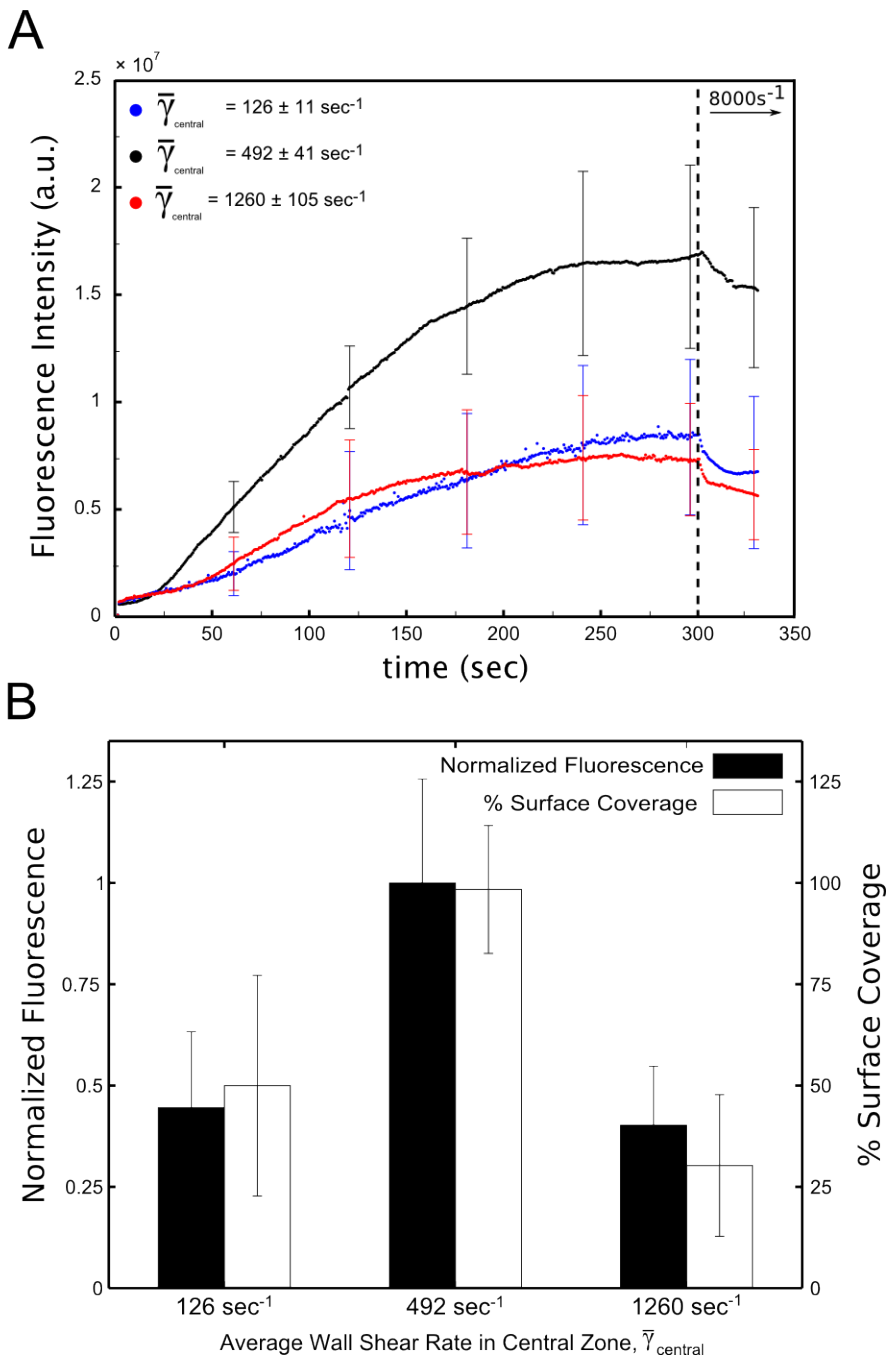

Figure 2.5: A. Kinetic traces of platelet accumulation for wild-type mouse blood at three shear rates. B. Endpoint fluorescence and surface area measurements of formed aggregates.

492 sec^{-1} (Figure 2.5B). At an average wall shear rate of 126 sec^{-1}, platelet adhesion was uniform across the width of the channel, but there were fewer platelet aggregates compared with 492 sec^{-1}. At an average wall shear rate of 1,260 sec^{-1}, there was little platelet accumulation in the center of the channel. The few platelet aggregates that were observed may be due to adsorption of vWF from from the plasma onto the collagen. While adsorption of vWF onto collagen from flowing mouse blood is expected during the experiment, platelet deposition will continually cover the collagen available for adsorption during the 300 sec perfusion. The observed biphasic response illustrated in Figure 2.5 was most likely a result of competing effects where increasing flow increases the platelet flux to the collagen surface but also increases the force loading on adhesive bonds, reduces interaction times, and dilutes reactive species, resulting in less efficient platelet adhesion at higher flow rates. This competition highlights an interesting and dynamic characteristic of platelet accumulation, and perhaps may inform some of the regulation that occurs to limit thrombus size *in vivo*. Among the key characteristics of any successful hemostatic system is the ability to prevent excessive clot formation that leads in either vessel occlusion or mechanically unstable clot formation, leading to dangerous and potentially deadly emboli. Save for the alterations in vascular smooth muscle tension and other systemic mediators of vascular tone, as thrombi continue to form into the blood vessel lumen, the shear rate continues to increase, assuming volumetric flow rates are maintained. This result may indicate that, among other transport considerations such as the removal of active species from the site of injury, the decreased interaction times and increased force load on bonds limits the amount of thrombus growth that prevents pathological clotting scenarios during healthy hemostasis.

For $\overline{\gamma}_{central} = 126$ sec^{-1}, extending the perfusion time to 20 min did not result in increased platelet accumulation as shown in Figure 2.6. For these longer experiments, we observed continuous addition and removal of platelets from the aggregate surface, but there was no net change in the integrated fluorescence intensity after the first 300

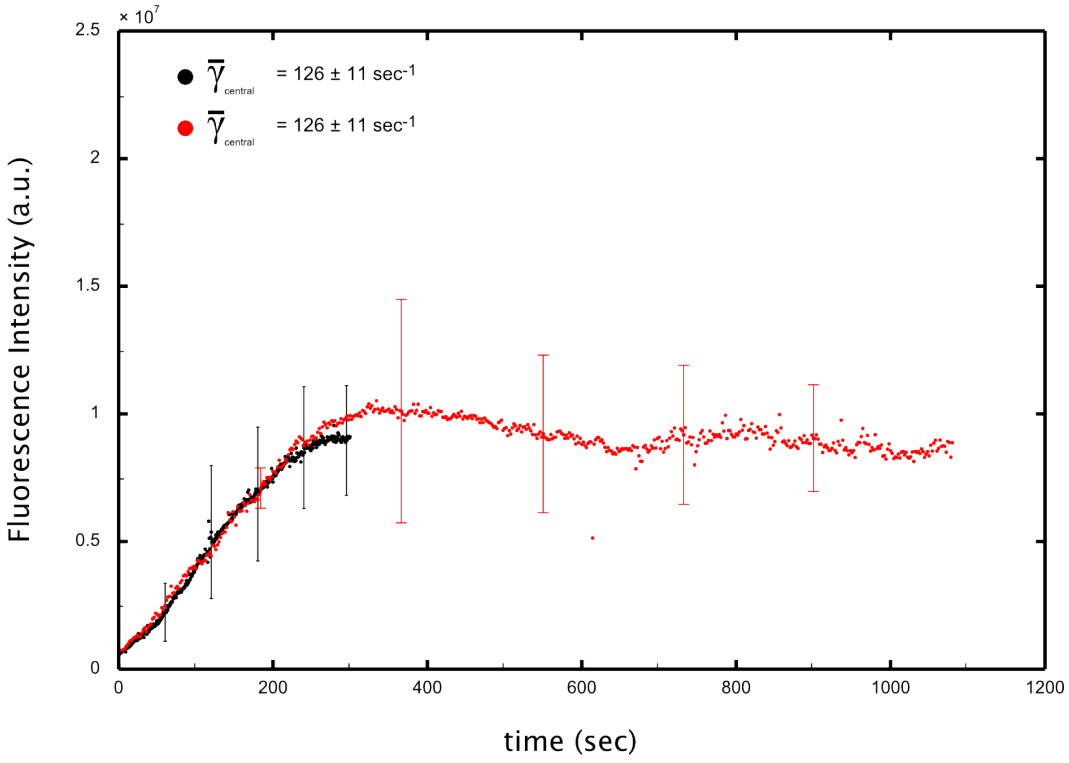

Figure 2.6: Kinetic traces of platelet accumulation for wild-type mouse blood for 5 and 20 min time courses (n = 6).

sec. These data suggest that the initial platelet layer on collagen dictates the final extent of thrombus growth in the absence of thrombin. Again, this is most likely the case for this model system without the generation of thrombin for subsequent platelet signaling and fibrin generation.

2.4.3 Accumulation of platelets with collagen receptor deficiencies

We performed flow experiments over patterned collagen with whole blood from mice deficient in one or both of the primary collagen receptors. Single knockout mice were deficient in the α_2 integrin subunit. A double knockout deficient in both FcRγ and α_2 was used as a negative control. The knockout mice have a mixed genetic background consisting of C57BL/6J, BalbC/ByJ and 129Sv/ImJ mice strains. Both C57BL/6J and BalbC/ByJ were used as wild type controls.

There was no statistical difference ($P = 0.75$) between platelet accumulation and aggregate fragmentation between the two wild-type controls as shown in Figure 2.7. While seemingly mundane, this is not an insignificant result. Inbred mice have long been the workhorse of hemostasis researchers in need of studying mutated proteins. However, the wide variety of wild-type mouse strains used during the genetic manipulation processes have exceedingly wide, upwards of an order of magnitude in circulating vWF levels [101]. This discrepancy arises from many known and unknown sources, from differences at the transcriptional, translational, execratory, and degradation aspects of soluble vWF homeostasis. The measurements confirming the lack of statistically significant difference between the two wild types provides solid background for the investigation of the genetic mutants.

Platelets deficient in the α_2 integrin subunit had a diminished ability to adhere to patterned acid soluble collagen at an average wall shear rate of 400 sec^{-1} as shown in Figure 2.8. There was a significant difference ($P = 0.0012$) in platelet accumulation for mice deficient in the α_2 integrin compared with wild-type mice.

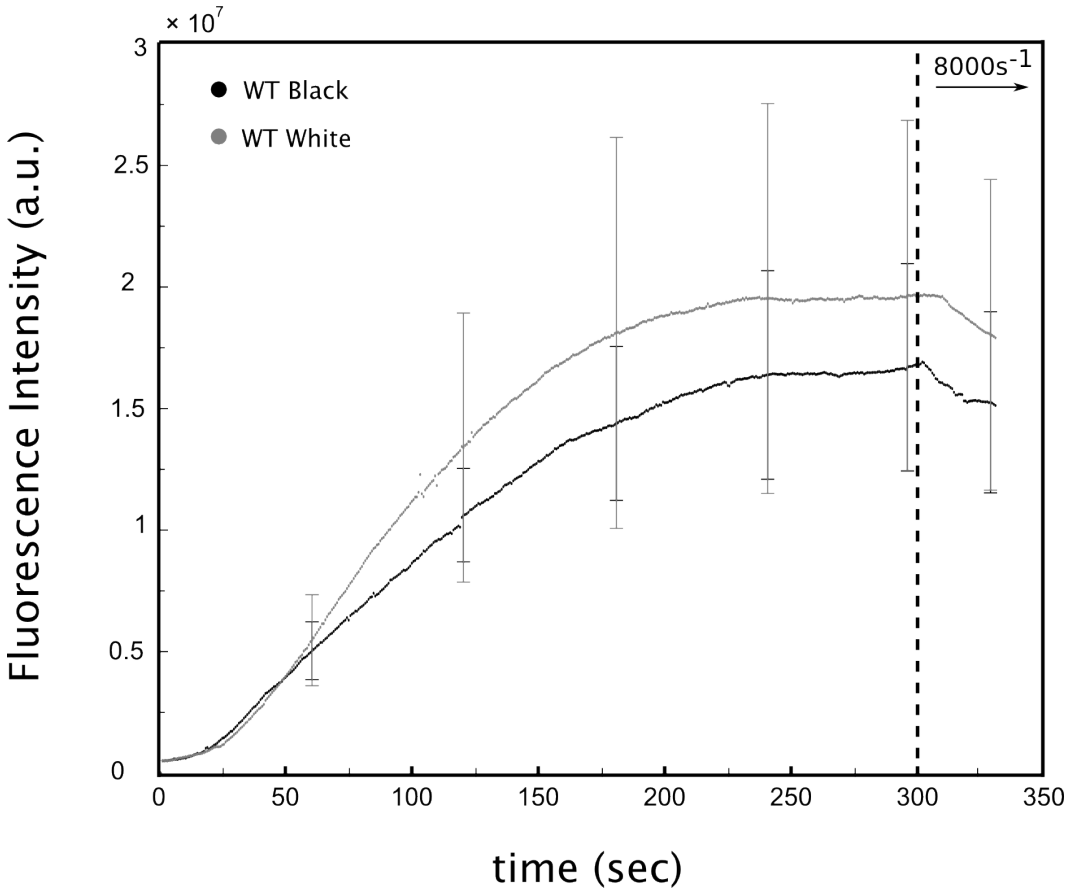

Figure 2.7: Kinetic traces of platelet accumulation for two wild-type control mouse strains (n = 6).

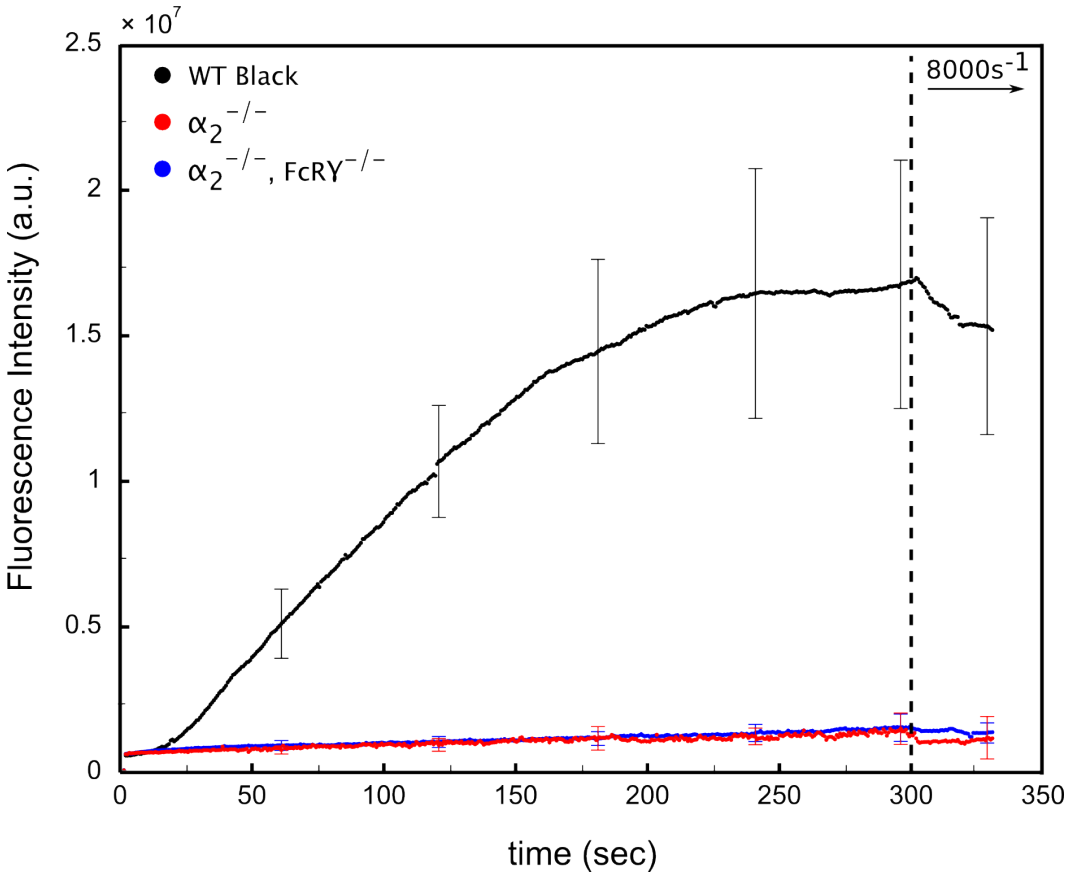

Figure 2.8: Kinetic traces of platelet accumulation for wild-type and two collagen receptor knockout mouse strains (n = 6).

The small number of platelets that did adhere was presumably initiated through the GPIb-IX-V complex on platelets and vWF from the plasma adsorbed to the collagen. These data show that the $\alpha_2\beta_1$ receptor was necessary for firm adhesion to acid-soluble collagen under flow. This data is in agreement with published results and will be discussed in further detail later in this Chapter.

2.4.4 Thrombus stability and PAR signaling

A useful feature of flow chambers is the ability to control the shear rate and make changes to it during the course of a single experiment. Microfluidic chambers, due to their small dead volumes, allow extremely high shear rates to be tested for extended periods of time even with very small reagent volumes. In each flow experiment, we monitored platelet accumulation for 5 min at a constant wall shear rate then increased the average wall shear rate to $\overline{\gamma}_{chan}$ = 8,000 sec^{-1} for 1 min. Thrombus stability for this was defined by the percentage decrease in integrated fluorescence intensity and loss in surface coverage following the step up in shear rate. During the 1 min exposure of the pre-formed thrombus to ultra high shear rates of 8,000 sec^{-1} (a level known to cause shear-induced platelet activation (SIPA) in cone-and-plate viscometers [100]), we found no indication that SIPA enhanced thrombus buildup during the 1 min exposure. As seen in Figures 2.5A and 2.8, total fluorescence intensity decreases by 15-25% for platelet aggregates formed at both venous and arterial shear rates. Platelets deficient in the α_2 subunit had a severe adhesion deficiency, covering less than 5% of the surface after the 5 min accumulation phase. Upon shear rate increase to 8,000 sec^{-1}, we observed a complete removal of platelets from the surface as shown in Figure 2.8, demonstrating strict requirement for $\alpha_2\beta_1$ in stable adhesion for murine platelets to acid soluble type I collagen.

Thrombin is critical in clot formation and stability by distinct pathways involving platelet activation via protease activated receptor (PAR) signaling, enhanced recruitment of additional platelets, and fibrin generation. In order to investigate

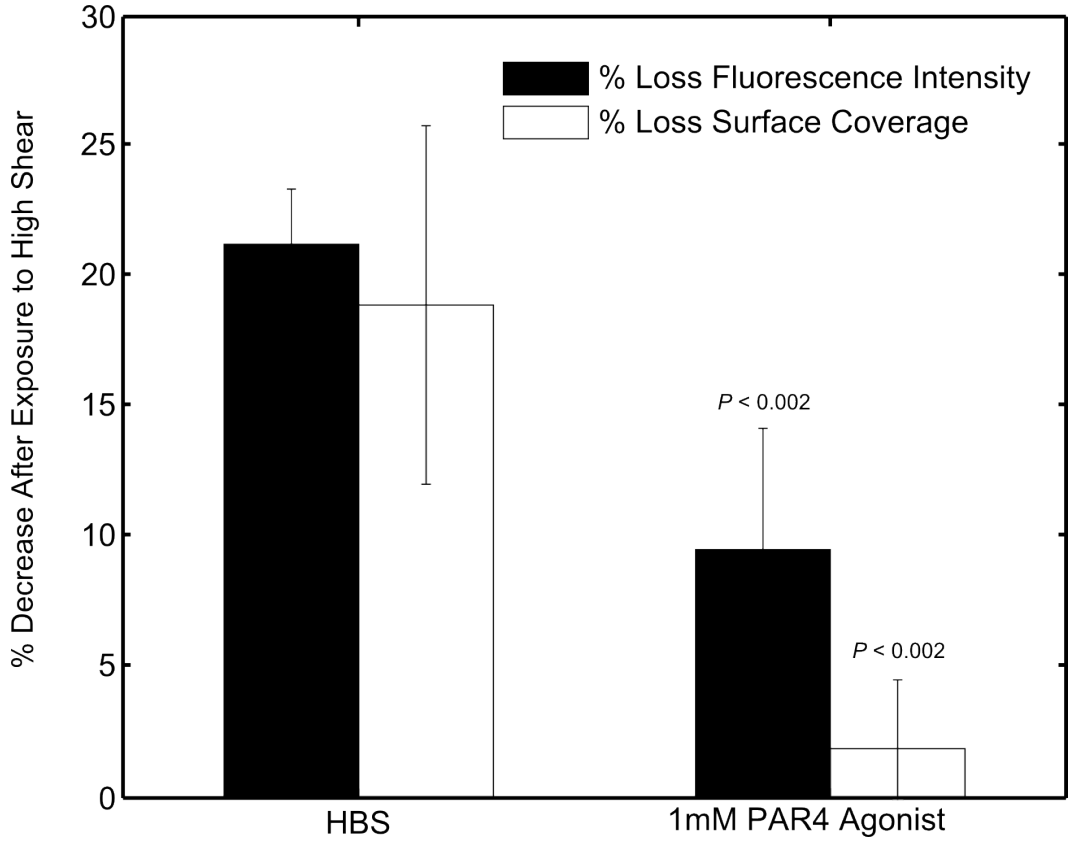

Figure 2.9: Changes in fluorescence intensity and surface coverage after thrombus exposure to HBS or PAR4 peptide (n = 6).

mouse PAR4 signaling in the absence of active thrombin (which was blocked by 93 μM PPACK throughout the entirety of the experiment) and fibrin formation, we introduced an activating peptide after the platelet thrombi were formed to induced platelet signaling via the G-protein coupled receptor. In addition to the signaling pathways activated by the collagen receptor GPVI and the feedback receptors of released secondary messengers (ADP and TxA_2), PAR4 activation leads to substantial phospholipase C β activation, resulting in large surges in intracellular calcium and subsequent integrin activation and granule release. By selectively infusing murine PAR4 activating peptide (AYPGKF) over pre-formed platelet aggregates, it was possible to determine the effect of PAR4 signaling on both platelet-platelet and platelet-collagen bond strength when subjected to a high shear challenge.

PAR4 activation of platelets following accumulation on collagen led to a stabilization of the thrombus compared with a buffer control as shown in Figure 2.9. There was a significant difference for both the percentage of total fluorescence intensity and area loss ($P = 0.002$) between the buffer control and the experimental group. While the initial size of each thrombus mass at 300 sec may vary due from experiment to experiment due to intrinsic intra-mouse variability (as indicated in 2.5), we found that every aggregate lost mass at 8,000 sec^{-1}, and that the percentage decrease in mass was highly consistent. Because each and every thrombus formed, regardless of variations in its initial size after 300 sec of formation time, displayed a decrease in fluorescence when exposed to 8,000 sec^{-1}, the percentage decrease in total fluorescence was measured to be 20 $\pm$ 3 % (n = 6).

In Figure 2.9, we report a 55% reduction in percentage thrombus volume loss with PAR4 agonist because an untreated thrombus has an approximately 20% decrease in fluorescence intensity after exposure to 8,000 sec^{-1}, while a thrombus treated with PAR4 agonist only has a 10% decrease in fluorescence intensity. This decrease is statistically significant (21.3 $\pm$ 2.1% loss with buffer vs. 9.5 $\pm$ 4.7% loss with PAR4 agonist, $P = 0.002$, n = 6). In terms of percent loss in surface coverage, we report in 2.9 a 90% reduction in percent surface loss with PAR4 agonist (18.9 $\pm$ 6.9% area loss with HBS vs. 1.9 $\pm$ 2.6 % loss with PAR4 agonist; $P = 0.002$, n = 6). Thus, regardless of the initial mass of the thrombus at 300 sec (which can vary somewhat between mice as shown in the error bars in Figure 2.5), each of these thrombi will lose about 20% of its volume when exposed to 8,000 sec^{-1} and this loss is substantially mitigated by 50% when the aggregates are exposed to a PAR4 agonist. While the total volume loss is only 20% with a shear step-up to 8,000 sec^{-1} under these experimental conditions, the clinical significance of embolism of 20% of total clot volume is substantial and results shown in Figure 2.9 provide a quantitative *in vitro* method to interrogate thrombus stability. The increase in stability of mouse

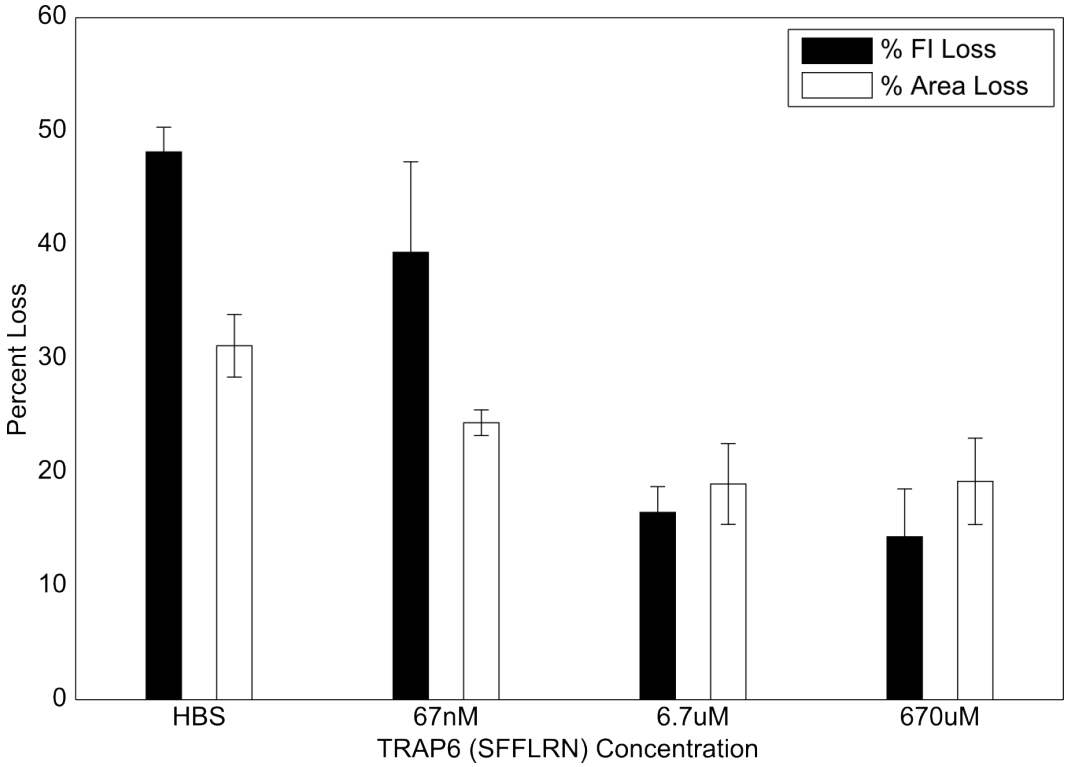

Figure 2.10: Changes in fluorescence intensity and surface coverage after human platelet thrombus exposure to HBS or PAR1 peptide (n = 6).

platelet aggregates was likely due to PAR4-mediated enhancement of both $\alpha_2\beta_1$-dependence platelet adhesion on collagen and $\alpha_{IIb}\beta_3$-dependence platelet-platelet interactions.

Similar results were obtained in analogous experiments performed with human platelet thrombi activated with the PAR1 agonist, SFLLRN, where 670 μM SFLLRN reduced percentage FI loss from 40% to 15% ($P = 0.001$, n = 8) compared with HBS control as shown in Figure 2.10.

2.5 Discussion

Microfluidic techniques are ideally suited for *ex vivo* phenotyping of blood, especially when minimal volumes are available, such as from genetically modified animals or

in point-of-care diagnostic situations. The shear stress is a user-defined parameter in this microfluidic model system that can be modulated during the course of an experiment. This feature allowed us to build up platelet aggregates at one shear rate and then probe the stability of platelet-ligand and platelet-platelet bonds at higher shear rates. We detected disaggregation of wild-type mouse platelets during a shear-up challenge of 8,000 sec^{-1}. There was evidence of platelet-platelet and platelet-collagen bond failure, indicating instabilities at this pathological wall shear rate. Platelet deposition was shear dependent and biphasic 2.5, revealing the competition of enhanced platelet delivery to the wall, reduced interaction times, and increased forces as flow increases. In α_2-deficient mice, those platelets that did adhere were almost completely removed after shear-up challenge, suggesting that stable adhesion to immobilized collagen was $\alpha_2\beta_1$ dependent. PAR4 activation led to increased stabilization to resist shear forces, suggesting a role for thrombin signaling in clot stability independent of platelet recruitment or fibrin generation.

By manipulating the thrombin-driven platelet signaling independently of fibrin formation due to thrombin activity, it was possible to begin dissecting the implications of PAR signaling on aggregate stability. PAR4 signaling significantly improved the ability of focal collagen-initialized platelet thrombi to remain adherent in under a pathological shear rate of 8,000 sec^{-1}. Measurements of loss of area coverage and total fluorescence intensity probed the stability of platelet-collagen ($\alpha_2\beta1$) and platelet-platelet ($\alpha_{IIb}\beta3$) bond strengths following PAR4 signaling, respectively. We observed that PAR4 signaling increased the stability of the initially bound platelets to collagen (i.e. reduced the percentage surface coverage loss) as well as increased platelet-platelet stability, most likely via $\alpha_{IIb}\beta_3$-fibrinogen complexes.

In this report, we have scaled down the conventional flow chamber assay to a microfluidic platform. The salient advantage of this adaptation is the small volumes sufficient to run a complete flow experiment under physiologically relevant flow conditions for hemostastically relevant times. Other reports of murine blood in *ex vivo*

flow assays using either pooled [56] or diluted [96, 75] whole blood and often require the sacrifice of several animals. Dilution reduces plasma protein concentrations and alters the effect of red blood cells on platelet drift toward the wall, which is crucial in focal injury models such as this one. With a microfluidic system, no dilution or pooling was necessary to run a flow experiment over a relevant time frame for thrombosis via a non-lethal blood collection method. An important parameter for any *ex vivo* function test of platelets is the time between blood collection and the start of the experiment, as changes effect the blood's characteristics due to lack of active mediators excreted by endothelium, such as nitric oxide and cyclic AMP. A system requiring more than 100 μL of blood would mandate a cardiac puncture and possibly the pooling of multiple animals' blood. These procedures can take 10 min to 1 hr depending on the number of animals and require the addition of additional factors to ensure that platelets remain quiescent. In our system, the time from blood draw to first platelet deposition in the image field was typically less than 1 min, a significant advantage in point-of-care diagnostic situations.

Microfluidic channels in combination with protein patterning more closely represents the focal nature of *in vivo* vascular injury models than conventional flow chambers that utilize uniformly coated surfaces across hemostatically irrelevant length scales (on the order of mm for most typical hemostasis injuries). While parallel plate chambers are amenable to surface patterning proteins [70, 80, 79], they have higher volume requirements than microfluidic channels. In addition, blood flow in microfluidic channels can more accurately mimics the hemodynamics found in arterioles and venuoles [103, 44]. Annual flow chambers such as glass capillary tubes have low volume requirements, but are less amenable to discrete surface patterning with collagen and other molecules of interest in the absence of sophisticated and complex patterning techniques [91]. In configurations where proteins are adsorbed to the entire surface, there can be marked boundary layer depletion of platelets where adhesion decreases with axial position [94]. Due to the short length of the collagen

patch in the direction of flow, platelet deposition was essentially uniform from the front of the patch to the back of the patch, especially within the central 60 μm region. Microfluidic techniques can be applied to explore several experimental conditions within a single device. For examples, current reports [38] have developed a device to study platelet adhesion over a range of shear stresses (0.5 to 50 dynes/cm^2), although without the focal patterning utilized in this system, with <100 μL of whole blood.

Our patterning of acid soluble type I collagen yielded a homogeneous and repeatable thin film. Previous work [97] used blocking antibodies with human platelets and found that adhesion to acid soluble type I collagen under flow was dominated by $\alpha_2\beta1$. Our observations that murine platelets deficient in the α_2 subunit cannot adhere to acid soluble collagen are consistent with these results. In contrast to soluble collagen, platelet arrest during flow over fibrillar collagen preferentially requires GPVI for adhesion and activation and demonstrates only a supporting role for $\alpha_2\beta1$ [75]. While we used platelet-collagen interactions as proof-of-principle in this report, micropatterning techniques can be extended to other prothrombotic molecules such as vWF [70, 80], fibrillar collagen and tissue factor [51, 79]. While fibrillar collagen is more physiological and has been tested in this system, the active area in the device is so small that the number of collagen fibers per test area was highly variable. This is because deposition of fibrillar collagen was heterogeneous at the micron length scale. Consequently, we chose to used a homogeneous, reproducible collagen thin film for system characterization.

2.6 Conclusions

As thrombosis and hemostasis researchers continue to develop genetically modified animals and injury models, *ex vivo* assays need to adapt and evolve to complement features of the *in vivo* animal models. Flow-based assays are especially important

because they mimic the shear stresses experienced by platelets in blood vessels. Here we applied microfluidic methods that have several advantages over conventional flow chambers including: (i) low volume requirements (<100 μL) that circumvent the need to dilute or pool murine whole blood, (ii) spatially defined presentation of a prothrombotic surface that mimics the focal nature of vascular injury with discrete boundaries at the injury site, and (iii) ability to probe thrombus stability at high shear stresses. These features allow a high number of replicates and may be useful for testing the pharmacological activity of small molecules or biologics in the presence of physiologically relevant flow.

This work served as a proof-of-principal that the combination of protein micropatterning with microfluidic blood perfusion can be used as a model system of thrombosis. The use of simple, single inlet, single outlet, single channel devices minimized the complexity of a new and unproven system. Some of the subtle flexibilities of investigating the role of thrombin receptor effects on thrombus stability proved that a wide range of previously physically unrealizable experiments could be performed utilizing the small material requirements and dead volumes of this microfluidic system. However, the method itself is limited in its throughput, though not as much as its contemporaries, in that experimental conditions are run one at a time. This limitation become prohibitive when working with human donors, who unlike a group mice, are not amenable to a series of blood draws when the next experiment is ready to commence. Rather, blood, especially platelet function, begins to significantly change when outside of the body for more than an hour, as can be understood by changes in temperature, flow, and soluble mediators continuously released by the endothelium *in vivo*.

Chapter 3

Platelet Antagonist Dose Responses

3.1 Abstract

Determination of patient-specific response to anti-platelet agents facilitates proper dosing for both acute and chronic prophylaxis. "Closed" systems (with or without flow) may fail to predict pharmacological potency in situations where platelets rapidly accumulate under flow conditions at a site of thrombosis ("Open" systems). Using an 8-channel microfluidic flow assay of human whole blood with corn trypsin inhibitor (± PPACK) perfused over focal zones of collagen, dose-response curves were measured for pharmacological agents at a wall shear rate of 210 sec^{-1}. The $P2Y_1$ inhibitor MRS 2179 ($IC_{50} = 0.233 \pm 0.132$ μM) and $P2Y_{12}$ inhibitor 2-MeSAMP ($IC_{50} = 2.558 \pm 0.799$ μM) were potent blockers of secondary platelet accumulation under flow, while the $P2X_1$ inhibitor (NF 449) and apyrase failed to reduce platelet accumulation. MRS 2179 and 2-MeSAMP had undetectable effects on initial platelet adhesion to collagen. Numerical simulation of convective-diffusive transport and apyrase-mediated catalytic degradation of ADP indicated that ultra-high concentrations of apyrase (∼2000 U/mL) would be required to have the same effect under

flow as much lower concentrations (1 U/mL) currently used in closed systems (aggregometry or cone-and-plate viscometer). This is the first evaluation of IC_{50}'s for $P2Y_{12}$ and $P2Y_1$ antagonists under controlled flow conditions. Evaluation of anti-platelet agents in open flow systems demonstrates that inhibition of either ADP by apyrase or antagonism of $P2X_1$ signaling had no effect on platelet accumulation. This technique provides a platform for rapidly investigating effective of anti-thrombitic therapies simultaneously in a model injury system.

3.2 Background

Anti-platelet therapies have been successful in preventing excessive clotting in patients with a wide range of pathologies [12, 10]. Targeting the thromboxane A_2 pathway with aspirin [113] or ADP feedback via the P2-family of platelet receptors [32, 41] reduces secondary platelet activation pathways [48] and reduce pathologically excessive clot formation while not interfering with primary platelet adhesion and activation necessary for general hemostasis. However, bleeding risks and variability of patient response to anti-platelet therapies often mandate careful monitoring of patients. For example, a significant number of patients fail to respond to anti-platelet drugs, clopidogrel in particular [112].

The most popular current target of anti-platelet therapy is the G protein-coupled receptor $P2Y_{12}$, which is one of the three P2-family proteins found on the platelet surface [58]. The receptor is activated by the binding of its ligand, ADP, released from activated platelets at the site of injury, which in turn causes activation of G_{i2}, inhibition of adenylyl cyclase, and activation of PI3 kinase, a rise of cytosolic calcium, and finally granule release and shape change [33]. $P2Y_1$ is the second G protein-coupled receptor that has been targeted as an anti-platelet therapeutic target. Binding of ADP to this other receptor on the platelet surface, which is G_q coupled [78], leads to phospholipase C β (PLCβ) activation and subsequent platelet

activation. The third P2-family receptor, the $P2X_1$ receptor, is an ATP ligand-gated ion channel [81], which directly leads to the influx of calcium from the extracellular milieu. The role of platelet $P2X_1$ signaling is less well defined with respect to platelet activation and thrombus formation than the P2Y receptors [77]. Finally, the enzyme apyrase (ATP-diphosphohydrolase E.C.3.6.1.5) which actively hydrolyzes both ADP and ATP to the mono-phosphorolated and hemostatically irrelevant AMP is used ubiquitously in aggregometry, cone-and-plate viscometry, and other *in vitro* experimental techniques to remove the ligands of the P2 family receptors from the bulk solution. Endogenous ATP- and ADP-ases exist throughout the vasculature (CD39) to keep circulating concentrations below activating levels. The therapeutic potential for recombinant apyrase [106] and solubilized CD39 [24] is currently being explored as a potential anti-platelet therapy.

Evaluation of platelet function and pharmacological agents can occur in *closed systems* of constant volume that lack flow (eg. intracellular calcium measurement, automated calibrated thrombography) or include flow (eg. aggregometry or cone-and-plate viscometry). However, these laboratory approaches fail to recreate the relevant transport characteristics in that intravascular thrombosis is an *open system* where blood is continually flowing over a thrombotic site. Various *in vitro* flow systems allow precise control of hemodynamics, surface characteristics, and inlet blood pharmacology [97, 20, 80, 72, 38] which have resulted in deeper understandings of the complicated interplay between flow, initiation, and thrombus growth. In open systems, the rapid accumulation of platelets at a surface leads to platelet concentrations greatly exceeding those found in whole blood, and the delivery/removal of species by convection may impact the efficacy of pharmacological agents. If an agent is potent in a closed system but lacks efficacy in an open system, then the therapeutic benefit of the agent may be limited with respect to reducing intravascular thrombosis under flow.

3.3 Materials and Methods

3.3.1 Blood collection and labeling

Blood was obtained from healthy individuals who had refrained from taking medications for at least ten days prior to donation. Informed consent was obtained from each volunteer, and phlebotomy was performed in accordance with IRB approval from the University of Pennsylvania's Office of Regulatory Affairs and the Declaration of Helsinki.

Whole blood was drawn via venipuncture into corn trypsin inhibitor (CTI, Haematologic Technologies Inc., Essex Junction, VT) to a final concentration of 50 μg/mL to inhibit Factor XIIa. Although the physiological relevance and importance of FXII is currently under investigation [109]. Aliquots of 200 μL whole blood were labeled with 4 μL of AlexaFluor 647 conjugated anti-CD41 (α_{IIb}) antibody (Clone PM6/248, AbD Serotec, Raleigh, NC), which had no effect on platelet function (results not shown). In order to inhibit thrombin function in some experiments, H-D-Phe-Pro-Arg-chloromethylketone (PPACK, Calbiochem, San Diego, CA) was added to a final concentration of 100 μM. CTI-treated whole blood was perfused through the fluidic chamber within 15 min of phlebotomy.

3.3.2 Microfluidic fabrication and protein patterning

Microfluidic devices were fabricated in poly(dimethylsiloxane) (PDMS, Sylgard 184, Ellsworth Adhesives, Germantown, WI) using well established techniques [22]. Detailed fabrication methods and patterning techniques were performed similarly to those detailed in Section 2.3.3. In order to ensure physical separation between the eight blood samples located in relative close proximity on the chip during the experiment, a simple second PDMS layer was used as pseduowells. PDMS (10:1 v:v base:curing agent) was mixed to a final volume of 99 mL and poured into a clean 150 mm petri dish. After allowing to cure at 80 °C for at least 4 hours, the solid

cylinder was removed. A pattern was placed beneath it and the single cylinder was cut into 20 individual well sections using an Xacto®knife that would fit on top of the devices with the microchannels. Using one flow device as a guide, the location of the eight inlets were marked on the surface of the plain PDMS using a felt marker. Large holes were then punched from the well-piece using a 4 mm diameter punch (Ted Pella, Redding, CA). The flow device and wells were irreversibly bonded by treating the two adjoining surfaces with a Tesla-coil-induced lab corona treater (115 V, Electro-Technics Products Inc., Chicago, IL) for 30 seconds, bringing the two sides immediately into contact, and curing overnight at 60°C under ∼2 lb of force. Briefly, glass slides (75 mm × 50 mm × 1 mm, Fisherbrand, Fisher Scientific, Pittsburg, PA) were cleaned with Methanol:HCl as described in Section 2.3.3, then functionalized with Sigmacote (Sigma-Aldrich, St. Louis, MO) to form a hydrophobic surface to aid collagen adsorption. Human Type-I collagen (Vitrocol 3.0 mg/mL, Advanced BioMatrix, San Diego, CA) was diluted to 300 μg/mL in HEPES buffered saline (HBS, 20 mM N-(2-Hydroxyethyl)piperazine- N'-2-ethanesulfonic acid, 150 mM NaCl, pH 7.4) with 10 μL 0.1 M sodium hydroxide solution to neutralize pH to 7.0 to a final volume of 1 mL. Microfluidic devices were then filled with the solution and allowed to incubate at room temperature for 150 min to polymerize the collagen into a thin film on the surface of the slide. Excess solution was then removed, immediately followed by placement of the flow device aligned on the formed collagen region. A solution of 0.5 % bovine serum albumin (BSA) in HBS was then filled through the channels and allowed to sit at room temperature for at least 60 min in order to prevent non-specific platelet binding to both the PDMS and the un-reacted glass surface. The device used to perfuse the blood over the collagen strip is shown in Figure 3.1.

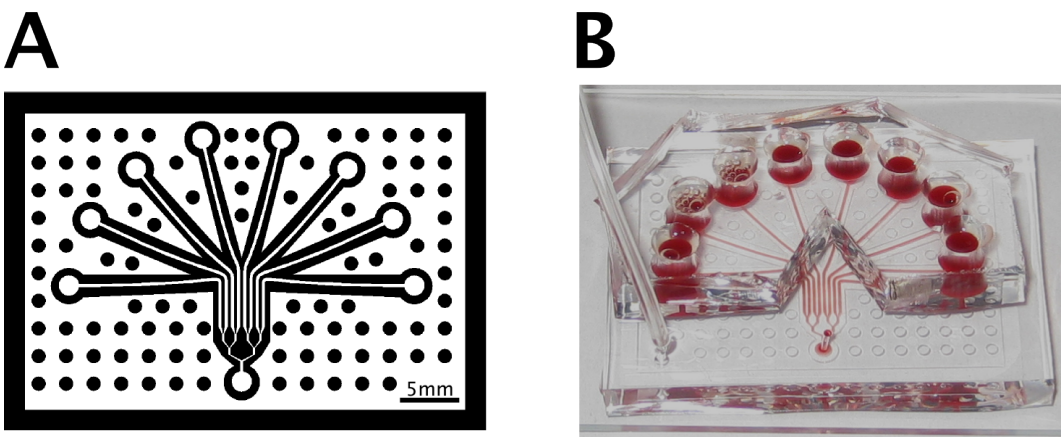

Figure 3.1: A. CAD schematic of eight channel device. B. Photograph of one device used.

3.3.3 Flow cytometry and device characterization

Fluorescent particles (FITC and PE-Cy5 Easy Calibration Kits, Spherotech, Lake Forest, IL) were diluted 1:9 (v:v) in 0.5 % BSA in HBS to a particle concentration of approximately 2 x 10^5 particles/mL. Control mixtures of 10 μL of each type of fluorescent particle (FITC Peaks 2, 3, 4, and 5 and PE-Cy5 Peaks 2, 3, 4, and 5) were mixed in a microcentrifuge tube. Particles were assigned to input positions on the flow device using a random number generator and perfused through the device using a gastight syringe (250 μL Hamilton Company, Reno, NV) mounted on a syringe pump (PHD 2000, Harvard Apparatus, Holliston, MA) at a volumetric flow rate of 16 μL/min for 5 min. The effluent was collected in Tygon tubing (0.020 in ID, 0.060 in OD, Fisher Scientific, Pittsburg, PA) and subsequently infused into a microcentrifuge tube for assaying. Flow cytometry was performed on an Accuri A6 flow cytometer (Accuri Cytometers Inc., Ann Arbor, MI) fitted with the CSample automated plate sampler. Gates were applied in CFlow Plus software and kept constant across all samples analyzed.

3.3.4 Inhibitor preparation

2'-Deoxy-N^6-methyl adenosine 3',5'-diphosphate (MRS 2179), Grave VIII apyrase from potato (*Solanum tuberosum*), 2-Methylthioadenosine 5'-monophosphate (2-MeS-AMP) (Sigma Aldrich, St. Louis, MO), and 4,4',4",4"'-[Crabonylbis(imino-5,1,3-benzenetriyl-bis(carbonylimino))]tetrakis-1,3-benzenedisulfonic acid (NF 449, Tocris Bioscience, Ellsiville, MO) were dissolved in HBS to working concentrations. Dilutions of compounds were made to ten fold the desired final concentration in HBS on the day of the experiment, after which the inhibitor was added at a ratio of 1:9 to fluorescently labeled whole blood and allowed to incubate at 5 min at room temperature, with gentle mixing at 2 min, except for apyrase which was added immediately prior to perfusion. Final inhibitor concentrations used were: MRS 2179 (0 - 10 μM), 2- MeSAMP (0 - 200 μM), NF 449 (0 - 10 μM) and apyrase (0 - 100 U/mL).

3.3.5 Platelet accumulation measurement

Blood samples incubated with the given inhibitors were introduced to the inlet of the flow device and immediately perfused through the device at a controlled volumetric flow rate of 15 μL/min for an average wall shear rate at the collagen patch of 210 sec^{-1} (for rectangular channels of cross sectional dimensions of 60 μm $\times$ 250 μm). Assembled devices were mounted on an inverted microscope (IX81, Olympus America Inc., Center Valley, PA) and imaged using a CCD camera (ORCA-ER, Hamamatsu, Bridgewater, NJ) illuminated with a mercury lamp (100W, 620 Ex / 700 nm Em). Fields of view were captured using a 2X objective, integrating for 1,000 ms every 5 sec for 5 min.

3.3.6 IC_{50} calculation

The far left and far right collagen regions were identified manually, with intermediate and corresponding background regions interpolated using a custom MATLAB script

(MathWorks, Natic, MA). Background-corrected fluorescence values were fit using a four parameter logical model shown in Equation 3.1:

$$FI = A + \frac{A - B}{1 + \left(\frac{[I]}{C}\right)^D} \tag{3.1}$$

with $[I]$ representing the inhibitor concentration, FI the background corrected fluorescence of the corresponding region, A and B the minimum and maximum intensities respectively, with C and D the fit parameters. The data were fit using a least-squares non-linear curve fitting routine (MATLAB, Data Analysis Toolbox).

3.3.7 Computational model of apyrase activity in open and closed systems

In order to investigate the effect of convective mass transport on the hydrolysis of ADP and ATP by apyrase, a set of finite element method numerical simulations were performed. A commercial software package (COMSOL Multiphysics, Burlington, MA) was used to solve both the steady-state flow profile and the coupled convection-diffusion-reaction system in a 2-dimensional domain approximating the 2 mm surrounding the 250 μm reactive zone with a height of 60 μm. The hydrolysis of ADP by apyrase was approximated by classic Michaelis-Menten kinetics using the published K_M for apyrase with ADP and ATP [17]. The influx of ADP at the reactive surface was set to an experimentally determined rate corresponding to full platelet activation [71], which is comparable to previously estimated values [37, 36], and a value calculated from the platelet flux to a collagen surface at the given shear rate [5] and the approximate ADP concentration per platelet [45]. Parameter values and boundary conditions are shown in Table 3.1.

Grid independence was performed by evaluating the near-wall average concentration for a series of increasingly refined grids consisting of 13,840, 55,360, 105,429, and 221,440 triangular elements, each with less than 0.001 % error from the estimate of

Table 3.1: Physical parameters and boundary conditions used in numerical simulations of ADP concentrations around at a growing thrombus surface. *: Calculated from the Wilkie-Change correlation for molecular diffusivity [11]. **: Determined by calculating the maximum velocity for a rectangular duct with cross-sectional dimensions of 150 μm $\times$ 60μm and a volumetric flow rate of 1.88 μL/min.

Parameter	Value	Reference
Density of whole blood	1.06 x 10^3 kg/m^3 (25 °C)	[36]
Viscosity of whole blood	4.7 x 10^{-3} Pa-sec (25 °C)	[36]
Diffusivity of ADP and ATP	1.14 x 10^{-10} m^2/sec	*
Flux of ADP (J_{ADP})	4.4 x 10^{-6} and 7.8 x 10^{-10} mol/m^2-sec	[71, 53]
Flux of ATP (J_{ATP})	2/3 x J_{ADP}	[45]
$v_{x,max}$	4.18x10^{-3} m/sec	**
$K_{M,ADP}$	0.25 mol/m^3	[17]
$K_{M,ATP}$	0.06 mol/m^3	[17]
k_{ADP}	100 μmol/min/mg	[17]
k_{ATP}	1,210 μmol/min/mg	[17]

the zero grid spacing solution using Richardson extrapolation [86]. The intermediate grid (105,429 elements) was used in order to optimize solution time and accuracy. Steady-state momentum and mass balance calculations were performed using a direct solver (UMFPACK) on a workstation (dual 2.2 GHz processors, 12 GB RAM).

$$ATP + apyrase \xleftrightarrow{K_{M,ATP}} ATP \cdot apyrase \xrightarrow{k_{ATP}} ADP + apyrase \tag{3.2}$$

$$ADP + apyrase \xleftrightarrow{K_{M,ADP}} ADP \cdot apyrase \xrightarrow{k_{ADP}} AMP + apyrase \tag{3.3}$$

Let $B_{ATP} = c_{ATP} \cdot apyrase$ and $B_{ADP} = c_{ADP} \cdot apyrase$.

$$\frac{dc_{ATP}}{dt} = -k_1 B_{ATP} \tag{3.4}$$

$$\frac{dc_{ADP}}{dt} = k_1 B_{ATP} - k_2 B_{ADP} \tag{3.5}$$

$$T_{apyrase} = B_{ATP} + B_{ADP} + Free \tag{3.6}$$

$$B_{ATP} = \frac{c_{ATP} \cdot Free}{K_{M1}} \tag{3.7}$$

$$B_{ADP} = \frac{c_{ADP} \cdot Free}{K_{M2}} \tag{3.8}$$

Combining Equations 3.6, 3.7, and 3.8

$$B_{ATP} = \frac{c_{ATP} \cdot T_{apyrase} \left(1 - \frac{c_{ADP}}{K_{M2}+c_{ADP}}\right)}{K_{M1} + c_{ATP} - \frac{c_{ATP} \cdot c_{ADP}}{K_{M2}+c_{ADP}}} \tag{3.9}$$

$$B_{ADP} = \frac{c_{ADP} \cdot T_{apyrase}}{K_{M2} + c_{ADP}} \left[1 - \frac{c_{ATP} \left(1 - \frac{c_{ADP}}{K_{M2}+c_{ADP}}\right)}{K_{M1} + c_{ATP} - \frac{c_{ATP} \cdot c_{ADP}}{K_{M2}+c_{ADP}}}\right] \tag{3.10}$$

The competition between ADP and ATP for hydrolysis by apyrase was modeled using classical Michaelis-Menten kinetics operating under the fast equilibrium assumption, shown by Equations 3.7, and 3.8.

The open simulations were simulated with the following settings: Subdomain conditions:

$$\nabla \bullet (-D_{ADP} \nabla c_{ADP}) = k_{ATP} B_{ATP} - k_{ADP} B_{ADP} - v_x(y) \bullet \nabla c_{ADP} \tag{3.11}$$

$$\nabla \bullet (-D_{ATP} \nabla c_{ATP}) = -k_{ATP} B_{ATP} - v_x(y) \bullet \nabla c_{ATP} \tag{3.12}$$

Boundary Conditions:

Inlet: $c_{ATP} = c_{ADP} = 0$

Reactive surface: $\frac{dc_{ATP}}{dy} = J_{ATP}$, $\frac{dc_{ADP}}{dy} = J_{ADP}$

Outlet: $J_{out,ATP} = v_x(y) c_{ATP}(x = L, y)$, $J_{out,ADP} = v_x(y) c_{ADP}(x = L, y)$

Walls and centerline: $\nabla c_{ATP} = \nabla c_{ADP} = 0$.

The closed system used the same binding kinetics and reaction terms (Equations 3.4, 3.5, 3.9, 3.10) with different ADP release.

$$\dot{m}_{ADP} = \frac{3}{\tau\sqrt{2\pi}} exp\left(\frac{-9(t-\tau)^2}{2\tau^2}\right) \cdot T_{ADP}, 0 < t \leq 2\tau$$
$$0, t > 2\tau \tag{3.13}$$

Equation 3.13 describes a normal distribution for ADP release to a cumulative total of T_{ADP}, with a time of maximal instantaneous release τ. The total ADP in the system was estimated by the typical volume and platelet count in an aggregometry cuvette (0.5 mL cuvette, 2×10^8 platelets/mL) with the same approximate ADP concentration per platelet used in the low flux value for the open system [45], with the maximal release time estimated from the maximal rate of ADP release [98, 18] at 30 sec, leading to a maximal ADP concentration of 6 μM in the absence of degradation. By matching effective flux values between the open and closed systems, the best attempt was made to create directly comparable numerical approximations of the corresponding *in vitro* systems.

3.3.8 Statistical analysis

Data were compared to appropriate controls using the Mann-Whitney U-test with p-values less than 0.01 considered statistically significant. All data are plotted as the mean ±standard deviation. All calculations were performed using the MATLAB Statistics Toolbox.

3.4 Results

3.4.1 Device characterization

To verify equal flow rates in each of the eight channels, each inlet reservoir was spiked with a unique bead tracer that was quantifiable by flow cytometry (Figure 3.1A). By measuring each tracer bead concentration in the combined exit stream of the microfluidic device (total flow = 16 μL/min for 5 min; channel wall shear

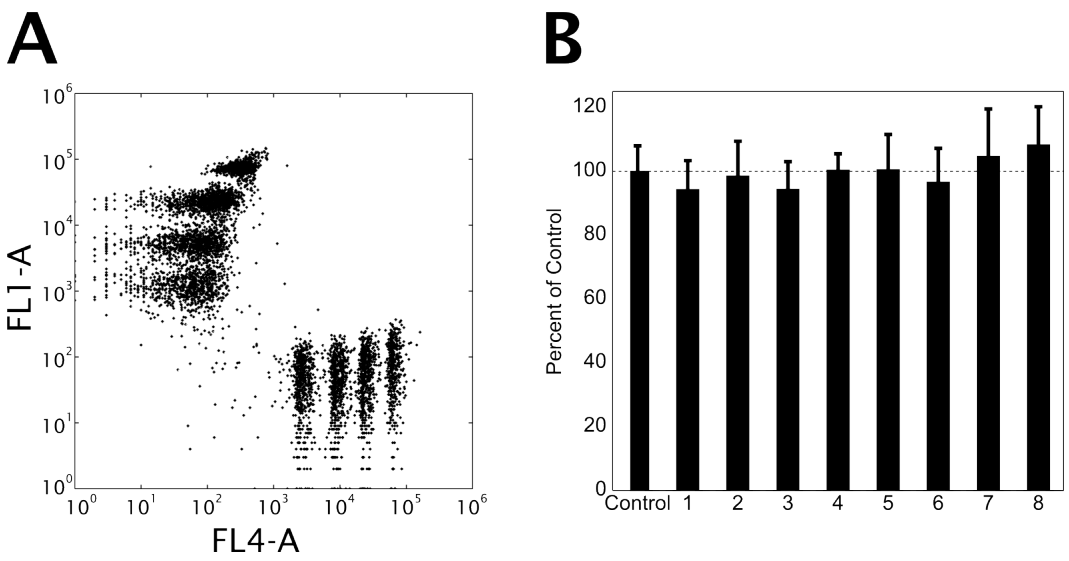

Figure 3.2: A. Flow cytometry identification of the eight distinct particle peaks. B. Comparison of relative percent of particles in the efflux of the flow device from 15 experiments using 5 different devices (bars are standard deviation, p >0.05 for all compared to control).

rate = 222 sec^{-1}), the flow rates were verified to be equal across the chambers (Figure 3.1B). This uniformity across the channels was validated in 15 different experiments using 5 different devices, thus confirming the designed intent that each reactive interaction zone is under statistically indistinguishable bulk hemodynamics and transport conditions. This characterization step, while somewhat mundane, is absolutely crucial to the remainder of this Chapter of work, and for other studies that utilize this design. While design principals and numerical simulations provide excellent guidance for the development of more complex and useful device geometries in this model system, careful, and perhaps painstakingly dull, experiments must be performed in order to verify the assumptions and output of numerical models.

Since thrombus buildup reached heights of <20% of the chamber height for such short distances, the pressure drop across an individual ∼250 μm long thrombus would be small compared to the pressure drop across the entire length of a channel. Thus, platelet accumulation at the collagen patch has a minimal effect on the flow distributions within the system.

3.4.2 IC_{50} for platelet P2-family inhibitors during thrombosis under flow

Three specific P2-family antagonists and apyrase were tested in a dose-response mode to calculate effective IC_{50}'s for collagen-induced platelet aggregate formation inhibition, in the presence and absence of thrombin generation capability. In each experiment, a total of eight simultaneously forming thrombi were imaged in real time as shown in Figures 3.3 and 3.4. Fluorescenetly labeled platelets accumulate only at the site of collagen exposure, with minimal non-specific upstream or downstream adhesion. The collagen displays substantial surface coverage due to platelet adhesion to collagen within 1 min and subsequent secondary platelet accumulation via platelet-platelet interactions over the 5 minutes as shown in Figure 3.4 with several important results that are not immediately apparent. Theoretically, these receptor antagonists should only have an effect on platelets that are recruited and activated via ADP induced signaling via the $P2Y_1$ receptor. Therefore, the initial adhesion and activation events of platelets directly binding to and signaling from the collagen exposure should remain unaffected. This is in fact the case, as the initial slopes of FI vs time during the first 90 seconds of the experiment, the time during which a majority of the adhesion events are platelet-collagen interactions. This observation serves as an internal control, and is only truly possible by the simultaneous measurement of an untreated positive control group in addition to the experimental groups.

Determination of total surface fluorescence at 5 min allowed a determination of the IC_{50} for each pharmacological agent as shown in Figure 3.5. The ability to measure these dose response curves for platelet receptor antagonists under flow with a direct comparison to untreated control samples on the same collagen surface has not been performed before. Due to the nature of blood changing from the moment it is removed from the flow forces and actively excreted factors from the endothelium which keep platelets in a quiescent state in the body, running proper control experiments is often very difficult. In addition, intra-donor variability can be

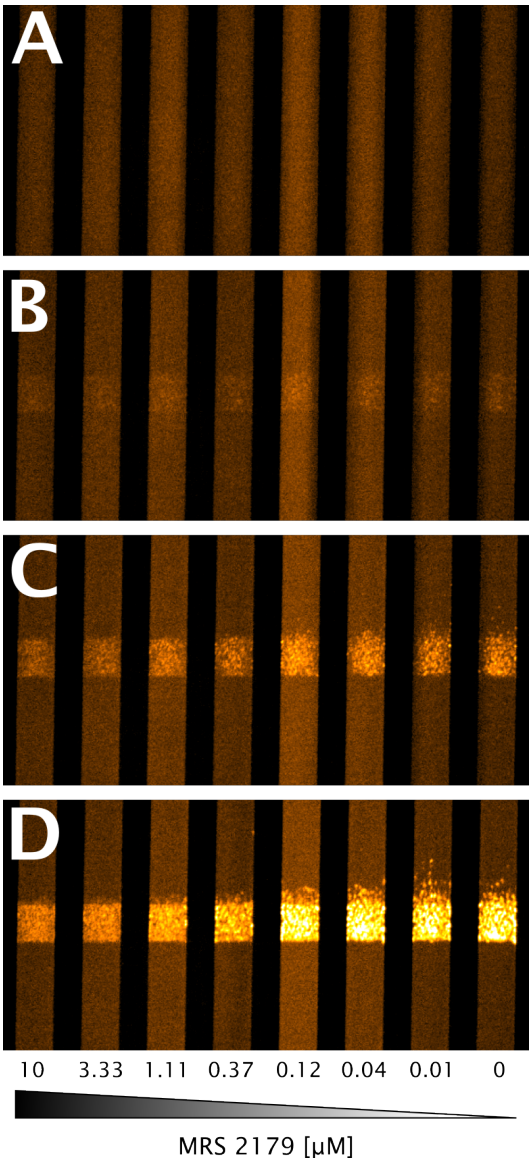

Figure 3.3: Micrographs of fluorescently labeled platelets at a collagen patch at 0 (A), 1 (B), 2 (C), and 5 (D) minutes at the given concentrations of a $P2Y_1$ inhibitor MRS 2179.

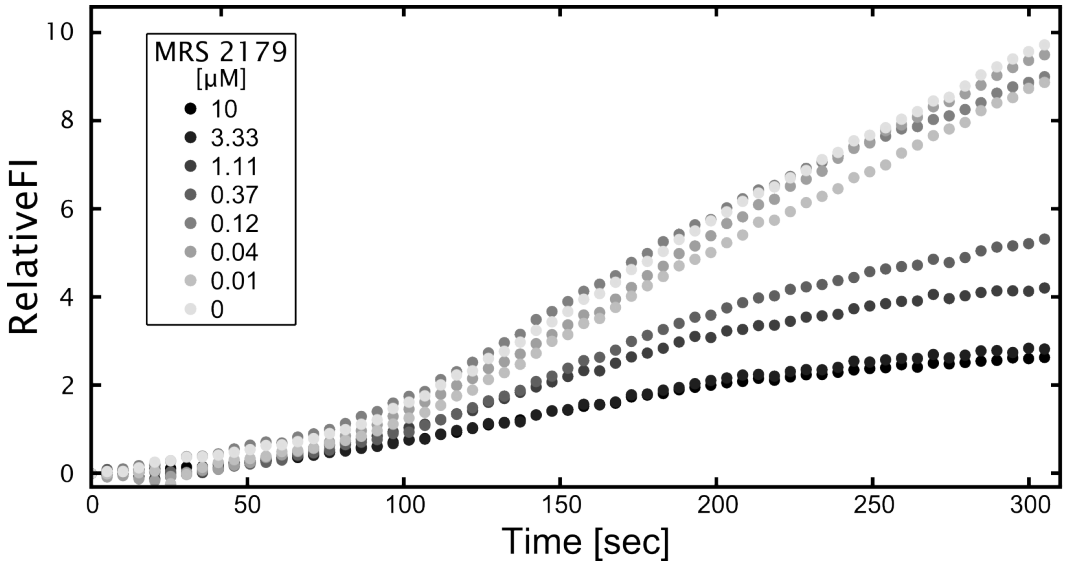

Figure 3.4: Kinetic trace of background corrected fluorescence at eight concentrations of MRS 2179 measured simultaneously.

among the major drawbacks to using freshly isolated human tissue for hemostatic experiments. However, this person to person difference can be an advantage with a model system such as this, since each experiment is compared within itself. The differences in platelet count, surface protein expression, soluble factor levels, and thousands of other metrics that have been shown to affect platelet assays can be accounted for, with the relative impact of pharmacological intervention determined on a given day at a specific time. This is one of the main attractive features for possible future development of these types of systems as diagnostic devices for point-of-care situations.

The $P2Y_1$ and $P2Y_{12}$ inhibitors displayed remarkably robust dose-dependent effects on limiting the accumulation of platelets at a localized collagen region. This is in contrast to the $P2X_1$ inhibitor which had no effect, as has been demonstrated previously at comparable shear rates in the lower physiological regime [42]. The thrombin generation in this system appears to be minimal, since there is no difference in the presence or absence of an irreversible thrombin inhibitor, as shown in the near identical measurements shown in Table 3.2 and Figure 3.5. The ability to

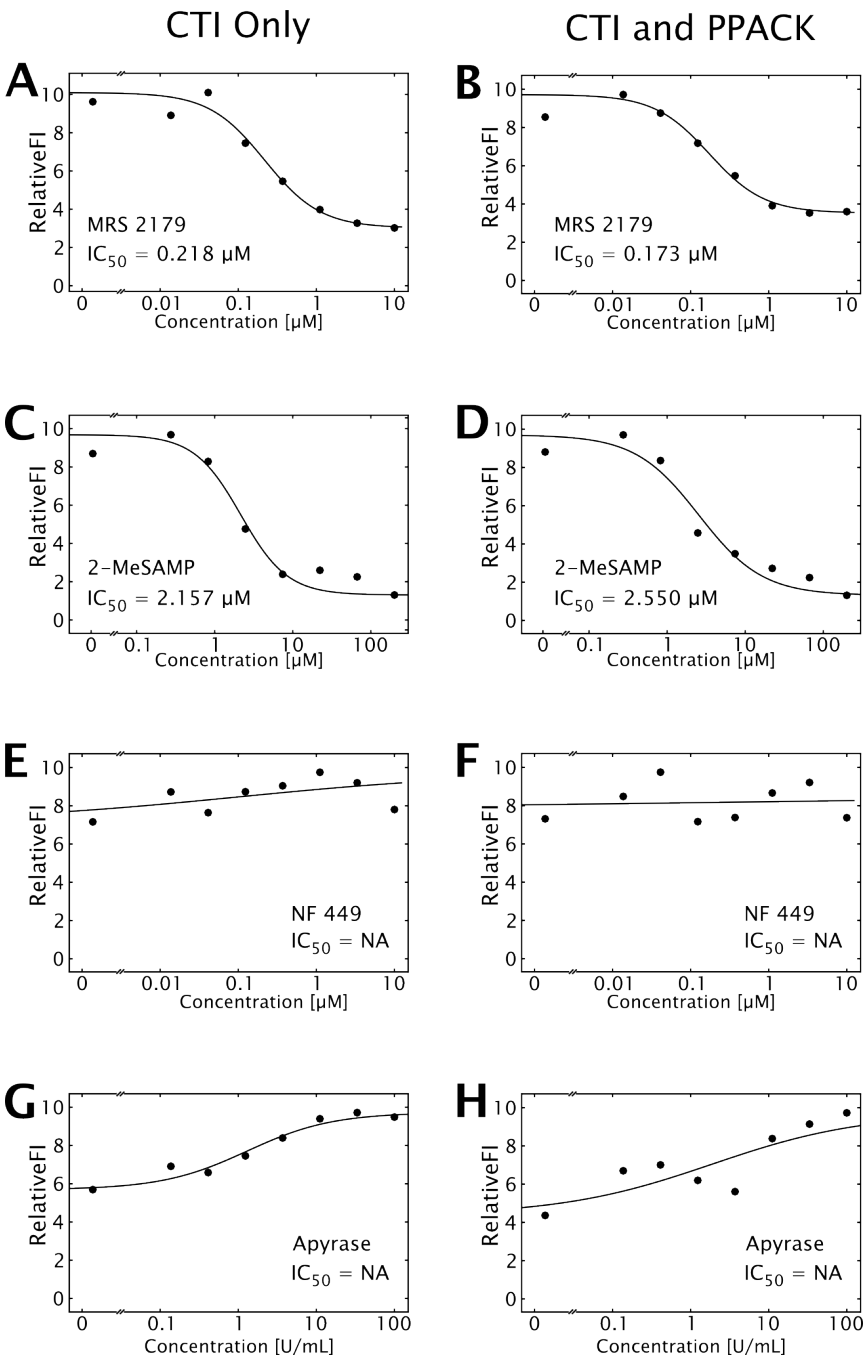

Figure 3.5: IC_{50} curves for the three pharmacological inhibitors and apyrase in the absence (A, C, E, G) or presence (B, D, F, H) of thrombin inhibition.

Table 3.2: IC_{50} values for the pharmacological inhibitors and apyrase (n = 4 different donors, P >0.39 between CTI only and CTI/PPACK

Compound	CTI only	CTI and PPACK
$P2Y_1$ (MRS 2179) [μM]	0.171 $\pm$0.093	0.227 $\pm$0.098
$P2Y_{12}$ (2-MeSAMP) [μM]	2.619 $\pm$0.994	2.497 $\pm$0.700
$P2X_1$ (NF 449) [μM]	NA	NA
Apyrase (U/mL)	NA	NA

run the number of experiments on the number of different donors for the range of inhibitor concentrations is solely due to the minimal material requirements of the microfluidic model system. Four interventions were measured at seven different concentrations for four different donors with the appropriate controls for five minutes of flow under venous shear rates. If these experiments were to be performed in classical parallel plate flow chamber assays, over 5 L of donor blood would have been required, in addition to over $7,000 for the labeling antibody alone, not to mention significantly more inhibitor and labor requirements. However, if positive controls were performed with each and every experiment, as were done in this study, the costs and material requirements would be increased by another factor of two. While the presence and role of blood derived tissue factor exposed on or accumulating at collagen-induced platelet activation is still under intense investigation, the relatively short experimental time (5 min) without exogenous tissue factor results in minimal thrombin and fibrin generation in this model system as expected [79].

In contrast to small molecular P2-receptor antagonists, apyrase operates by a different mechanisms in preventing platelet activation by nucleotide substrate by enzymatic hydrolysis. In the microfluidic focal injury model, apyrase was unable to prevent collagen-initiated platelet accumulation, even at extremely high levels (100 U/mL) of the enzyme. This lack of effect was not mediated by incubating the enzyme with the blood sample for up to 10 min (results not shown).

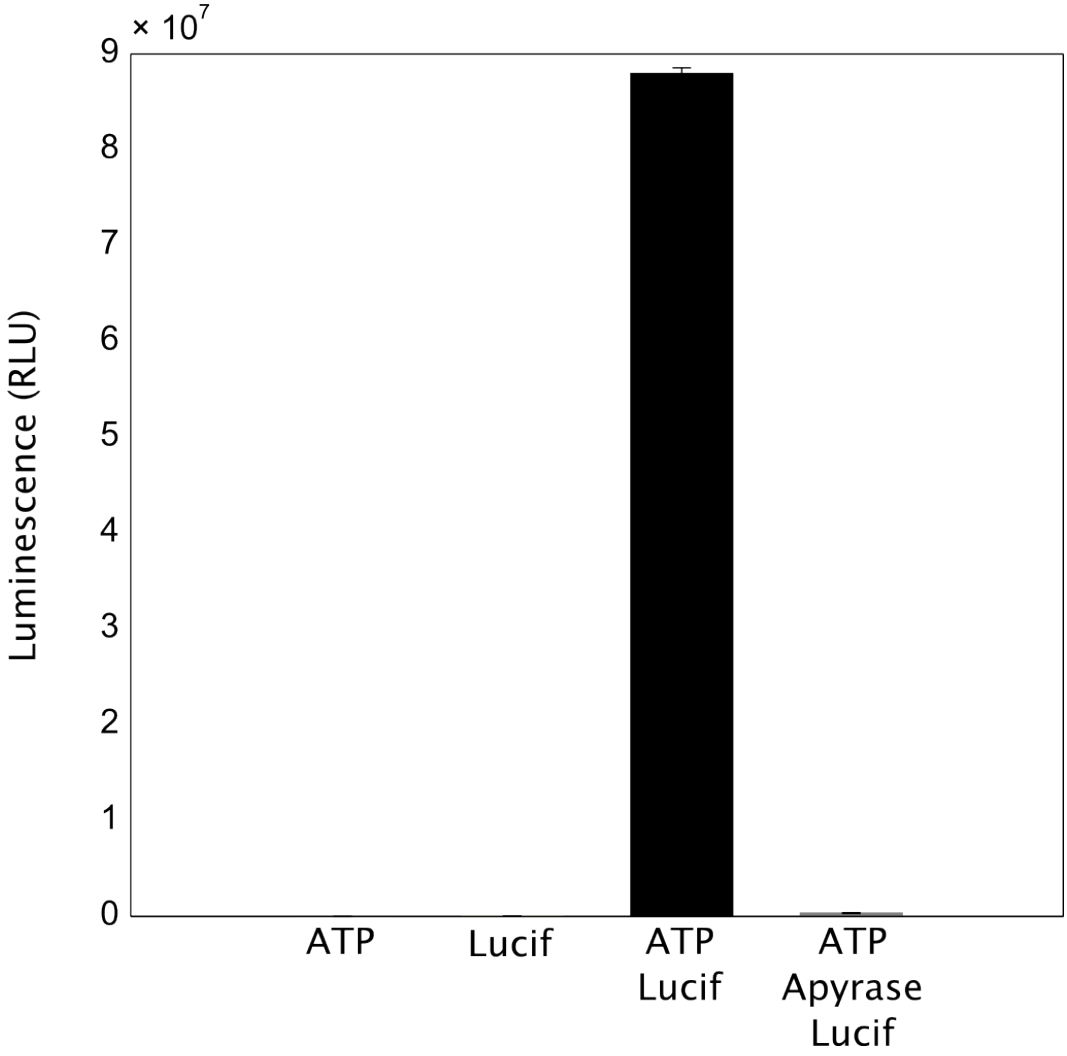

Figure 3.6: Apyrase activity confirmed by incubating 0.5 U/mL apyrase with 5 μM ATP for 10 min prior to luciferase addition (n = 3, p <0.01 between ATP with luciferase and ATP preincubated with apyrase and luciferase).

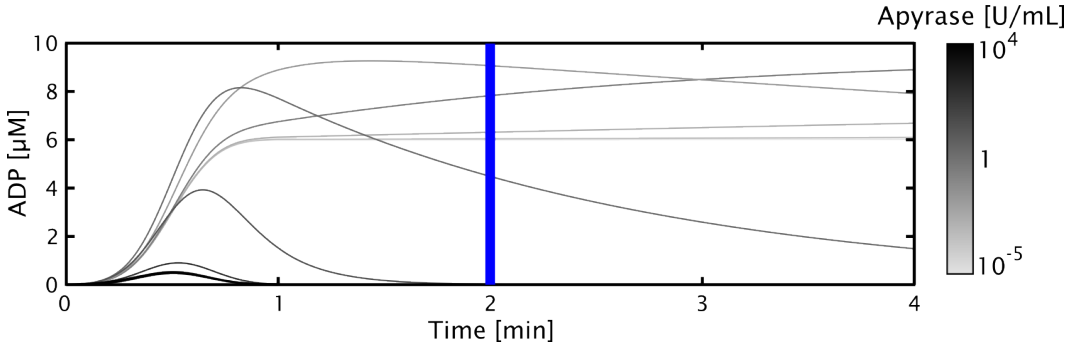

Figure 3.7: Results of closed system approximating ADP release by collagen activated platelets and subsequent hydrolysis by varying concentrations of apyrase.

Enzyme activity was confirmed by reduction of ATP-mediated luciferase signal as shown in Figure 3.6. The slight enhancement of platelet deposition at 10 U/mL may be due to conversion of released ATP to ADP compared to the kinetically slower reaction and weaker binding of ADP to apyrase compared to ATP.

3.4.3 Numerical simulation of apyrase-mediated ADP hydrolysis in open and closed systems

The closed system of an aggregometry cuvette was model using Equations 3.4, 3.5, 3.9, 3.10, 3.13, with the instantaneous ADP concentration at 2 min used to determine dose dependence, as seen in Figure 3.7. In order to approximate the amelioration of the 'active cloud' [47] of ADP generated at the site of platelet activation of apyrase, average ADP concentration in a region 5 μm above the length of the reactive zone were calculated using a finite element method coupled to a convective flow field. This numerical exercise validates the practice of using relatively moderate concentrations (between 0.5 and 3 U/mL) of apyrase while performing aggregometry studies to ameliorate ADP and ATP receptor activation.

These calculations were made across a range of apyrase concentrations of 1×10^{-5} to 3×10^{4} U/mL, with representative samples shown in Figure 3.8. The steady-state concentrations in the reactive zone were plotted as a function of bulk apyrase

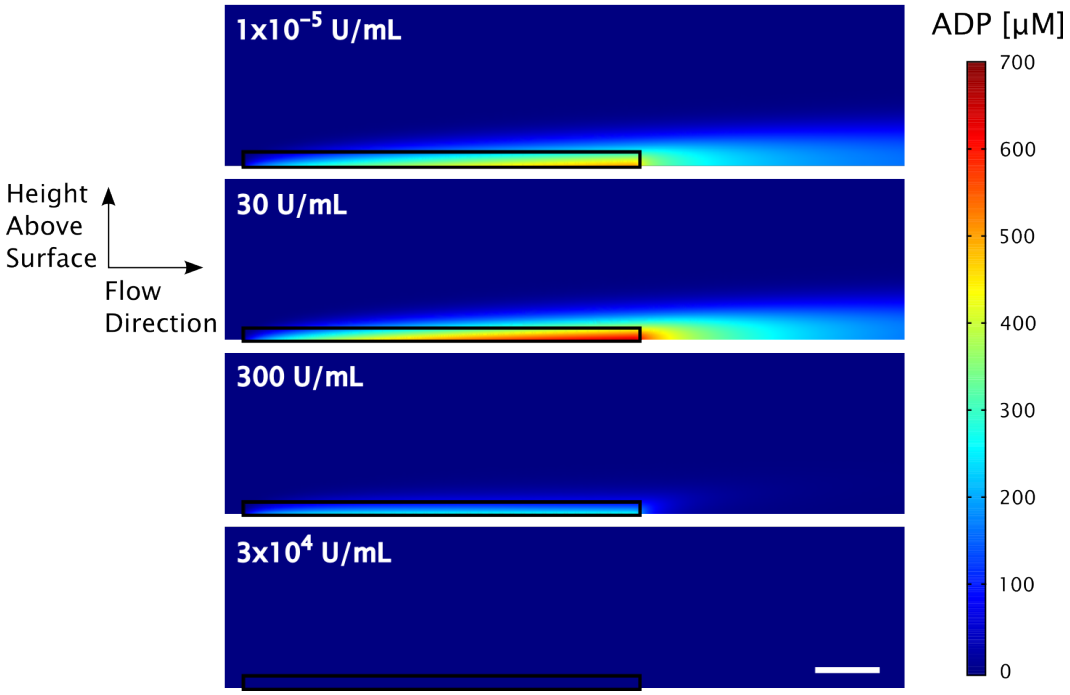

Figure 3.8: Results of open system approximating ADP release by collagen activated platelets and subsequent hydrolysis by varying concentrations of apyrase.

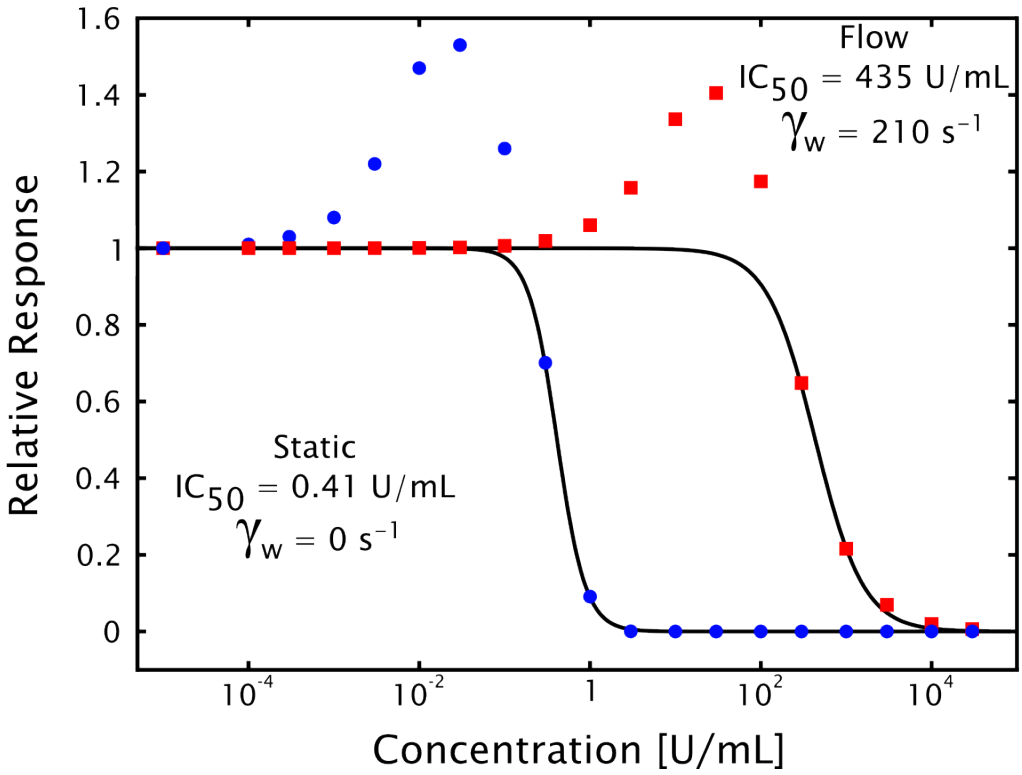

Figure 3.9: IC_{50} calculations for numerical simulations for both open (red squares) and closed (blue circles) systems.

concentration, calculating an effective IC_{50} using Equation 3.1. Unlike the closed system analogous to an aggregometry cuvette, where the control volume was drawn around the entire experimental volume, the only region of interested in the open system is that immediately above the active region. The reason for this is the focal nature of the collagen exposure and the passivization of the remainder of the glass surface and device walls. Since this model system is intended to investigate the effect of these inhibitory treatments on localized injuries, it is presumed that endothelial cells upstream and downstream of the injury site are not compromised, hence platelet accumulation is limited to the site of injury.

The dose dependent behavior is shown in Figure 3.9. As shown, increasing the apyrase concentration effectively abolished any ADP in the closed system at 1 U/mL, the concentration which is most commonly used in aggregometry.

The slight but reproducible increase in platelet accumulation under high (10, 30, and 100 U/mL) apyrase concentrations observed in the experimental system was hypothesized to be the result of preferential conversion of ATP to ADP by apyrase at the location of the growing thrombus. There are two prevalent isozymes of the apyrase enzyme, with relative ATPase:ADPase activity ratios of 12:1 and 1:1 [53], with most apyrase reagents supplied as mixtures of the two. By running the numerical simulations with both pairs of binding and kinetic rate parameters, it was possible to show that in both the closed and open systems, an apyrase-mediated increase in ADP is generated due to preferential conversion of ATP released simultaneously during platelet degranulation as shown in Figure 3.9.

The dose dependent behaviors are not sensitive to the flux imposed at the reactive surface of the open system, which is important since literature estimates for the ADP flux from a growing thrombus vary over four orders of magnitude [72, 5], indicating that the phenomena is independent of the actual ADP flux at the surface as shown in Figure 3.10.

3.5 Discussion

The 8-channel microfluidic focal injury model allows the rapid determination of the effective concentration of anti-platelet and antithrombotic agents under flow conditions. By designing and fabricating a pair of microfluidic devices for patterning collagen and perfusion with tight spatial control, this system is able to measure the accumulation of fluorescent platelets at 8 independent sites of collagen exposure simultaneously. By dosing small volumes (90 μL) of whole blood from a single donor with correspondingly small volumes (10 μL) of inhibitor, it is possible to generate a full response curve from a single experiment. The dose response behavior observed in this system for both 2-MeSAMP and MRS 2179 was similar to previously reported data [14, 105, 9], implying that the inhibitors maintained their operational range in

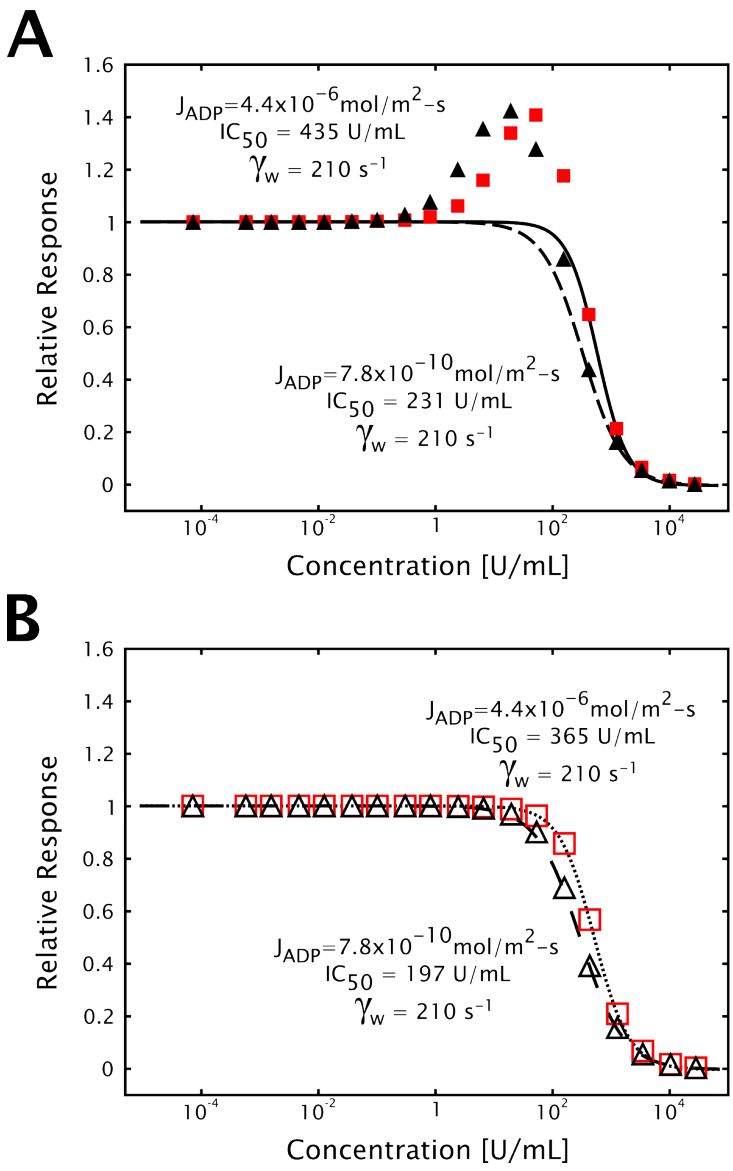

Figure 3.10: In the open system with unequal (A, closed symbols) and equal (B, open symbols) ATP:ADP rate parameters, the dose dependence of apyrase mediated ADP depletion is largely unaffected by flux over four orders of magnitude (high in red squares, low in black triangles).

spite of a more complex and rigorous experimental system.

The biochemical modes of action of the $P2Y_1$ and $P2Y_{12}$ inhibitors used in this work are different from the family of compounds currently used as to inhibit the receptors as anti-platelet therapeutics (the thienopyridines). These compounds require metabolism to turn the administered pro-drug into the active compound, which then binds its target receptor irreversibly and prevents ligand binding and subsequent G-protein signaling. This mode of action is in contrast to the reversible binding, direct acting compounds used in this work (MRS 2179 and 2-MeSAMP) and next generation therapies under investigation (ARC69931MX). The reversibility of the compound interactions with the receptor may be a concern, as shown by lack of efficacy leading to the early termination of the ARC69931MX trial (ClinicalTrials.gov identifier NCT00306162). However, the activity of MRS 2179 (IC_{50} 200 nM) in this system was comparable to the published K_i of 138 nM [9], while 2-MeSAMP required a concentration approximately 10 fold higher than its calculated K_d (0.23 μM) [49] for half-maximal effect in this assay ($IC_{50} \sim 2.5$ μM), which could be accounted for by the presence of a high affinity ADP binding site on platelets [46].

The inability of apyrase to prevent platelet accumulation at a collagen surface and the corresponding numerical simulations of both open and closed systems have several relevant and important implications. The mode of action of an enzymatic degradation of receptor ligand in the bulk phase is fundamentally distinct from direct receptor antagonism. By preincubation of small molecule inhibitors with the blood sample, ample time is given for diffusion to, recognition of, and equilibration with the antagonist's given receptor, thereby disabling the ability of the receptor to bind its ligand and signal. However, enzymatic degradation of ligand must occur in the time between ligand exposure, in this case ADP release from dense granules upon primary platelet activation, and receptor binding. In closed, well mixed systems, such as aggregometry cuvettes, the ligand, enzyme, and receptor are all equally distributed throughout the control volume. Under flow conditions where platelets

accumulate to levels that are 10 to 50-fold greater than in normal whole blood, apyrase is kinetically unable to degrade locally released ADP, even with convective removal of ADP. The experiments and simulations were performed at relatively low (210 sec^{-1}) shear rates compared to the arterial vasculature, which is the targeted region of action for anti-platelet agents. The slower flow rates, and correspondingly low convective transport of ADP away from the growing thrombus, representing higher agonist concentrations and a more rigorous test of compound potency.

Upon further investigation of the preferential hydrolysis of ATP to ADP for a specific isozyme of apyrase, it was determined that local ADP concentrations, in the presence of the right amount of apyrase, could actually be higher than in the absence of apyrase.

While this is easily rectified by using an enzyme with, at the absolute minimum, an equal affinity for both ATP and ADP, the effects of convection on the system still dominate, as shown in Figure 3.11. The system modeled here only takes into account the species released from platelets. It is well established that red blood cells are key factors in regulating vascular tone, using ATP as one of the main mediators [25]. Red cells can release very significant amounts of ATP, especially in hypoxic conditions, upwards of 2×10^7 molecules per cell, leading to local ATP concentrations of over 160 μM. In this regard, red blood cells act as sources of ATP, which in the presence of circulating apyrase, could lead to increased ADP concentrations at growing thrombi. This analysis implies that dosing high concentrations of adenosine phosphatases required to have an effect under flow conditions of could actually increase platelet accumulation at the site of injury which was observed in this model system (at apyrase concentrations of 10, 30, and 100 U/mL), putting individuals at risk for atherothrombosis at higher risk for pathological clot formation.

However, the open system described in this work is fundamentally different from classical aggregometry experiments. Rather than an isotropic release throughout the control volume, the focal nature of the injury necessitates that ADP generation

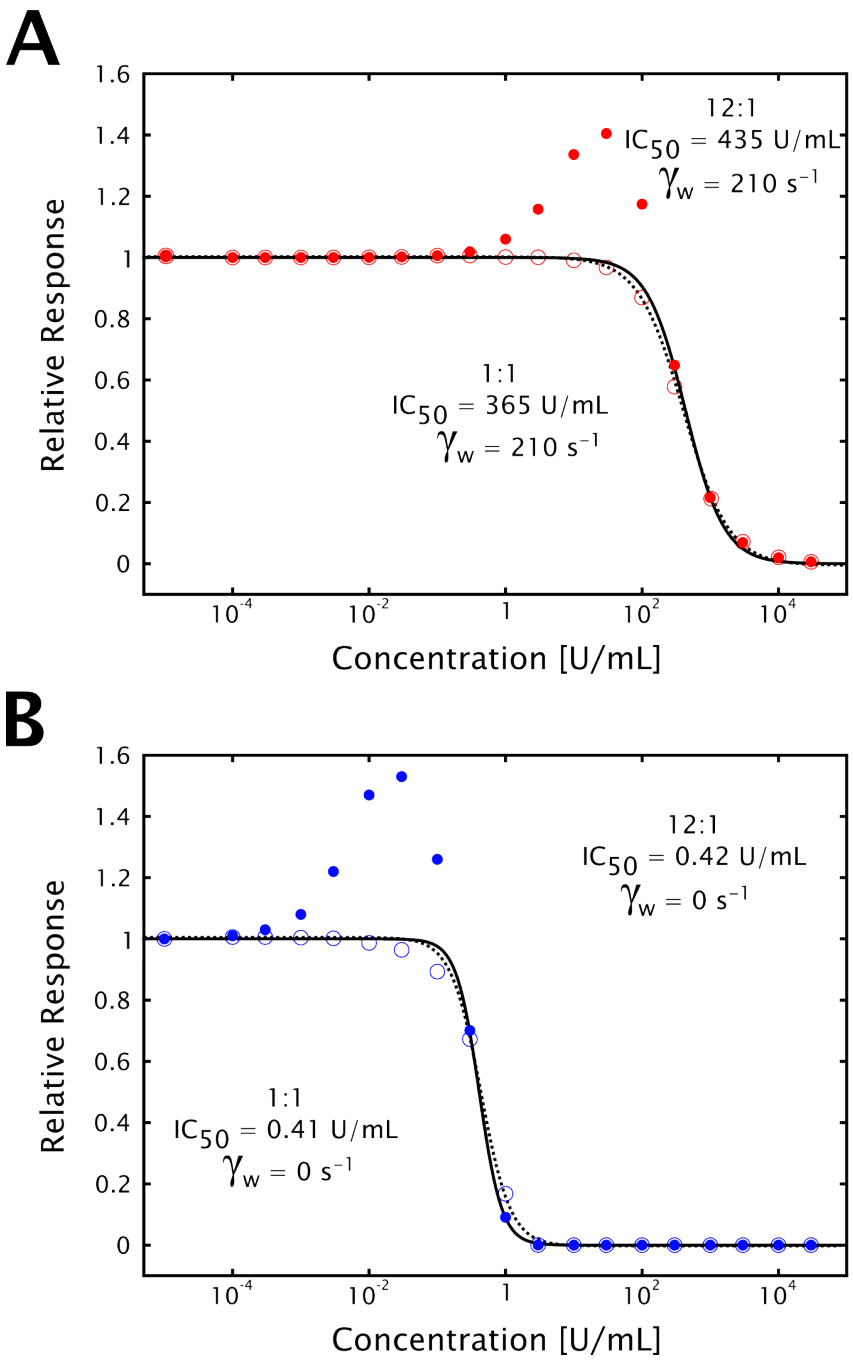

Figure 3.11: In the open system with unequal (A) and equal (B) ATP:ADP rate parameters, the dose dependence of apyrase mediated ADP depletion is largely unaffected by flux over four orders of magnitude.

is also localized to the growing thrombus site. While laminar flow is characteristic of physiological conditions found in a large majority throughout the vasculature, it necessarily is accompanied by poor radial mixing, especially of non-ionic molecular species (MW >100 Da).

$$Da = \frac{U \cdot L}{V \cdot c_A} \tag{3.14}$$

The competing phenomena of reaction and convective transport is characterized in a dimensionless number typically used to describe chemical reactor efficiency, called the Dämkohler number [11], defined by Equation 3.14, with U, L, V, and c_A representing characteristic reaction rate, length, velocity, and concentration respectively. As the Dämkohler number approaches infinity, the reaction approaches completion as it would under no flow conditions (i.e. $V \rightarrow 0$) within the interaction zone. However, as the Dämkohler number approaches zero, convection dominates the system meaning the reaction is minimal within the region of interest. In the experimental system and open system simulation, the Dämkohler number is $2{\times}10^{-3}$, or close to zero. This is manifested in the fact that the simulation results suggest that exceedingly high apyrase concentrations would be required to have an effect on the local ADP concentration for a given flow profile. It is worthwhile to reiterate that the experiments and simulations were performed at wall shear rates of 210 sec^{-1}, a relatively low physiological shear rate. Higher shear rates, and correspondingly higher velocities, would only decrease the Dämkohler number and decrease the effect of any bulk phase enzymatic based agonist depletion.

The simple dimensional analysis provided by the Dämkohler number leads to several important clinical implications. This work indicates that enzyme-mediated ligand removal for localized surface-mediated events occurring under bulk convective transport will be limited, not due to enzyme specificity, but rather by the time required to react compared to convection away from the zone of interest. A number of nucleotide phosphohydrolase therapies currently undergoing testing for diminishing

ADP-induced excessive platelet accumulation in thrombotic pathologies have shown early success in one of two major ways. The first is to use a model injury system that includes an element of stasis, either an ischemic stroke model [84] or an ischemia/reperfusion thrombosis model [55]. While these *in vivo* model systems are highly relevant, their intrinsic lack of blood flow at the site of injury necessarily provides the soluble enzyme the time required to act, in contrast to injury models in which blood flow is maintained. The second and newer approach is by which the enzymatic domain of CD39 is covalently bound to a targeting moiety, hence allowing local enzyme concentration to greatly increase compared to the bulk concentration at the site of injury [19]. This surface-bound enzyme increases the residence time of the enzyme at the active site, provide more enzymatic activity at the site of ADP action.

3.6 Conclusions

In summary, this chapter has shown that a microfluidic focal injury model is capable of measuring the responsiveness of platelets to a set of inhibitors by measuring changes in collagen-induced accumulation under flow. While inhibitors of the $P2Y_1$ and $P2Y_{12}$ receptors displayed dose-dependent efficacy, the $P2X_1$ antagonist did not have any effect in this model system. Similarly, the phosphohydrolase apyrase was not able to reduce platelet accumulation by hydrolyzing ADP and preventing its action on subsequent activation of additional platelets. Numerical simulations have given us insight into why apyrase is able to function at moderate (1 U/mL) concentrations in aggregometry and other closed systems, however significantly higher concentrations (1,000 U/mL) would be required for similar abolition of ADP induced platelet activation under single-pass flow conditions. In addition, the preferential hydrolysis of ATP to ADP by a non-specific apyrase can increase the local ADP concentration to levels higher than in the absence of the enzyme, increasing

platelet accumulation on a focal collagen region. This work represents a step towards what could be a functional assay used to rapidly estimate a patient's response to anti-platelet therapy, prior to or during prophylactic treatment.

This Chapter has outlined how improvements in experimental throughput in combination with simple finite element method mathematical modeling has help to illuminate the potential issues with a therapy currently undergoing treatment. Two aspects of this model system were crucial for this finding: namely the small material requirements and the simultaneous experimentation. Large quantities of commercially available apyrase were required in order to obtain final concentrations of 100 U/mL in a small ($\sim$100 μL) sample for these experiments. This would have been completely cost prohibitive were it to be performed in a classical parallel plate flow chamber, which would have required over $ 7,000 worth of fluorescent antibody and over 5 L of donor blood, not to mention other materials requirements. Secondly, and perhaps more importantly, the ability to repeatedly see relative increases in platelet accumulation to simultaneously running control blood samples from the same donor on the same collagen preparation was the critical step to investigating the enzyme specificity. While integrated signals were noticeably different, the apparent accumulation during the experiment was only slight. The ability to compare multiple repeats of the experimental condition to a simultaneous control were invaluable. While these changes greatly increased the power of this model system over that described in Chapter 2, it is important to note that the system used in this Chapter remains simplistic. The power of protein micropatterning and soft lithography coupled with replicate molding is in the integration of more complex and realistic surfaces and flow conditions, not simply straight channels and a collagen zone.

Chapter 4

On the Impact of Secondary Surface and Bulk Flow Modifications in Thrombus Formation

4.1 Abstract

The ultimate goal of *ex vivo* model system development is to provide the user with control over as many of the experimental variables as possible, while including as much of the complexity and realism of the *in vivo* situation. Realistically, this approach towards *in vivo* conditions has to occur gradually, and preferably modularly: providing opportunities to increase the system complexity when it is desired, while retaining the ability to revert back to simpler, perhaps more well established, system operation modes. Hemostasis research is no different in that there is a continuum of *in vitro* systems that are useful for the investigation into new aspects of platelet and coagulation biology. The addition of a coagulation inhibitor, tissue factor, to the

initial surface condition, and the manipulation of the flow history of a blood sample are two logical steps towards the recreation of the complex biological situation of thrombosis. Significant engineering advances are required for the localization of known amounts of active tissue factor on a surface in a repeatable and physiologically relevant way, the initial steps of which are investigated here. Furthermore, the flexibility of soft lithographic techniques to form complex, yet physically relevant, geometries to mimic pathologies commonly encountered in diseased individuals allows for the initial studies of the impact of shear exposure to thrombogenic potential. In both cases, this work outlines both the advances and remaining hurdles that exist to further develop model systems of thrombosis and hemostasis that being to approach the complexity and richness of the their *in vivo* analogues, while maintaining the control of *in vitro* experimental procedures.

4.2 Background

4.2.1 Tissue Factor

Tissue factor is a 41 kDa protein that is expressed in cells throughout the body, with highest expression levels in the brain, the adventitial around blood vessels, and skins cells [62]. While the importance of tissue factor in a proper hemostasis response is important and will be discussed in more detail, there are other critical signaling roles of tissue factor. The tissue factor knockout is an embryonic lethal mutation, with incomplete blood vessel development [63]. The role of tissue factor in vascular development and tone are linked to both its proteolytic cofactor activity as it is in the extrinsic hemostatic cascade as shown in Figure 1.3, but also as an important signaling molecule in the proper maintenance of blood vessels, the uterus, the placenta and the heart [63].

The source of tissue factor during injury is currently still under investigation and a controversial topic among researchers in the field. There are a large number

of proposed sources of tissue factor in the vasculature: *de novo* synthesis [99] and pre-formed exposure [83] in platelets, microparticles [34] as well as tissue factor that is ubiquitously expressed in the subendothelial space [13]. In addition to the physical source of the tissue factor protein, biochemical changes that are induced in the protein are equally important to its activity. Some of the hypotheses that are currently under investigation include tissue factor de-encryption by protein disulfide isomerase [3] or negative phospholipid exposure [4].

Tissue factor is a transmembrane protein that requires a negatively charged phospholipid surface for the proper assembly and activity. Upon activation, platelets exchange their lipid content from the inner membrane leaflet to the extracellular side, providing phosphatidylserine for assembly. As platelets continue to accumulate and activate within a growing thrombus, the surface for coagulation assembly and propagation greatly expands, while platelets become physical barriers to convective removal of activated species from the reaction zone. It is important to note that only a few of the coagulation reactions require a negatively charged phospholipid surface (as shown in the gray boxes in Figure 1.1), convective removal of products dominates the reaction rates in almost all types of thrombus formation, as described in Equation 3.14.

The role of tissue factor in *in vitro*, *ex vivo*, and *in vivo* injury model systems remains under research and a source of controversy. Models of arterial thrombosis stain positively for tissue factor during thrombus growth [31], with fibrin forming in the injured area. While a significant fraction of the tissue factor in *in vivo* models most likely is derived from activated endothelial cells and the vascular bed, including smooth muscle cells [110]. In contrast, most *ex vivo* and *in vitro* flow experiments do not incorporate exogenous tissue factor in the surface preparation. Those that do either do use as the sole initiator [91], or in combination with other matrix proteins [79, 80]. While these experiments have led to interesting and important realization

about tissue-factor driven coagulation under flow, the ability to investigate the long-time thrombin generation and clot formation is limited in these systems due to their volume requirements. The microfluidic system used in this work provides the ability to investigate the role of tissue factor in collagen-induced thrombosis under flow, since relatively long (30 min) experiments can be performed repeatedly and with reasonable ($\sim$5 mL) blood volume requirements.

4.2.2 Von Willebrand Factor and effects of shear

Among the proteins involved in clot formation, von Willebrand Factor (vWF) is the largest and perhaps most complicated in terms of production, release, function, signaling, and degradation. Originally formed in both endothelial cells and megakaryoctes [29]. Upon synthesis, vWF undergoes a number of complicated post-translational modifications, the final result of which is being packaged into granules (Weibel-Palade bodies or α-granules in endothelial cells and platelets respectively). These vesicles are exocytosed upon activation signals, leading to locally high concentrations of the protein, in addition to the ubiquitous circulating concentration of approximately 10 μM in the blood plasma [2]. The advanced processing and packaging of vWF leads to a wide size distribution of multimers both within intracellular stores and in the circulating species [60]. The protein assumes a mostly globular structure while circulating in the blood stream, however previous work has shown that upon either high amounts of shear stress or upon platelet tethering, these large multimers can stretch out into a string-like form [76, 107]. The prevailing theory is that vWF-mediated transient platelet adhesion is crucial at elevated shear rates, where platelet collagen bonds are too slow to form and signal during the short interaction times in elevated flows, such as the arteriole system [115, 21].

There has been much work to date that describes the importance of vWF, from its clinical origins when discovered in 1926 Erik von Willebrand in Finland, to the

protein crystal structure of its platelet-interacting subunits [23]. By presenting protein domains that bind both to collagen repeats and proteins on the platelet surface, specifically glycoprotein Ib (GPIb) and integrin $\alpha_{IIb}\beta_3$, multimers of vWF monomers serve as potent potentiators of platelet accumulation. Several *in vitro* experimental results describe the critical role of vWF in shear-induced platelet activation (SIPA), whereby platelets undergoing a shear force in a cone-and-plate viscometer become activated and aggregate together, mostly via vWF-GPIb interactions [82]. Recent work has also indicated that the local shear conditions may be directly responsible for platelet activation [73], although in a complicated and non-focal nature. However, it is known that during the progression of coronary heart disease, atherosclerotic plaques build up well into the luminal space of a diseased vessel, which can lead to either complete blockage via a thrombotic event or simply vessel collapse [89]. Immediately prior to full vessel collapse, blockages of up to 98 % luminal cross-sectional area have been reported, which results in local pathological shear rates of up to 50,000 sec^{-1} [16, 90]. While these shear rates have induced SIPA *in vitro*, the relatives times of pathological shear exposure *in vivo* and those required to activate platelets or bind to collagen *in vitro* are separated by orders of magnitude (tens of ms to tens of sec) [61].

A majority of the work done to investigate the behavior of platelets, vWF, and collagen under high shear flows have been performed under uniform high shear across a large surface coated either with collagen or vWF [97, 114, 85]. While these experimental conditions may approximate the dynamics of what would be considered plaque failure at the throat of a stenosis, the inflexibility of flow chamber designs has severely limited the ability of research to examine how the flow history of blood affects its behavior when presented with an injury mimetic. Even very brief exposures to very high forces are proposed to have potentially significant effects on thrombus formation [67]. Additionally, some of the signalling mechanisms within platelets activated by binding of surface proteins to shear-exposed vWF domains

can significantly alter the procoagulant and subsequent platelet recruitment activity [69]. By beginning to parse out the effect of shear exposure and the effect of surface-mediated vWF accumulation under shear is an important aspect to understanding the systemic effects of a high shear region within the vascular system.

4.3 Materials and Methods

4.3.1 Blood collection and labeling

Blood was obtained and labeled as described in Section 3.3.1.

4.3.2 Device fabrication, characterization, and validation

PDMS devices were fabricated, characterized, and validated as described in Sections 2.3.3 and 3.3.3.

4.3.3 Electron microscopy

In order to more closely investigate the aggregates formed during the experiments, samples were imaged with a scanning electron microscope. After perfusion of blood for the specified time through the device, the blood in the inlet reservoir was replaced with fresh HBS. The flow rate was maintained for 1 min while the buffer cleared a majority of the unbound red cells through the device. The inlet reservoir was then filled with 1.6 % paraformaldehyde, then 2 % glutaraldehyde (Sigma-Aldrich, St. Louis, MO) in HBS, and perfused for 5 min each. The flow was then stopped and the thrombus allowed to fix *in situ* for at least 3 hr at room temperature. After the incubation, the device was carefully removed from the glass slide, ensuring that the thrombi formed remained intact and adhered to the glass surface. After device removal, the thrombi were fixed in in the following order: A, A, A, B, A, A, A, with 'A' designating 0.2 M sodium cacodylate buffer (pH 7.0), and 'B' 2 % glutaraldehyde

in HBS, each for 10 min at room temperature. The last fixative was left on the sample overnight at 4°C. The following day, glass slides were scored to isolate the reactive zone where the thrombi are formed. The small glass areas were then dehydrated in the following percentage 100 % ethanol in 0.2 M sodium cacodylate for 10 min each: 50, 70, 80, 90, 100, 100. The dehydration was then finalized by incubating the sample in 50:50, then 100:0 hexamethyldisilazane (HMDS, United Chemical Technologies Inc., Bristol, PA) : 100 % ethanol for 15 min each. Samples were then immediately mounted with double sided carbon tape on an aluminum stub (11 mm, Ted Pella, Redding, CA). Samples were then sputter coated with platinum/palladium using a sputter coater (Cressington Scientific Instruments Ltd., Watford, UK) for 35 sec at an argon overpressure of 0.08 mbar, with a current between 25 and 30 mA. Samples were imaged on a JEOL 7500 FEG-SEM (JEOL Ltd., Peabody, MA) in Gentle-Beam (GB-H) mode, with a net accelerating voltage of 2 kV with a 2 kV sample bias at a current of 10 μA in secondary electron imaging mode at a probe current of 7.

4.3.4 Tissue factor lipidation and activity assay

Tissue factor requires a negatively charged phospholipid surface for its activity. *In vivo*, this surface is dependent upon platelet and endothelial cell activation and intracellular processes that flip phosphatidylserine (PS) from the inner to the outer platelet membrane. In addition, when platelets are activated, they undergo radical shape changes, supplying significantly more surface area than a non-activated platelet for surface mediated reactions to occur on. In order to capitalize on the variety of synthetic functionalized lipids available, recombinant human tissue factor was relipidated into custom functionalized liposomes according to previously published methods [74]. Briefly, lipid mixtures of the desired final molar ratio were mixed well in chloroform, followed by drying to a lipid film under vacuum for at least 4 hours. After removal of the solvent, the film was rehydrated by incubating in HBS overnight at 4 °C. Liposomes were formed by thorough vortexing of the rehydrated

lipid film. The non-ionic lipid detergent 3-[(3-Cholamidopropyl)dimethylammonio]-1-propanesulfonate (CHAPS, Pierce, Rockford, IL) was used to solubilized the liposomes which were mixed with purified recombinant human tissue factor (expressed in *S. frugiperda*, EMD Biosciences, Gibbstown, NJ). The detergent was dialyzed away by placing the solution in a 10 kDa cutoff membrane dialysis cartridge (Pierce, Rockford, IL) and exchanging against three changes of 1 L HBS, allowing each to equilibrate for 12 hours at 4 °C. Following dialysis, the relipidated protein was stored at -20 °C until used.

The activity of the tissue factor was evaluated using a three component purified system. Equal volumes of relipidated tissue factor was added to a 96 well plate containing varying amounts of activated Factor VII (FVIIa, Haematologic Technologies, Essex Junction, VT) along with a fixed concentration of the fluorogenic substrate Boc-Val-Pro-Arg-AMC (Bachem, Torrance, CA). Fluorescence cleavage of the substrate was monitored every minute for three hours on a fluorescence plate reader (EnvisionII, Perkin Elmer, Waltham, MA). The change in fluorescence was calculated for each time point and best fit to a line. The slopes were then plotted as a function of total VIIa concentration.

4.3.5 Tissue factor immobilization for controlled *in vitro* thrombin generation

In order to localize tissue factor at the site of collagen exposure for focal thrombin production, a series of chemical linkages were employed. There are two design goals for this section: specific targeting of the tissue factor bearing liposomes to the collagen patch and retention of tissue factor activity when bound to the targeted surface. The first technique approach was to use streptavidin-coated beads as a physical linker between the collagen surface and the liposomes. The streptavidin-biotin interaction is extremely specific and effectively irreversible with a dissociation constant $K_d \approx 10^{-14}$ M. Superparamagnetic beads are commercially available, commonly

used for the isolated of biotinylated gene products from cell lysates or releasates, available in a range of sizes. For this work, 1.8 μm superparamagnetic streptavidin-coated beads (Polysciences Inc., Warrington, PA) were used in conjunction with a bench-top magnetic separator (Invitrogen, Carlsbad, CA). Biotinylated liposomes were mixed in a 99:1 molar ratio with a biotinylated antibody (anti-collagen, Type I, biotin conjugated, Chemicon/Millipore, Billerica, MA) and allowed to equilibrate. Particles were then added and allowed to mix under slight agitation at room temperature for 30 min. After the liposomes containing the tissue factor and antibody have equilibrated with the particles, the excess soluble agents are removed by three cycles of magnetic separation and re-suspension in fresh buffer. The second linkage was using the same biotinylated antibody with a direct streptavidin linkage to the biotinylated liposome, utilizing the multi-valency of the streptavidin molecule. For those experiments used with a soluble streptavidin linker, fluorescently labeled streptavidin (Streptavidin-Cy3 from *Streptomyces avidinii*, Sigma-Aldrich, St. Louis, MO) was used.

4.3.6 Shear effects on thrombus formation

In order to investigate the results of a short exposure to pathologically high shear rates, devices were designed and fabricated. Numerical simulations were performed as previously described in Section 3.3.7, utilizing symmetry conditions at both the x-y and x-z centerlines in order to increase grid density within the desired region. Grid independence was confirmed again by Richardson extrapolation [86]. Fluorescent-conjugated antibodies used to stain for the presence of adsorbed vWF (anti-von Willebrand Factor (FITC), Abcam, Cambridge, MA) either to the collagen region or within the formed thrombi. For experiments with platelet free plasma, etylene-diaminetetraacetic acid disodium salt solution (EDTA, Sigma-Aldrich, St. Louis, MO) was used to a final concentration of 5 mM to chelate calcium during phlebotomy, preventing both coagulation and platelet integrin activation. Whole blood

was centrifuged at 2500 g for 15 min, and the supernatant (platelet poor plasma) removed. That sample was subsequently centrifuged at 16,100 g for 15 min to pellet any residual platelets or red blood cells, with the resulting supernatant considered to be platelet free plasma (PFP).

4.4 Results

4.4.1 Tissue factor activity in custom functionalized liposomes

In order to verify the activity and determine the specific amount of active tissue factor presented on the apical surface of the liposomes post-dialysis, a functional assay was performed. The substrate Boc-Val-Pro-Arg-AMC was used, despite its intention as a thrombin specific substrate. The substrate was converted by both FVIIa and the tissue factor FVIIa (TF-VIIa) complex, but at different rates.

$$TF + VIIa \overset{K_{M,1}}{\longleftrightarrow} TF \cdot VIIa \tag{4.1}$$

$$VIIa + VPR - AMC \overset{K_{M,2}}{\longleftrightarrow} VIIa \cdot VPR - AMC \overset{k_2}{\longrightarrow} VIIa + AMC \tag{4.2}$$

$$TF{\cdot}VIIa + VPR - AMC \overset{K_{M,3}}{\longleftrightarrow} TF{\cdot}VIIa{\cdot}VPR - AMC \overset{k_3}{\longrightarrow} TF{\cdot}VIIa + AMC \tag{4.3}$$

The reaction network is shown in Equations 4.1, 4.2, 4.3. Reaction progress is monitored by measuring the fluorescence of the AMC group upon cleavage from the peptide substrate.

This conversion is shown in Figure 4.1 and the cleavage rate increases linearly with the FVIIa concentration as shown in Figure 4.2.

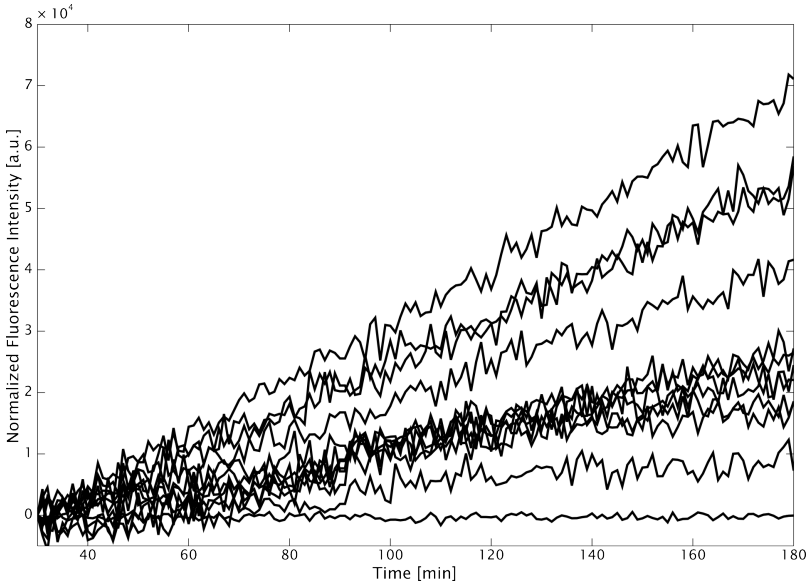

Figure 4.1: Fluorescence traces of the cleavage of AMC from the peptidyl substrate Boc-Val-Pro-Arg-AMC by a range of concentrations of purified FVIIa.

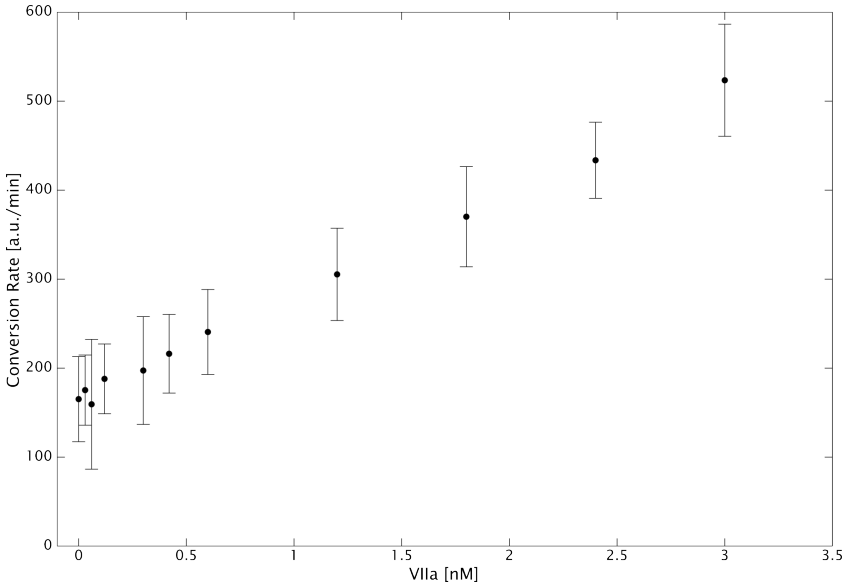

Figure 4.2: FVIIa concentration dependent substrate cleavage of fluorogenic substrate (n = 8).

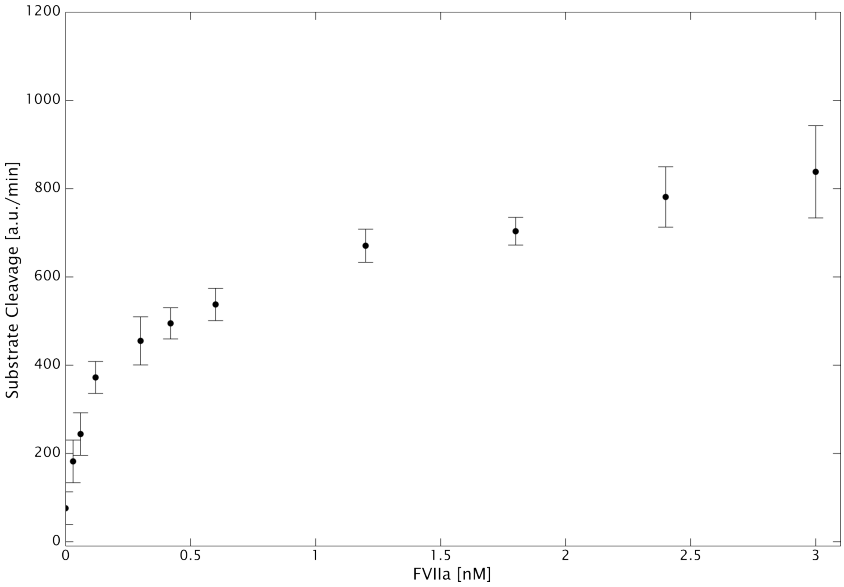

Figure 4.3: TF-catalyzed FVIIa-mediated substrate cleavage of fluorogenic substrate, with blank liposomes at the same concentration (n = 8).

When the FVIIa enzyme is in the TF-VIIa complex assembled on the surface of a phospholipid vesicle, this cleavage rate increases significantly, as shown in Figure 4.3. The infection point, at approximately 0.5 nM of FVIIa, indicates the concentration of tissue factor in the system, as explained by Equations 4.1, 4.2, 4.3, with $K_{M,3} > K_{M,2}$ and $k_2 < k_3$.

This effect was not due to the lipid from the tissue factor, as shown in Figure 4.4. By examining the inflection point of the conversion rate with added FVIIa, it was possible to estimate within a factor of two the active concentration of tissue factor incorporated into the liposomes. This concentration corresponded to approximately half of the molar concentration of molecular tissue factor introduced prior to dialysis. This decrease of expected concentration is due to the equal probability of the tissue factor protein incorporating into the membrane with its active surface on the apical and basolateral surfaces of the liposome during formation.

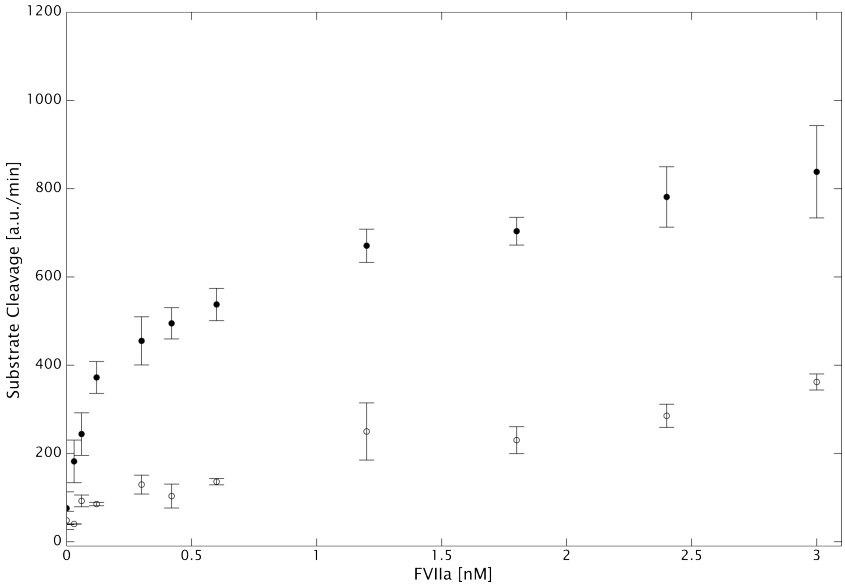

Figure 4.4: TF-catalyzed FVIIa-mediated substrate cleavage of fluorogenic substrate, with blank liposomes at the same concentration shown in open circles with tissue factor liposomes in filled circles (n = 8).

4.4.2 Tissue factor immobilization on beads for *in vitro* thrombin generation

Characterizing the amount of tissue factor immobilized on the streptavidin-coated superparamagnetic particles was the first step in utilizing them for surface-initiated thrombin generation. While it would have been ideal to use the same activity assay used to characterize the free liposomes, the number of particles required for significant signal would be prohibitive even in the case of ideal liposome-particle binding. In order to circumvent this issue, the self-amplification of thrombin production in whole blood as the result of tissue factor initiation was used. A well-plate based assay, using 10x diluted whole blood drawn into sodium citrate (to chelate calcium) and CTI (to block contact-pathway-dependent FXIIa formation and subsequent FX-ase activity), was re-calcified after mixing with varying concentrations of either TF bound to particles or in free liposomes. Thrombin formation was measured using Boc-VPR-AMC cleavage at known kinetic rates. Thrombin formation was distilled

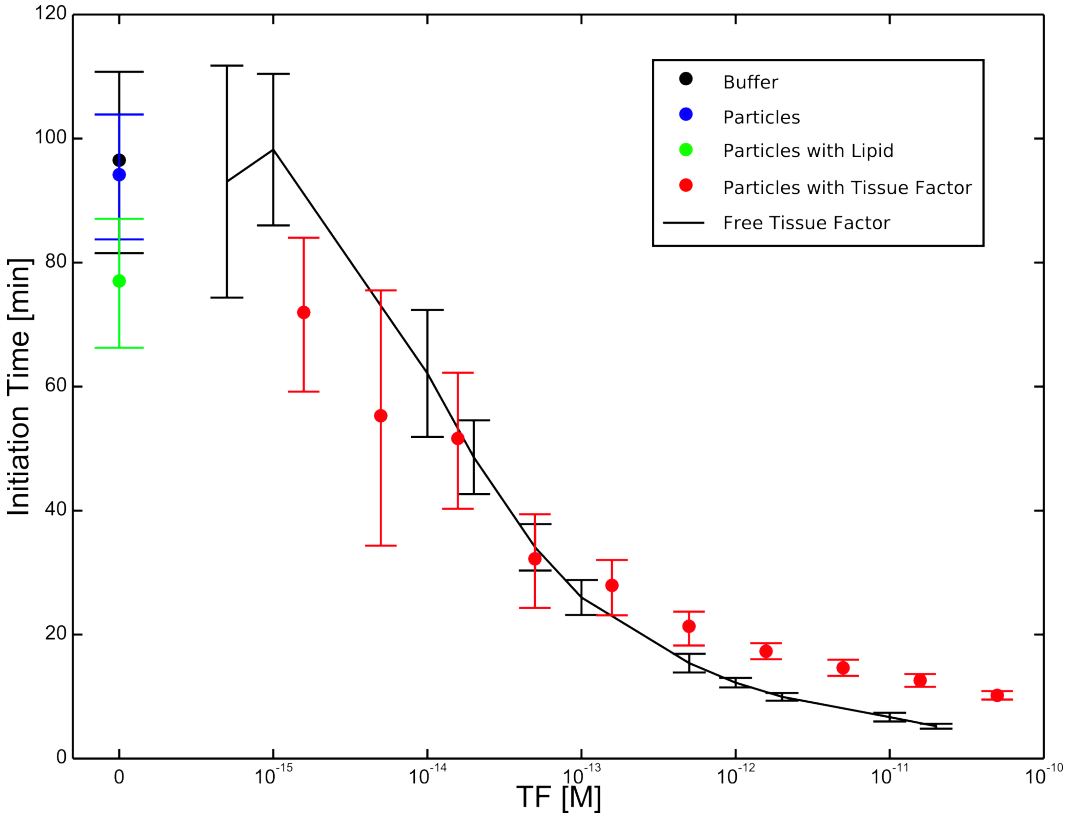

Figure 4.5: Initiation time measurements for determining particle-bound tissue factor concentrations. Conversion of 5 % of Boc-VPR-AMC was set to be the initiation time (n = 8).

to an initiation time, or the time at which 5% of the substrate was cleaved.

The results of the initiation time experiments are shown in Figure 4.5. From this data, it is possible to approximate the concentration of active tissue factor molecules at 350 molecules per particle, or a tissue factor density of 35 molecules per μm^2 of bead surface. This value is well within the range of published reports for active tissue factor concentrations under flow [79]. It is interesting to note in Figure 4.5 that the inclusion of lipids without active tissue factor to the assay results in a slight, yet statistically insignificant, decrease in initiation time. This is in concert with the prevailing notion that negatively charged phospholipid surface is, to an extent, one of the limiting reagents in this assay.

Once the particles were fully characterized, their ability to specifically bind to

micropatterned collagen was evaluated. Soluble human type I collagen was allowed to polymerize on a Sigmacote-treated glass slide for approximately 3 hr as described in Sections 2.3.3 and 3.3.2. Following collagen formation, the patterning device was rinsed with ∼100 μL of 0.5 % BSA in HBS. Loaded particles were then diluted to approximately 10^7 particles/mL and allowed to fill the channel at a controlled flow rate of 5 μL/min.

As can be seen in Figure 4.6, the particles co-localize with the collagen strip, but there is uneven distribution of particles across the surface of the collagen. Secondly, the particles tend not to adhere to the collagen as single, independent particles, but rather as aggregates of various sizes. Adjustments in antibody:TF:particle ratios were made in order to sample some of the available operating space to solve these problems, however none was successful. Slight improvements in coating homogeneity were accomplished by cycling bulk flow of particles on and off through the channel at 30 min intervals, essentially filling the channel space with particles, allowing them to encounter and bind to the collagen. Alleviation of particle aggregation was attempted by including low concentrations (0.1 to 1%) of a low molecular weight (2,000 Da) poly(ethylene glycol) during lipid and antibody binding. This slightly mediated some of the particle aggregate formation, but nonspecifically adsorbed to the collagen once introduced to the channel, quenching its biological affinity and activation of platelets when exposed under whole blood flow.

The activity of the tissue factor immobilized on targeted beads on a collagen surface was examined in several ways. The first attempts to flow recalcified plasma over the beads at a low flow rate were unsuccessful. There are a number of reasons that would explain this, namely the relatively small amount of lipid surface area for coagulation complex assemblies, specifically extrinsic prothrombinase (XaVa). Attempts were made to visualize both fibrin formation and cleavage of Boc-VPR-ACM by epifluorescence, but neither readout revealed any activity. The next attempt was to perfuse whole blood that had been treated with CTI only to inhibit the

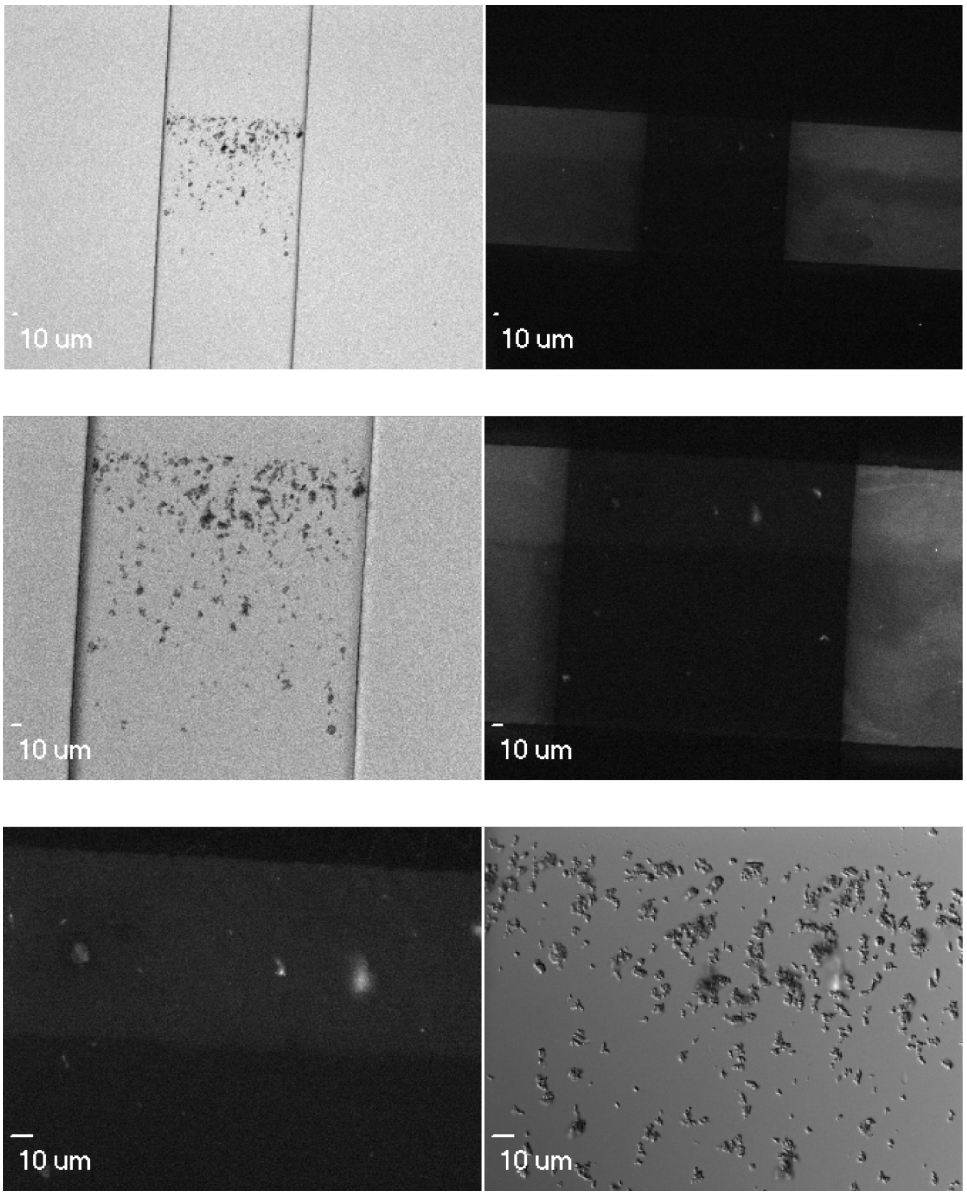

Figure 4.6: Micrograph of streptavidin-coated superparamagnetic beads linked to tissue-factor containing biotinylated liposomes and biotinylated anti-collagen antibody localized on micropatterned human type I collagen. The left channel shows the fluorescently labeled collagen, with differential interference contrast micrograph of the beads on the right at three magnifications (10X, 20X, and 40X from top to bottom).

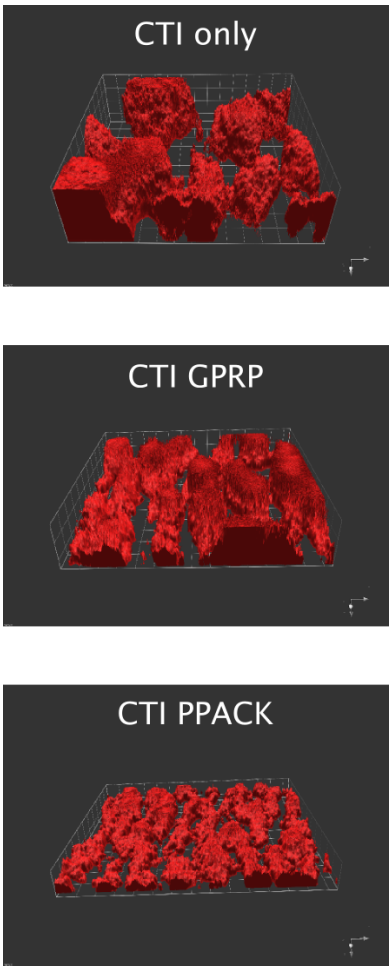

Figure 4.7: Confocal reconstructions of thrombi formed on collagen and tissue factor coated particles. Flow is from from to back with 10 μm grids.

contact pathway over the TF beads on the collagen surface. Platelet adhesion to the collagen was minimally affected when monitored with AlexaFluor 647 anti-CD41 antibody signal compared with a purely collagen surface.

As can be seen in Figure 4.7, even in the presence of fibrin polymerization inhibitor Gly-Pro-Arg-Pro (GPRP), the platelet thrombus volume is higher in the sample with thrombin production allowed compared to the thrombin inhibitor PPACK.

The fibrin forming capability of the tissue factor on the particles is shown in Figure 4.8. Clearly the tissue factor on the beads has initiated enough of the coagulation cascade to produce significant amounts of thrombin and therefore form fibrin fibers.

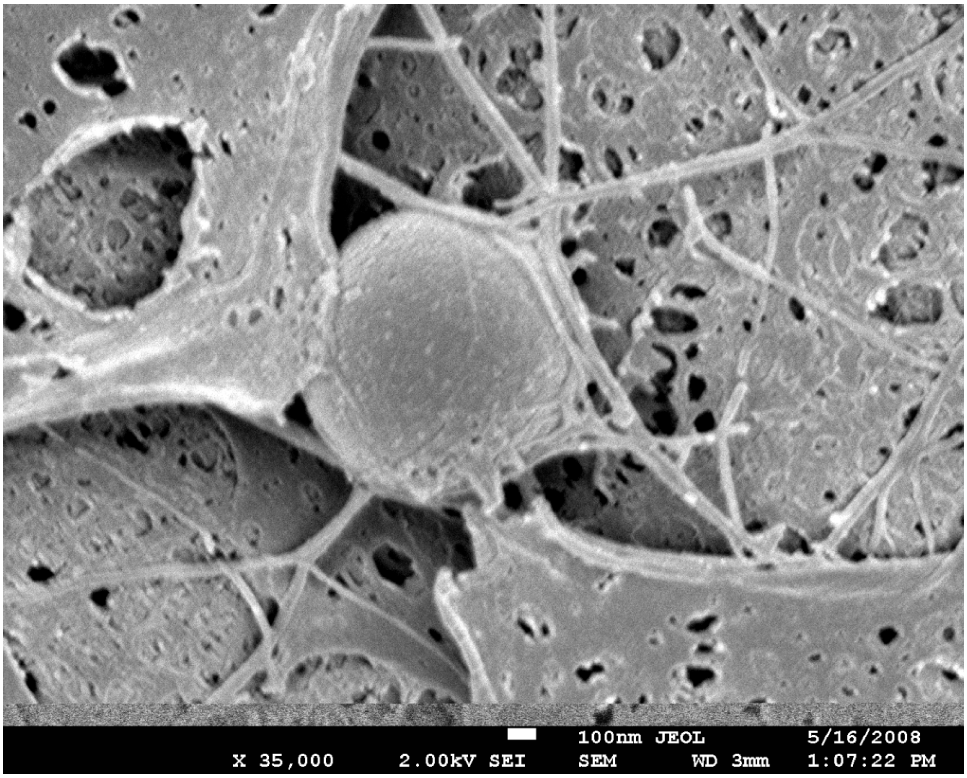

Figure 4.8: Scanning electron micrograph of fibrin formed around tissue factor coated particle, flow from left to right.

However, these experimental results were difficult to duplicate and necessarily hard to quantify.

4.4.3 Direct tissue factor immobilization on collagen for *in vitro* thrombin generation

Due to the problematic nature of getting even tissue factor bearing bead distribution on the collagen surface, a second more simplistic approach was used. Capitalizing again on the specificity and irreversibility of the streptavidin-biotin bond, a layer-by-layer approach was taken. After the collagen film was formed, sequential solutions containing biotinylated anti-collagen antibody (various dilutions), soluble streptavidin (10 μg/mL), and biotinylated relipidated tissue factor ($\sim$ 2 nM) separated by rinses in 0.5 % BSA in HBS were performed. In order to investigate the effectiveness of using the bulk antibody concentration to control the extent of surface coverage with the streptavidin, and subsequently the tissue factor, a titration of the antibody was performed using the fluorescent streptavidin binding as the readout.

As is shown in Figure 4.9, there is a marked decrease in fluorescence at the collagen region with increasing antibody dilution, indicating that controlling the bulk concentration gives a handle on the amount of antibody coverage. The activity of the streptavidin-linked tissue factor was evaluated by perfusing human blood over a collagen strip coated with antibody diluted at 1:1000 in 0.5% BSA in HBS, which appeared in Figure 4.9 to give an relatively high (approximately 5 % surface coverage) coating.

As is seen in Figure 4.10, the thrombi formed with active tissue factor at the surface in addition to collagen grow to significantly larger size. However, the most striking difference between thrombi formed on collagen alone and those formed with surface-immobilized tissue factor is the stability of those thrombi. It is clear that by 20 min, all of the thrombi had embolized from the collagen region. This behavior was observed even at antibody dilutions of $1{:}10^5$, or less than 1 % surface coverage

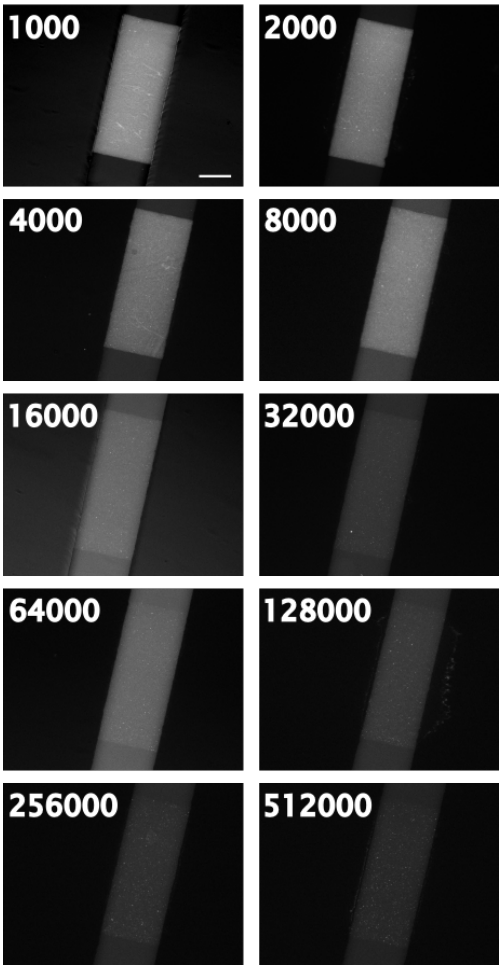

Figure 4.9: Micrographs of Cy3-streptavidin bound to biotinylated anti-collagen antibody on a collagen surface, exhibiting dose-dependent fluorescence, with the ratio of 0.5 % BSA in HBS to antibody indicated by the number in the upper left of each image (scale bar is 50 μm).

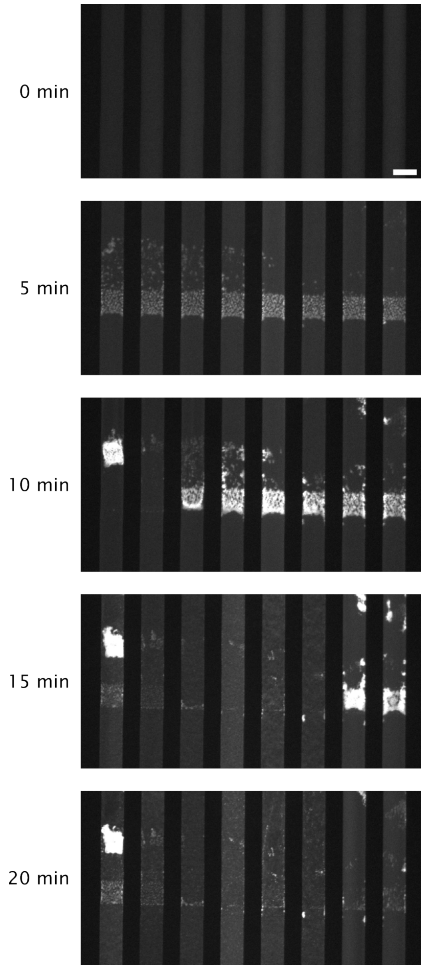

Figure 4.10: Micrographs of thrombi forming on a tissue factor coated collagen surface. Flow is from bottom to top at an average wall shear rate of 210 sec^{-1} (scale bar is 500 μm, CTI human whole blood).

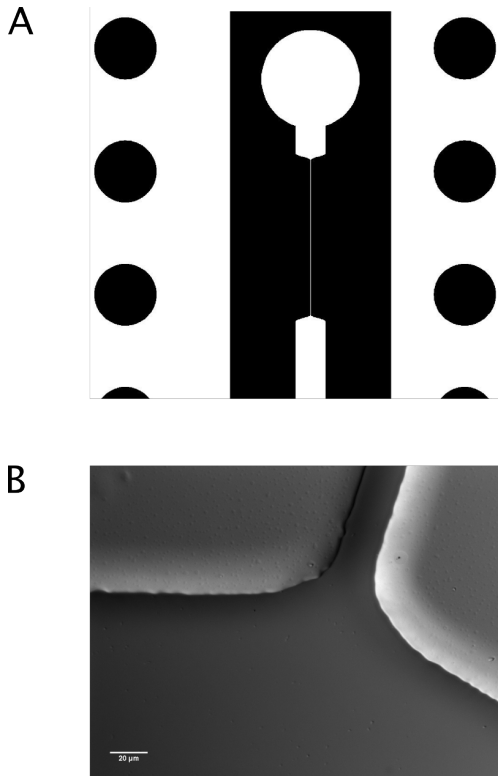

Figure 4.11: A. CAD design of stenosis device, with 500 μm wide inlet and outlet regions surrounding a 10 μm wide stenosis region, in this case 2.5 mm long. B. Differential interference contrast micrograph of the inlet section of a finished device.

of the lipid.

4.4.4 Characterization of stenosis mimetic device

To investigate the extent to which flow history has on the adsorption of vWF and the accumulation of platelets on collagen, a set of microfluidic devices were designed as stenosis mimetics.

The design that accomplished this is shown in Figure 4.11. Similar designs were fabricated with stenosis lengths of 1, 2.5, and 5 mm, each of which had a width of 10 μm with inlet and outlet widths of 500 μm. Among the key design criteria of this device was to ensure that the flow profiles through the inlet and outlet regions of the stenosis did not result in flow separation and recirculation zones. While

these complicated fluid dynamics may occur *in vivo*, especially in the case of stent placement for percutaneous coronary intervention [50], the first approximation of atherosclerotic blockages are relatively gradual increases and decreases in effective luminal cross-section, hence the assumption of fully-developed, laminar (at least pre- and post-stenosis) flow. In order to confirm the desired gentle inlet and outlet of the stenosis mimetic, a series of computational fluid dynamics simulations were performed.

As seen in Figure 4.12A, the fluid dynamics simulations indicate that streamlines enter and exit the stenosis region with smoothed, continuous traces. Figure 4.12B indicates that the shear rate in the stenosis region decreases rapidly at the expansion zone back to that found in a non-stenosed device of the same (500 μm) width within 500 μm of the stenosis exit. To confirm the indications of the mathematical modeling, fluorescent 1.8 μm beads were perfused through the fabricated devices at a controlled flow rate.

The indication of Figure 4.13 is that the stream lines predicted in the calculations are in fact observed in the actual device when operating under conditions to be used in experimentation. After confirming the ideality of the inlet and outlet regions of the stenosis zone, the device was used to investigate the effect of flow history on thrombus formation. This was performed by utilizing flow channels that included a 5 mm long stenosis region (10 μm width) with 500 μm wide inlet and outlet regions, and a channel on the same physical device of a constant 500 μm width. The devices used were fabricated to a height of 53 μm. Platelets were labeled as before (3.3.1) while visualization of vWF was attempted using the FITC-conjugated antibody. CTI and PPACK treated human whole blood was perfused at a flow rate of 10 μL/min, corresponding to an average wall shear rate of 1,000 sec^{-1} in the inlet and outlet zones and a shear rate of approximately 50,000 sec^{-1} in the stenosis region across a 500 μm wide collagen patch of human type I collagen.

As is seen in Figure 4.14, the morphology and kinetics of thrombus formation

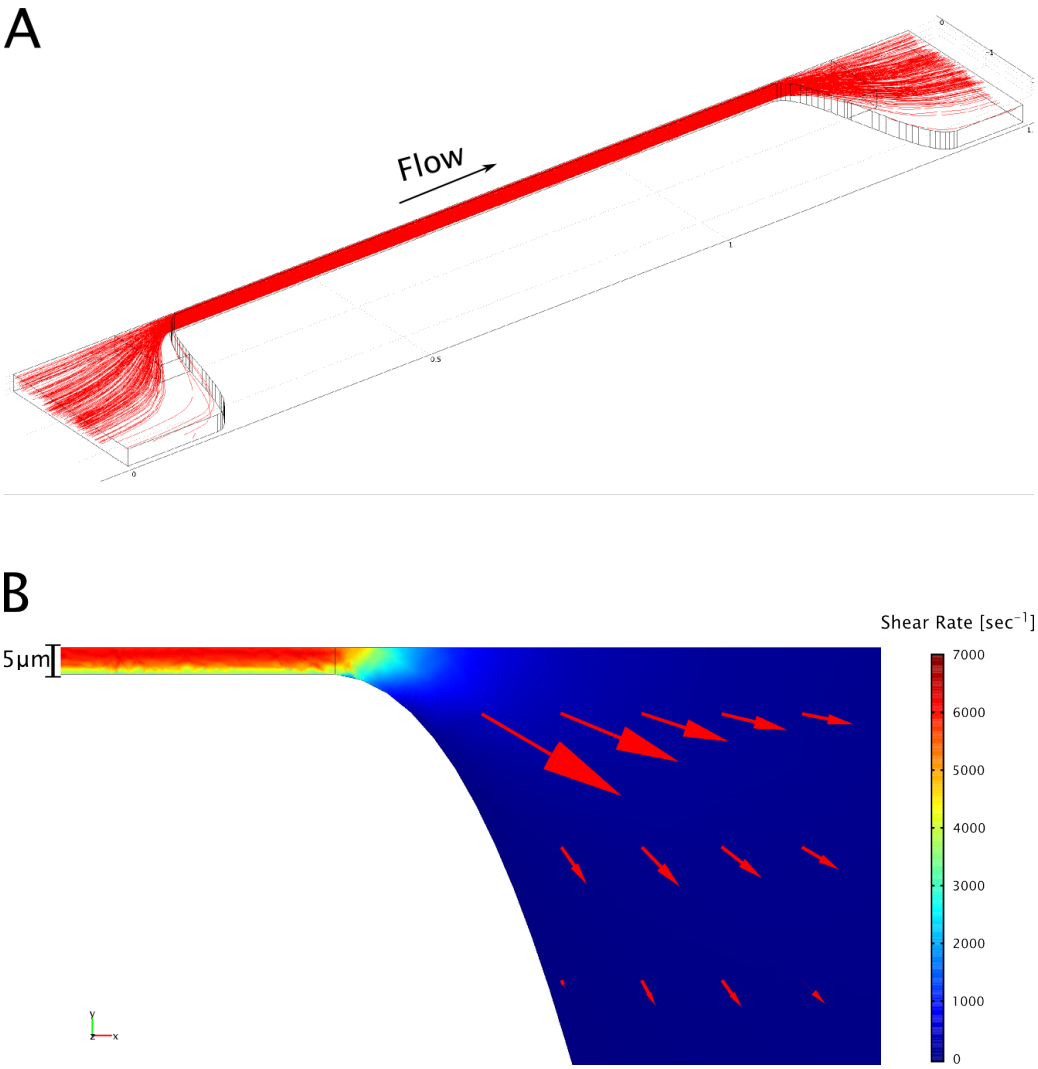

Figure 4.12: A. Streamline approximations of the inlet and outlet regions of the stenosis mimetic device. B. Local shear rate (surface) and velocity field (red arrows) at the outlet of the stenosis region.

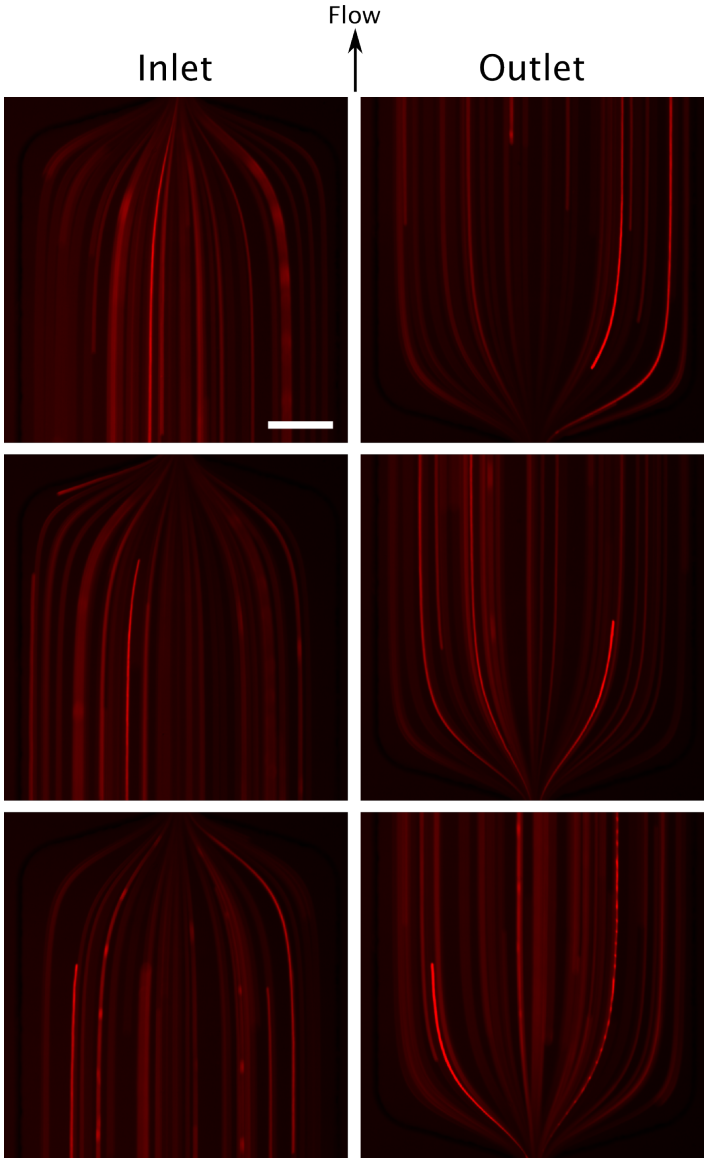

Figure 4.13: Long exposure (5 sec) micrographs of fluorescent beads entering and exiting the stenosis region in a device depicted in Figure 4.11 (2 μL/min flow rate, scale bar is 100 μm).

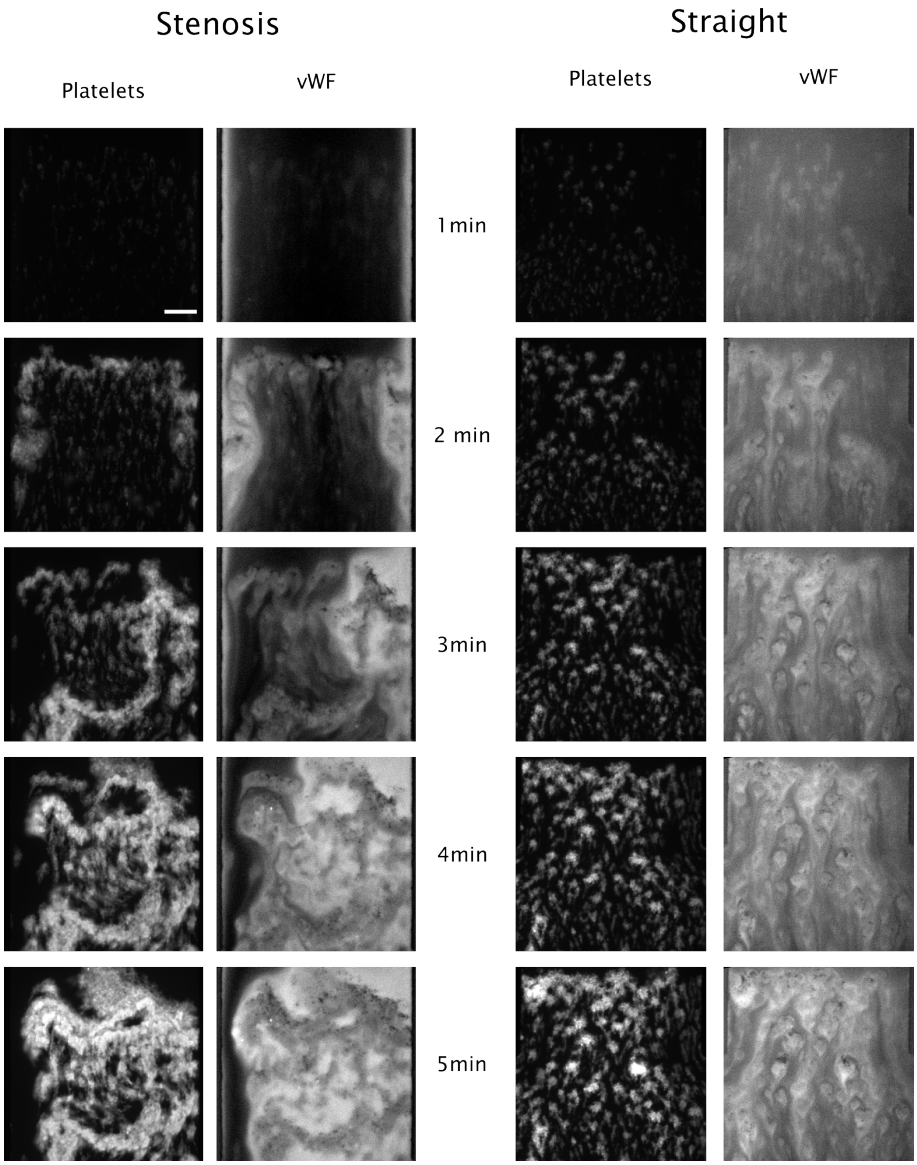

Figure 4.14: Time course of platelet and vWF accumulation at the collagen zone of human whole blood either passing through a stenosis region or not. Flow is from top to bottom and scale bar is 100 μm, CTI/PPACK human whole blood.

are relatively different between the same donor blood, on the same collagen, with the only difference being a short, yet very severe, exposure to shear, comparable to what may be found in a severely stenosed coronary artery.

4.5 Discussion

As presented in Chapters 2 and 3, measuring the accumulation of platelets on a collagen surface through a straight channel can lead to novel and interesting insights into the biology of platelet receptors and receptor antagonists. However, there is still a significant gap between the complicated exposure of subendothelial proteins and matrix components that are exposed upon injury. In fact, the composition and type of subendothelium differ throughout the vasculature, depending on the size, location, and purpose of the vessel, as one would expect for such a dynamic and wide-functioning mass contacting system. Additionally, imperfections and geometrical complications of the vascular system are frequently overlooked when investigating the already complicated dynamics of platelet accumulation and thrombus formation. This work begins to delve into the complex yet more realistic arena of injury mimetic systems.

4.5.1 Role of surface-bound tissue factor in *ex vivo* thrombus formation

The ability to immobilize tissue factor on the surface to initiate coagulation has been a challenge in the field of hemostasis research for years. Recently, a number of advances have been made, however each with their own set of limitations. Contact protein arrays [79] have been used to show the dose-dependence of tissue factor to significant fibrin formation under whole blood flow. Other microfluidic methods in conjunction with sophisticated lipid patterning techniques [51, 52, 91, 102] to investigate some of the transport issues that are relevant to active species formation

and transport during clot formation. Other mathematical models have been used to interrogate some of the unknown reaction dynamics that are characteristic of thrombin formation during coagulation processes [39, 28, 27]. Other work has focused on using endothelial cells, treated with a molecule to induce an injury-like response [57], relying on the endothelial cells themselves to release the appropriate soluble factors and express the proper surface antigens to stimulate platelet adhesion and activation.

The most trusted and comprehensive model system of thrombosis to date is the laser-induced cremaster muscle murine model [26, 30]. It had not been until late 2009 that the extent and type of this injury was well understood in terms of what area of subendothelium, what depth into the subendothelial layer, and the resulting thrombus composition and size were with respect to the intensity of the laser injury [43]. While the injury model has been revolutionary in its ability to focally and reliably create similar injuries within the arterioles or venuoles of living mice, this is the first study to truly examine the implications of this type of injury. The authors found that several endothelial cells were completely ablated by the injury, with some of the injuries resulting in tissue destruction several tens of microns into the media of the blood vessel. This injury model system involves the formation of thrombin and the generation of fibrin at the injured vessel wall, as shown in both the original work and multiple subsequent studies. This thrombin generation is mostly likely due to tissue factor exposure to the flowing blood due to the removal of the endothelial cell barrier, and possibly subsequent additions by various blood-borne sources. The important aspect with respect to this work is the fact that not only is tissue factor exposed at a finite location, but also that numerous additional matrix proteins, not the least important collagen, are simultaneously exposed in conjunction with endothelial cell, and in some cases smooth muscle cell, lysate.

In terms of the relevance of the work presented here, there are a number of important differences when compared with previous *ex vivo* model systems. Firstly,

the work utilizing a purified lipid surface, on which the active tissue factor is assembled and allowed to react with either plasma or purified components lacks a number of important variables. Without a collagen substrate, the only activator of platelets would be thrombin formed from the reactive surface, hence deposition and subsequent feedback of platelet activation is severely dampened. Secondly, the use of platelet rich plasma removes the largest cellular fraction of the blood in the red blood cells, which are critical for proper hemodynamic conditions within the vessel, causing numerous alterations to local platelet concentrations and applying forces to other cells during flow. Working with endothelial cell layers may prove to be the next generation of thrombosis model systems, especially with the constant advances of on-chip cell culture and angiogenic practices to essentially grow blood vessels under controlled conditions, on which subsequent experiments could be performed [116]. However, the current technology and robustness of forming proper and repeatable blood vessels *in vitro* are limiting both the realism and reliability of results from such experiments. Perhaps the most realistic model system to date has been the inclusion of tissue factor to other matrix proteins such as collagen and vWF during contact microarray experiments while performed in a parallel plate flow chamber. By allowing human whole blood to encounter a number of proteins which they would be exposed to upon injury in a relatively focal region remains the best realization of a tissue factor-including thrombosis model.

This work has approached a system with a key advantage over that of any other work. Specifically, the ability to specifically measure and control the amount of tissue factor on the surface of a focal exposure to blood in addition to collagen. While the work of [79] attempted to measure concentration effects, the reported concentrations were given in bulk soluble tissue factor concentrations without any knowledge of the amount or extent of active protein remaining on the surface after initial rinsing steps. The advantage with a pseudo layer-by-layer approach to building a tissue factor surface on top of collagen is the ability to control the precise amount of tissue

factor with known activity on the surface, by controlling bead density, antibody coverage, and tissue factor:lipid ratio during relipidation. This control is of the utmost importance when working with a system with such a tight and strong operating threshold such as tissue factor. This switch-like behavior is paramount for its *in vivo* activity, either thrombin must be formed in order to stem blood loss from an injury, or it must not to prevent excessive clot formation and subsequent stasis. The main issue that has arisen in this work with tissue factor on a collagen surface has been the ability of the thrombi formed on the surface to remain. There are a number of potential causes for this, the first of which is simply a lack of completeness of the model system. As noted, the electron microscopy of the injured vessels from the *in vivo* model system show a large section of subendothelium exposed, not simply a region of type I collagen with some purified lipid and protein intermixed. The embolization of the thrombi formed during this work always showed a failure at the collagen-platelet interface. Most likely, this failure was due to a significant fraction of the collagen region being covered by lipid, necessary for the tissue factor's activity. The mechanical failure of the thrombi to remain adherent may also be due to a necessary evil of *ex vivo* hemostasis research, that is the contact pathway. In order to prevent coagulation due to the contact of blood with negatively charged plastic surfaces that it is necessarily in contact with up to the point of perfusion over the collagen strip, inhibitors (CTI) must be used. Recent work has shown that the contact pathway plays a significant role in the attenuation and magnitude of thrombin generation in a collagen-induced injury system [109]. This may be important in continuing thrombin generation to create fully activated and adherent platelets on an otherwise slightly 'slippery' lipid-rich collagen surface.

4.5.2 Effects of shear history on thrombus formation

The second aspect of this work that begins to capitalize on the flexibility and scale of microfluidics is the experimentation with stenotic flow models. It is well known

that the narrowing of arteries, specifically in the coronary vasculature and the blood vessels within the brain, complete blockages of which lead to heart attacks and strokes respectively, are the largest cause of death within the developed world. Perhaps the reason that atherosclerosis as a disease in particular is a promising target for prevention is that it is a chronic condition that occurs as plaques build up over years of improper diet, lack of exercise, and in some cases genetic mutations with faulty or non-existing gene products. This gradual progression of the disease often remains unnoticed until some catastrophic event, either a vessel collapse or plaque rupture and thrombosis, which can either block the blood flow at the site of rupture, or send large and deadly thrombi throughout the vasculature resulting in a range of pathologies. Currently, there are no good means of early detection for patients at risk for atherosclerosis, as imaging technologies continue to attempt to visualize differences in flow without the high collateral damage associated with invasive scope procedures.

The work described with investigating the effects of exposing whole blood to pathologically high shear conditions for very finite periods of time is very promising on a number of accounts. Firstly, it speaks to the very fast mechanisms by which blood can change its state.

Figure 4.15 shows that even 2 μm from the wall, the fluid is moving at approximately half of the maximum velocity, indicating that platelets and plasma in the red cell depleted outer layer experience the high shear in a 5 mm stenosis at 50,000 sec^{-1} for less than 200 ms. This high stress zone is quickly dissipated back out into a physiologically normal 1,000 sec^{-1} where it encounters the injury mimetic collagen strip. What is not immediately obvious from Figure 4.14 is that the thrombi formed after the shear exposure were very prone to thrombosis, similar to those shown in the tissue factor work. The causes are not directly comparable, as no tissue factor or lipid was present in the collagen that was encountered by blood after the stenosis.

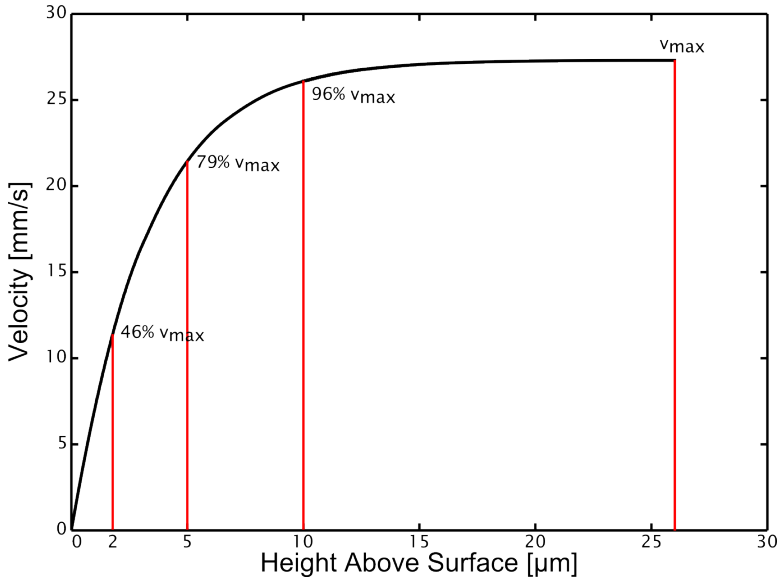

Figure 4.15: A plot of the velocity in the stenosis region across the z-midline.

The platelet aggregates formed on the same collagen preparation without being subjected to the high shear zone formed stable thrombi analogous to control aggregates formed throughout the work.

The implications and potential value of these initial findings are very interesting. Firstly, the cause of the alteration due to shear exposure is of interest. Total transit time post-stenosis is less than 1 sec, indicating that whatever mechanism is leading to altered platelet deposition must occur rapidly, either through a series of messengers with platelets or red cell mediated ATP release. However, a potentially more fundamental and important phenomena may be working on the large vWF multimers found circulating in the blood stream. The soluble protein is constantly in equilibrium with GPIb receptors on the platelet surface while circulating throughout the blood stream with rapid on and off events which prevent further aggregation in unneeded situations. Assuming that this model is correct, as the blood enters the stenosis region, a small but finite fraction of vWF is bound to platelets. If the literature models are correct in that the vWF-GPIb bond is in fact a catch bond, then the high stresses applied during transgression across the stenosis region would

increase the stability of the bond. This high stress on the globular vWF molecule could open up the conformation into an extended, much more hemostatically active molecule. In effect, the platelet transiently bound to the molecule would be acting in a manner similar to a sail, greatly increasing the effective area for shear forces to pull on the condensed quaternary structure of quiescent vWF. This elongated vWF molecule then under goes some relaxation once it exits the stenosis region, however since the collagen region in this work is in close proximity to the outlet of the stenosis, some fraction of the molecules remain in their elongated conformation. This increased vWF deposition on the collagen surface then mediates much more platelet-surface interaction than the collagen alone, leading to larger thrombus formation, and perhaps due to steric coverage of collagen sites required for full signaling and platelet activation, less stable thrombi.

If exposure, even for a very brief amount of time, to high shear can cause a conformational change for vWF into an elongated form, there are several interesting avenues to be pursued. Most striking would be the use of elongated vWF multimers as markers of atherosclerosis progression and even location. By sampling the amount and relative state of vWF multimers circulating in a patient's blood stream from different locations throughout the body (immediately before and after athero-prone zones such as the aortic arch or coronary arteries), it may be possible to determine both the extent and the relative location of dangerous atherosclerotic lesions in a manner much less invasive than current imaging modalities provide. As a biomaker of overall vascular tone, elongated vWF levels may aid those at higher risk for atherosclerosis, or those with known cases of atherosclerosis, to monitor the progression or regression of the disease with a simple blood-based analysis.

4.6 Conclusions

This chapter has outlined some of the secondary alterations to both the initial (surface) and inlet (flow history) conditions of the blood that encounters a reactive surface. While this system is far from ideal and the *in vivo* model systems from which it is modeled, the strengths of continual improvement and iterative design principals are touched on. Improvements in injury mimetic, with the introduction of a tissue factor source that is both repeatable and directly titratable remains the logical and critical next step in building a thrombosis model system that can incorporate both the coagulation cascade and platelet activation simultaneously but in balance with the other. In addition, using known physiological and pathological conditions as design inspiration in concert with the flexible and precise fabrication method that soft lithography and replicate molding offers, it is possible to extract new biological behavior from systems that may be occurring and naturally reporting on flow conditions throughout the body. Investigating the wide range of secondary surface and flow interactions provides a rich area for further work with thrombosis in microfluidic model systems.

4.7 Future Work

Among the most immediate goals for furthering the understanding of secondary modifications to both the injury mimetic surface and the flow geometry, the successful development of a repeatable and controllable tissue factor source remains the most important. A lack of thorough understanding about the specific location, distribution, and form of tissue factor exposed to blood during an injury even has not aided, but does not serve as an excuse for the unsuccessful development of a surface bound tissue factor model injury. Perhaps the single most difficult obstacle to overcome is the functional necessity of tissue factor to be incorporated into a lipid membrane bilayer for biological activity. While other groups have continued to experiment with

new and exciting formulations of active tissue factor [68], the ability to create a robust thrombosis model that includes surface immobilized tissue factor remains a goal of the hemostasis community. The simplicity of protein micropatterning lends itself to this problem, insofar as any series of fluid phase species are easily introduced to the surface in series or parallel in order for proper assembly and retention of hemostatic activity for all components involved, specifically collagen signaling and tissue factor activity.

The initial worked laid out for the use of stenosis-like flow patterns to investigate the potential shear-induced opening of vWF molecules into extended confirmation likewise has many avenues for further investigation. Initial attempts were made to visualize extended vWF multimers in platelet free or platelet rich plasma, however with the current detection systems no strands were visualized. Previous work has shown that vWF strands can assemble on collagen [7], however the difference with this work is that the vWF in our system only experiences high shear rates while inside the stenosis region while the capture occurs at a lower shear rate. Direct visualization of these extended confirmation vWF multimers would be the first step towards their utilization as potential biomarkers of atherosclerotic progress. A second interesting arena for further study would be in the stability of thrombi formed after exposure to a shear insult. Sorting out the exact mechanism of the mechanical instability when compared to unsheared blood may further lead down avenues that explain thrombi vulnerabilities in individuals.

Bibliography

[1] P. A. Aarts, S. A. van den Broek, G. W. Prins, G. D. Kuiken, J. J. Sixma, and R. M. Heethaar. Blood platelets are concentrated near the wall and red blood cells, in the center in flowing blood. *Arteriosclerosis*, 8(6):819–24, 1988.

[2] G. A. Adams and I. A. Feuerstein. Maximum fluid concentrations of materials released from platelets at a surface. *Am J Physiol*, 244(1):H109–14, 1983.

[3] J. Ahamed, H. H. Versteeg, M. Kerver, V. M. Chen, B. M. Mueller, P. J. Hogg, and W. Ruf. Disulfide isomerization switches tissue factor from coagulation to cell signaling. *Proc Natl Acad Sci U S A*, 103(38):13932–7, 2006.

[4] R.R. Bach. Tissue factor encryption. *Atherioscler Thromb Vasc Biol*, 26(3):456–61, 2006.

[5] L. Badimon, J.J. Badimon, V.T. Turitto, S. Vallabhajosul, and V. Fuster. Platelet thrombus formation on collagen type i. a model of deep vessel injury. influence of blood rheology, von willebrand factor, and blood coagulation. *Circulation*, 78(6):1431–42.

[6] V. Balasubramanian, E. Grabowski, A. Bini, and Y. Nemerson. Platelets, circulating tissue factor, and fibrin colocalize in ex vivo thrombi: real-time fluorescence images of thrombus formation and propagation under defined flow conditions. *Blood*, 100(8):2787–92, 2002.

[7] A. Barg, R. Ossig, T. Goerge, M.F. Schneider, H. Schillers, H. Oberleithner, and S.W. Schneider. Soluble plasma-derived von willebrand factor assembles into a haemostatically active filimentous network. *Thromb Haemost*, 97(4):514–26, 2007.

[8] H. R. Baumgartner. The role of blood flow in platelet adhesion, fibrin deposition, and formation of mural thrombi. *Microvasc Res*, 5(2):167–79, 1973.

[9] A. Baurand, P. Raboisson, M. Freund, C. Leon, J.P. Cazenave, J.J. Bourguignon, and C. Gachet. Inhibition of platelet function by administration of mrs2179, a p2y1 antagonist. *Eur J Pharmacol*, 412(3):213–21, 2001.

[10] D. L. Bhatt and E. J. Topol. Scientific and therapeutic advances in antiplatelet therapy. *Nat Rev Drug Discov*, 2(1):15–28, 2003.

[11] R. Byron Bird. *Transport phenomena*. Wiley, New York, 1960.

[12] L. F. Brass, L. Zhu, and T. Stalker. Novel therapeutic targets at the platelet-vascular interface for arteriosclerosis, thrombosis, and vascular biology. *Arterioscler Thromb Vasc Biol*, 2008.

[13] S. Butenas and K. G. Mann. Active tissue factor in blood? *Nat Med*, 10(11):1155–6; author reply 1156, 2004.

[14] E. Camaioni, J.L Boyer, A. Mohanram, T.K. Harden, and K.A. Jacobson. Deoxyadenosine bisphosphate derivates as potent antagonists at p2y1 receptors. *J Med Chem*, 41(2):183–190, 1998.

[15] J. Chen, T. G. Diacovo, D. G. Grenache, S. A. Santoro, and M. M. Zutter. The alpha(2) integrin subunit-deficient mouse: a multifaceted phenotype including defects of branching morphogenesis and hemostasis. *Am J Pathol*, 161(1):337–44, 2002.

[16] P.F. Davies. Flow-mediated endothlial mechanotransduction. *Physiol Rev*, 75(3):519–60, 1995.

[17] G. Del Campo, J. Puente, M. A. Valenzuela, A. Traverso-Cori, and O. Cori. Hydrolysis of synthetic pyrophosphoric esters by an isoenzyme of apyrase from solanum tuberosum. *Biochem J*, 167(3):525–9, 1977.

[18] T. C. Detwiler and R. D. Feinman. Kinetics of the thrombin-induced release of adenosine triphosphate by platelets. comparison with release of calcium. *Biochemistry*, 12(13):2462–8, 1973.

[19] Crikis S Dwyer K Selan C Robson S D'Apice A Cowan P Nandurkar H Dezfouli S, Zhang X. Development of rsolcd29-psgl as a novel therapeutic with anti-thrombotic and anti-inflammatory effects. *XXII Congress of the International Society on Thormbosis and Haemostasis*, pages Session AS–TH–025, 2009.

[20] S. L. Diamond, S. G. Eskin, and L. V. McIntire. Fluid flow stimulates tissue plasminogen activator secretion by cultured human endothelial cells. *Science*, 243(4897):1483–5, 1989.

[21] T. A. Doggett, G. Girdhar, A. Lawshe, J. L. Miller, I. J. Laurenzi, S. L. Diamond, and T. G. Diacovo. Alterations in the intrinsic properties of the gpibalpha-vwf tether bond define the kinetics of the platelet-type von willebrand disease mutation, gly233val. *Blood*, 102(1):152–60, 2003.

[22] D. C. Duffy, J. C. McDonald, O. J. A. Schueller, and G. M. Whitesides. Rapid prototyping of microfluidic systems in poly(dimethylsiloxane). *Analytical Chemistry*, 70(23):4974–4984, 1998.

[23] J. J. Dumas, R. Kumar, T. McDonagh, F. Sullivan, M. L. Stahl, W. S. Somers, and L. Mosyak. Crystal structure of the wild-type von willebrand factor a1-glycoprotein ibalpha complex reveals conformation differences with a complex

bearing von willebrand disease mutations. *J Biol Chem*, 279(22):23327–34, 2004.

[24] K. M. Dwyer, S. C. Robson, H. H. Nandurkar, D. J. Campbell, H. Gock, L. J. Murray-Segal, N. Fisicaro, T. B. Mysore, E. Kaczmarek, P. J. Cowan, and A. J. d'Apice. Thromboregulatory manifestations in human cd39 transgenic mice and the implications for thrombotic disease and transplantation. *J Clin Invest*, 113(10):1440–6, 2004.

[25] M.L. Ellsworth, T. Forrester, C.G. Ellis, and H.H. Dietrich. The erythrocyte as a regulator of vascular tone. *Am J Physiol*, 269(6 Pt 2), 1995.

[26] S. Falati, P. Gross, G. Merrill-Skoloff, B. C. Furie, and B. Furie. Real-time in vivo imaging of platelets, tissue factor and fibrin during arterial thrombus formation in the mouse. *Nat Med*, 8(10):1175–81, 2002.

[27] A. L. Fogelson and N. Tania. Coagulation under flow: The influence of flow-mediated transport on the initiation and inhibition of coagulation. *Pathophysiol Haemost Thromb*, 34(2-3):91–108, 2005.

[28] B. J. Folie, L. V. McIntire, and A. Lasslo. Effects of a novel antiplatelet agent in mural thrombogenesis on collagen-coated glass. *Blood*, 72(4):1393–400, 1988.

[29] M. Franchini and P.M. Mannucci. Von willebrand factor: Another janus-faced hemostasis protein. *Semin Thromb Hemost*, 34(7):663–9, 2008.

[30] B. Furie and B. C. Furie. Thrombus formation in vivo. *J Clin Invest*, 115(12):3355–62, 2005.

[31] B. Furie and B. C. Furie. Mechanisms of thrombus formation. *N Engl J Med*, 359(9):938–49, 2008.

[32] C. Gachet. The platelet p2 receptors as molecular targets for old and new antiplatelet drugs. *Pharmacol Ther*, 108(2):180–92, 2005.

[33] C. Gachet. Regulation of platelet functions by p2 receptors. *Annu Rev Pharmacol Toxicol*, 2005.

[34] P. L. Giesen, U. Rauch, B. Bohrmann, D. Kling, M. Roque, J. T. Fallon, J. J. Badimon, J. Himber, M. A. Riederer, and Y. Nemerson. Blood-borne tissue factor: another view of thrombosis. *Proc Natl Acad Sci U S A*, 96(5):2311–5, 1999.

[35] M. S. Goel and S. L. Diamond. Factor viia-mediated tenase function on activated platelets under flow. *J Thromb Haemost*, 2(8):1402–10, 2004.

[36] H. L. Goldsmith and V. T. Turitto. Rheological aspects of thrombosis and haemostasis: basic principles and applications. icth-report–subcommittee on rheology of the international committee on thrombosis and haemostasis. *Thromb Haemost*, 55(3):415–35, 1986.

[37] E. F. Grabowski, J. T. Franta, and P. Didisheim. Platelet aggregation in flowing blood in vitro. ii. dependence of aggregate growth rate on adp concentration and share rate. *Microvasc Res*, 16(2):183–95, 1978.

[38] Edgar Gutierrez, Brian G. Petrich, Sanford J. Shattil, Mark H. Ginsberg, Alex Groisman, and Ana Kasirer-Friede. Microfluidic devices for studies of shear-dependent platelet adhesion. *Lab on a Chip*, 8(9):1486–1495, 2008.

[39] J. J. Hathcock and Y. Nemerson. Platelet deposition inhibits tissue factor activity: in vitro clots are impermeable to factor xa. *Blood*, 104(1):123–7, 2004.

[40] C. L. Haycox, B. D. Ratner, and T. A. Horbett. Photoenhancement of platelet adhesion to biomaterial surfaces observed with epifluorescent video microscopy (evm). *J Biomed Mater Res*, 25(10):1317–20, 1991.

[41] B. Hechler, M. Cattaneo, and C. Gachet. The p2 receptors in platelet function. *Semin Thromb Hemost*, 31(2):150–61, 2005.

[42] B. Hechler, N. Lenain, P. Marchese, C. Vial, V. Heim, M. Freund, J. P. Cazenave, M. Cattaneo, Z. M. Ruggeri, R. Evans, and C. Gachet. A role of the fast atp-gated p2x1 cation channel in thrombosis of small arteries in vivo. *J Exp Med*, 198(4):661–7, 2003.

[43] B. Hechler, C. Nonne, A. Eckly, S. Magnenat, J.-Y. Rinckel, C.V. Denis, M. Freund, J.-P. Cazenave, F. Lanza, and C. Gachet. Arterial thrombosis: relevance of a model with two levels of severity assessed by histological, ultrastructural, and functional characterization. *J Thromb Haemost*, pages DOI: 10.111/j.1538–7836.2009.03666.x, 2009.

[44] J. M. Higgins, D. T. Eddington, S. N. Bhatia, and L. Mahadevan. Sickle cell vasoocclusion and rescue in a microfluidic device. *Proc Natl Acad Sci U S A*, 104(51):20496–500, 2007.

[45] H. Holmsen and H. J. Weiss. Secretable storage pools in platelets. *Annu Rev Med*, 30:119–34, 1979.

[46] J. Hua, S. Suguro, K. Iwabuchi, Y. Tsutsumi-Ishii, K. Sakamoto, and I. Nagaoka. Glucosamine, a naturally occurring amino monosaccharide, suppresses the adp-mediated platelet activation in humans. *Inflamm Res*, 53(12):680–8, 2004.

[47] J. A. Hubbell and L. V. McIntire. Platelet active concentration profiles near growing thrombi. a mathematical consideration. *Biophys J*, 50(5):937–45, 1986.

[48] S. P. Jackson and S. M. Schoenwaelder. Antiplatelet therapy: in search of the 'magic bullet'. *Nat Rev Drug Discov*, 2(10):775–89, 2003.

[49] H.M. Jantzen, L. Gousset, V. Bhaskar, D. Vincent, A. Tai, E.E. Reynolds, and P.B. Conley. Evidence for two distinct g-protein-coupled adp receptors mediating platelet activation. *Thromb Haemost*, 81(1):111–7, 1999.

[50] J.M. Jimenez and P.F. Davies. Hemodynamically driven stent strut design. *Ann Biomed Eng*, 37(8):1483–44, 2009.

[51] C. J. Kastrup, M. K. Runyon, F. Shen, and R. F. Ismagilov. Modular chemical mechanism predicts spatiotemporal dynamics of initiation in the complex network of hemostasis. *Proc Natl Acad Sci U S A*, 103(43):15747–52, 2006.

[52] C. J. Kastrup, F. Shen, M. K. Runyon, and R. F. Ismagilov. Characterization of the threshold response of initiation of blood clotting to stimulus patch size. *Biophys J*, 2007.

[53] A.M. Kettlun, L. Uribe, V. Calvo, J. Rivera, M. Mancilla, M.A. Valenzuela, and A. Traverso-Cori. Properties of two apyrases from solanum tuberosum. *Phytochemistry*, 21(3):551–8, 1982.

[54] D. Kirchhofer, T. B. Tschopp, P. Hadvary, and H. R. Baumgartner. Endothelial cells stimulated with tumor necrosis factor-alpha express varying amounts of tissue factor resulting in inhomogenous fibrin deposition in a native blood flow system. effects of thrombin inhibitors. *J Clin Invest*, 93(5):2073–83, 1994.

[55] D. Kohler, T. Eckle, M. Faigle, A. Grenz, M. Mittelbronn, S. Laucher, M. L. Hart, S. C. Robson, C. E. Muller, and H. K. Eltzschig. Cd39/ectonucleoside triphosphate diphosphohydrolase 1 provides myocardial protection during cardiac ischemia/reperfusion injury. *Circulation*, 116(16):1784–94, 2007.

[56] S. Konstantinides, J. Ware, P. Marchese, F. Almus-Jacobs, D. J. Loskutoff, and Z. M. Ruggeri. Distinct antithrombotic consequences of platelet glycoprotein ibalpha and vi deficiency in a mouse model of arterial thrombosis. *J Thromb Haemost*, 4(9):2014–21, 2006.

[57] C. J. Ku, T. D. Oblak, and D. M. Spence. Interactions between multiple cell types in parallel microfluidic channels: Monitoring platelet adhesion to an endothelium in the presence of an anti-adhesion drug. *Analytical Chemistry*, 80(19):7543–7548, 2008.

[58] S. P. Kunapuli and J. L. Daniel. P2 receptor subtypes in the cardiovascular system. *Biochem J*, 336 (Pt 3):513–23, 1998.

[59] K. D. Kurz, B. W. Main, and G. E. Sandusky. Rat model of arterial thrombosis induced by ferric chloride. *Thromb Res*, 60(4):269–80, 1990.

[60] H.L. Lemmerhirt, J.A. Shavit, G.G. Levy, S.M. Cole, J.C. Long, and D. Ginsburg. Enhanced vwf biosynthesis and elevated plasma vwf due to a natural variant in the murine vwf gene. *Blood*, 108(9):3061–7, 2006.

[61] F. Li, J. L. Moake, and L. V. McIntire. Characterization of von willebrand factor interaction with collagens in real time using surface plasmon resonance. *Ann Biomed Eng*, 30(9):1107–16, 2002.

[62] N. Mackman. Regulation of tissue factor gene. *Faseb J*, 9(10):883–9, 1995.

[63] N. Mackman. Role of tissue factor in hemostasis, thrombosis, and vascular development. *Atheroscler Thromb Vasc Biol*, 24(6):1015–22, 2004.

[64] H. Matsuno, T. Uematsu, S. Nagashima, and M. Nakashima. Photochemically induced thrombosis model in rat femoral artery and evaluation of effects of heparin and tissue-type plasminogen activator with use of this model. *J Pharmacol Methods*, 25(4):303–17, 1991.

[65] E. W. Merrill and G. A. Pelletier. Viscosity of human blood: transition from newtonian to non-newtonian. *J Appl Physiol*, 23(2):178–82, 1967.

[66] Alan Michelson and Alan D. Michelson. *Platelets*. Elsevier Academic Press, Burlington, MA ; San Diego, 2nd edition, 2007.

[67] H. Miyazaki and T. Yamaguchi. Formation and destruction of primary thrombi under the influence of blood flow and von willebrand factor analyzed by a discrete element method. *Biorheology*, 40(1-3):265–72, 2003.

[68] J.H. Morrissey, V. Pureza, R.L. Davis-Harrison, S.G. Sligar, Y.Z. Ohkubo, and E. Tajkhorshid. Blood clotting reactions on nanoscale phospholipid bilayers. *Thromb Res*, 112 Suppl 1:S23–6, 2008.

[69] I.C. Munnix, K. Gilio, P.R. Siljander, N. Raynal, M.A. Feijge, T.M. Hackeng, H. Deckmyn, P.A. Smethurst, R.W. Farndale, and J.W. Heemskerk. Collagen-mimetic peptides mediate flow-dependent thrombus formation by high or low affinity binding of integrin alpha2beta1 and glycoprotein vi. *J Thromb Haemost*, 6(12):2132–42, 2008.

[70] D. D. Nalayanda, M. Kalukanimuttam, and D. W. Schmidtke. Micropatterned surfaces for controlling cell adhesion and rolling under flow. *Biomed Microdevices*, 9(2):207–14, 2007.

[71] K. B. Neeves and S. L. Diamond. A membrane-based microfluidic device for controlling the flux of platelet agonists into flowing blood. *Lab Chip*, 8(5):701–9, 2008.

[72] K. B. Neeves, S. F. Maloney, K. P. Fong, A. A. Schmaier, M. L. Kahn, L. F. Brass, and S. L. Diamond. Microfluidic focal thrombosis model for measuring murine platelet deposition and stability: Par4 signaling enhances shear-resistance of platelet aggregates. *J Thromb Haemost*, 2008.

[73] W. S. Nesbitt, E. Westein, F. J. Tovar-Lopez, E. Tolouei, A. Mitchell, J. Fu, J. Carberry, A. Fouras, and S. P. Jackson. A shear gradient-dependent platelet aggregation mechanism drives thrombus formation. *Nat Med*, 15(6):665–73, 2009.

[74] P. F. Neuenschwander, M. M. Fiore, and J. H. Morrissey. Factor vii autoactivation proceeds via interaction of distinct protease-cofactor and zymogen-cofactor complexes. implications of a two-dimensional enzyme kinetic mechanism. *J Biol Chem*, 268(29):21489–92, 1993.

[75] B. Nieswandt, C. Brakebusch, W. Bergmeier, V. Schulte, D. Bouvard, R. Mokhtari-Nejad, T. Lindhout, J. W. Heemskerk, H. Zirngibl, and R. Fassler. Glycoprotein vi but not alpha2beta1 integrin is essential for platelet interaction with collagen. *Embo J*, 20(9):2120–30, 2001.

[76] L. Novak, H. Deckmyn, S. Damjanovich, and J. Harsfalvi. Shear-dependent morphology of von willebrand factor bound to immobilized collagen. *Blood*, 99(6):2070–6, 2002.

[77] A. T. Nurden. Does atp act through p2x(1) receptors to regulate platelet activation and thrombus formation? *J Thromb Haemost*, 5(5):907–9, 2007.

[78] S. Offermanns. Activation of platelet function through g protein-coupled receptors. *Circ Res*, 99(12):1293–304, 2006.

[79] U. M. Okorie, W. S. Denney, M. S. Chatterjee, K. B. Neeves, and S. L. Diamond. Determination of surface tissue factor thresholds that trigger coagulation at venous and arterial shear rates: amplification of 100 fm circulating tissue factor requires flow. *Blood*, 111(7):3507–13, 2008.

[80] U. M. Okorie and S. L. Diamond. Matrix protein microarrays for spatially and compositionally controlled microspot thrombosis under laminar flow. *Biophys J*, 91(9):3474–81, 2006.

[81] C. Oury, M. J. Kuijpers, E. Toth-Zsamboki, A. Bonnefoy, S. Danloy, I. Vreys, M. A. Feijge, R. De Vos, J. Vermylen, J. W. Heemskerk, and M. F. Hoylaerts. Overexpression of the platelet p2x1 ion channel in transgenic mice generates a novel prothrombotic phenotype. *Blood*, 101(10):3969–76, 2003.

[82] C. Oury, E. Sticker, H. Cornelissen, R. De Vos, J. Vermylen, and M. F. Hoylaerts. Atp augments von willebrand factor-dependent shear-induced platelet aggregation through ca2+-calmodulin and myosin light chain kinase activation. *J Biol Chem*, 279(25):26266–73, 2004.

[83] O. Panes, V. Matus, C.G. Saez, J. Pereira, and D. Mezzano. Human platelets synthesize and express functional tissue factor. *Blood*, 109(12):5242–50, 2007.

[84] D. J. Pinsky, M. J. Broekman, J. J. Peschon, K. L. Stocking, T. Fujita, R. Ramasamy, Jr. Connolly, E. S., J. Huang, S. Kiss, Y. Zhang, T. F. Choudhri, R. A. McTaggart, H. Liao, J. H. Drosopoulos, V. L. Price, A. J. Marcus, and C. R. Maliszewski. Elucidation of the thromboregulatory role of cd39/ectoapyrase in the ischemic brain. *J Clin Invest*, 109(8):1031–40, 2002.

[85] R. Polanowska-Grabowska, Jr. Simon, C. G., and A. R. Gear. Platelet adhesion to collagen type i, collagen type iv, von willebrand factor, fibronectin, laminin and fibrinogen: rapid kinetics under shear. *Thromb Haemost*, 81(1):118–23, 1999.

[86] Patrick J. Roache. *Verificaiton and validation in computational science and engineering*. Hermosapublishers, Albuquerque, NM, 1998.

[87] E. D. Rosen, S. Raymond, A. Zollman, F. Noria, M. Sandoval-Cooper, A. Shulman, J. L. Merz, and F. J. Castellino. Laser-induced noninvasive vascular injury models in mice generate platelet- and coagulation-dependent thrombi. *Am J Pathol*, 158(5):1613–22, 2001.

[88] J. M. Ross, L. V. McIntire, J. L. Moake, and J. H. Rand. Platelet adhesion and aggregation on human type vi collagen surfaces under physiological flow conditions. *Blood*, 85(7):1826–35, 1995.

[89] R. Ross. Atherosclerosis–an inflamatory disease. *N Engl J Med*, 340(2):115–26, 1999.

[90] Z. M. Ruggeri, J. N. Orje, R. Habermann, A. B. Federici, and A. J. Reininger. Activation-independent platelet adhesion and aggregation under elevated shear stress. *Blood*, 108(6):1903–10, 2006.

[91] M. K. Runyon, C. J. Kastrup, B. L. Johnson-Kerner, T. G. Ha, and R. F. Ismagilov. Effects of shear rate on propagation of blood clotting determined using microfluidics and numerical simulations. *J Am Chem Soc*, 130(11):3458–64, 2008.

[92] U. J. Sachs and B. Nieswandt. In vivo thrombus formation in murine models. *Circ Res*, 100(7):979–91, 2007.

[93] K. S. Sakariassen, P. A. Aarts, P. G. de Groot, W. P. Houdijk, and J. J. Sixma. A perfusion chamber developed to investigate platelet interaction in flowing blood with human vessel wall cells, their extracellular matrix, and purified components. *J Lab Clin Med*, 102(4):522–35, 1983.

[94] K. S. Sakariassen and H. R. Baumgartner. Axial dependence of platelet-collagen interactions in flowing blood. upstream thrombus growth impairs downstream platelet adhesion. *Arteriosclerosis*, 9(1):33–42, 1989.

[95] K. S. Sakariassen, R. Joss, R. Muggli, H. Kuhn, T. B. Tschopp, H. Sage, and H. R. Baumgartner. Collagen type iii induced ex vivo thrombogenesis in humans. role of platelets and leukocytes in deposition of fibrin. *Arteriosclerosis*, 10(2):276–84, 1990.

[96] K. L. Sarratt, H. Chen, M. M. Zutter, S. A. Santoro, D. A. Hammer, and M. L. Kahn. Gpvi and alpha2beta1 play independent critical roles during platelet adhesion and aggregate formation to collagen under flow. *Blood*, 106(4):1268–77, 2005.

[97] B. Savage, M. H. Ginsberg, and Z. M. Ruggeri. Influence of fibrillar collagen structure on the mechanisms of platelet thrombus formation under flow. *Blood*, 94(8):2704–15, 1999.

[98] T. D. Schraw, T. W. Rutledge, G. L. Crawford, A. M. Bernstein, A. L. Kalen, J. E. Pessin, and S. W. Whiteheart. Granule stores from cellubrevin/vamp-3 null mouse platelets exhibit normal stimulus-induced release. *Blood*, 102(5):1716–22, 2003.

[99] H. Schwertz, N. D. Tolley, J. M. Foulks, M. M. Denis, B. W. Risenmay, M. Buerke, R. E. Tilley, M. T. Rondina, E. M. Harris, L. W. Kraiss, N. Mackman, G. A. Zimmerman, and A. S. Weyrich. Signal-dependent splicing of tissue factor pre-mrna modulates the thrombogenicity of human platelets. *J Exp Med*, 203(11):2433–40, 2006.

[100] H. Shankaran, P. Alexandridis, and S. Neelamegham. Aspects of hydrodynamic shear regulating shear-induced platelet activation and self-association of von willebrand factor in suspension. *Blood*, 101(7):2637–45, 2003.

[101] J.A. Shavit, A. Manichaikul, H.L. Lemmerhirt, K.W. Browman, and D. Ginsburg. Modifiers of von willebrand factor identified by natural variation in inbred strains of mice. *Blood*, 114(26):5368–74, 2009.

[102] F. Shen, C. J. Kastrup, Y. Liu, and R. F. Ismagilov. Threshold response of initiation of blood coagulation by tissue factor in patterned microfluidic capillaries is controlled by shear rate. *Arterioscler Thromb Vasc Biol*, 28(11):2035–41, 2008.

[103] S. S. Shevkoplyas, S. C. Gifford, T. Yoshida, and M. W. Bitensky. Prototype of an in vitro model of the microcirculation. *Microvasc Res*, 65(2):132–6, 2003.

[104] J. J. Sixma, P. G. de Groot, H. van Zanten, and I. Jsseldijk M. A new perfusion chamber to detect platelet adhesion using a small volume of blood. *Thromb Res*, 92(6 Suppl 2):S43–6, 1998.

[105] S. Srinivasan, F. Mir, J.S. Huang, F.T. Khasawneh, S.C. Lam, and G.C. Le Breton. The p2y12 antagonists, 2-methylthioadensoine 5'-monophosphate triethylammonium salt and cangrelor (arc69931mx), can inhibit human platelet aggregation through a gi-independent increase in camp levels. *J Biol Chem*, 284(24):16108–17, 2009.

[106] D. Sun, A. McNicol, A. A. James, and Z. Peng. Expression of functional recombinant mosquito salivary apyrase: a potential therapeutic platelet aggregation inhibitor. *Platelets*, 17(3):178–84, 2006.

[107] E. Themistou, I. Singh, C. Shang, S.V. Balulyer, P. Alexandridis, and S. Neelamegham. Application of fluorescence spectroscopy to quantify shear-induced protein conformation change. *Biophys J*, 97(9):2567–76, 2009.

[108] V. T. Turitto. Blood viscosity, mass transport, and thrombogenesis. *Prog Hemost Thromb*, 6:139–77, 1982.

[109] P. E. van der Meijden, I. C. Munnix, J. M. Auger, J. W. Govers-Riemslag, J. M. Cosemans, M. J. Kuijpers, H. M. Spronk, S. P. Watson, T. Renne, and J. W. Heemskerk. Dual role of collagen in factor xii-dependent thrombus formation. *Blood*, 2009.

[110] L. Wang, C. Miller, R.F. Swarthout, M. Rao, N. Mackman, and M.B. Taubman. Vascular smooth muscle-derived tissue factor is critical for arterial thrombosis after ferric chloride-indcued injury. *Blood*, 113(3):705–13, 2009.

[111] Frank M. White. *Viscous fluid flow*. McGraw-Hill series in mechanical engineering. McGraw-Hill Higher Education, New York, NY, 3rd edition, 2006.

[112] S. D. Wiviott and E. M. Antman. Clopidogrel resistance: a new chapter in a fast-moving story. *Circulation*, 109(25):3064–7, 2004.

[113] K. K. Wu. Platelet activation mechanisms and markers in arterial thrombosis. *J Intern Med*, 239(1):17–34, 1996.

[114] Y. P. Wu, T. Vink, M. Schiphorst, G. H. van Zanten, I. Jsseldijk MJ, P. G. de Groot, and J. J. Sixma. Platelet thrombus formation on collagen at high shear rates is mediated by von willebrand factor-glycoprotein ib interaction and inhibited by von willebrand factor-glycoprotein iib/iiia interaction. *Arterioscler Thromb Vasc Biol*, 20(6):1661–7, 2000.

[115] T. Yago, J. Lou, T. Wu, J. Yang, J. J. Miner, L. Coburn, J. A. Lopez, M. A. Cruz, J. F. Dong, L. V. McIntire, R. P. McEver, and C. Zhu. Platelet glycoprotein ibalpha forms catch bonds with human wt vwf but not with type 2b von willebrand disease vwf. *J Clin Invest*, 118(9):3195–207, 2008.

[116] H. Yin, N. Pattrick, X. Zhang, N. Klauke, H. C. Cordingley, S. J. Haswell, and J. M. Cooper. Quantitative comparison between microfluidic and microtiter plate formats for cell-based assays. *Anal Chem*, 80(1):179–85, 2008.